



National Library
of Canada

Bibliothèque nationale
du Canada

Canadian Theses Service

Services des thèses canadiennes

Ottawa, Canada
K1A 0N4

CANADIAN THESES

THÈSES CANADIENNES

NOTICE

The quality of this microfiche is heavily dependent upon the quality of the original thesis submitted for microfilming. Every effort has been made to ensure the highest quality of reproduction possible.

If pages are missing, contact the university which granted the degree.

Some pages may have indistinct print especially if the original pages were typed with a poor typewriter ribbon or if the university sent us an inferior photocopy.

Previously copyrighted materials (journal articles, published tests, etc.) are not filmed.

Reproduction in full or in part of this film is governed by the Canadian Copyright Act, R.S.C. 1970, c. C-30.

**THIS DISSERTATION
HAS BEEN MICROFILMED
EXACTLY AS RECEIVED**

AVIS

La qualité de cette microfiche dépend grandement de la qualité de la thèse soumise au microfilmage. Nous avons tout fait pour assurer une qualité supérieure de reproduction.

S'il manque des pages, veuillez communiquer avec l'université qui a conféré le grade.

La qualité d'impression de certaines pages peut laisser à désirer, surtout si les pages originales ont été dactylographiées à l'aide d'un ruban usé ou si l'université nous a fait parvenir une photocopie de qualité inférieure.

Les documents qui font déjà l'objet d'un droit d'auteur (articles de revue, examens publiés, etc.) ne sont pas microfilmés.

La reproduction, même partielle, de ce microfilm est soumise à la Loi canadienne sur le droit d'auteur, SRC 1970, c. C-30.

**LA THÈSE A ÉTÉ
MICROFILMÉE TELLE QUE
NOUS L'AVONS REÇUE**

THE UNIVERSITY OF ALBERTA

NONINVASIVE ASSESSMENT OF GASTRIC MOTOR FUNCTION IN HUMANS

by

Babajide Olufemi FAMILONI

A THESIS

SUBMITTED TO THE FACULTY OF GRADUATE STUDIES AND RESEARCH IN
PARTIAL FULFILMENT OF THE REQUIREMENTS FOR THE DEGREE OF DOCTOR
OF PHILOSOPHY

THE DEPARTMENT OF ELECTRICAL ENGINEERING

EDMONTON, ALBERTA

SPRING, 1986

Permission has been granted to the National Library of Canada to microfilm this thesis and to lend or sell copies of the film.

The author (copyright owner) has reserved other publication rights, and neither the thesis nor extensive extracts from it may be printed or otherwise reproduced without his/her written permission.

L'autorisation a été accordée à la Bibliothèque nationale du Canada de microfilmer cette thèse et de prêter ou de vendre des exemplaires du film.

L'auteur (titulaire du droit d'auteur) se réserve les autres droits de publication; ni la thèse ni de longs extraits de celle-ci ne doivent être imprimés ou autrement reproduits sans son autorisation écrite.

ISBN 0-315-30325-5

Babajide O. FAMILONI,
Elect. Engineering Dept.
Univ. of Alberta,
Edmonton.
T6G 2G7. Alberta.
Canada.

March 4, 1986.

Dear Sir,

I wish to use the illustrative material attached, copied from

"A concept of gastrointestinal motility" by C.F. Code et al

In: Handbook of Physiology, section 6, Alimentary canal,

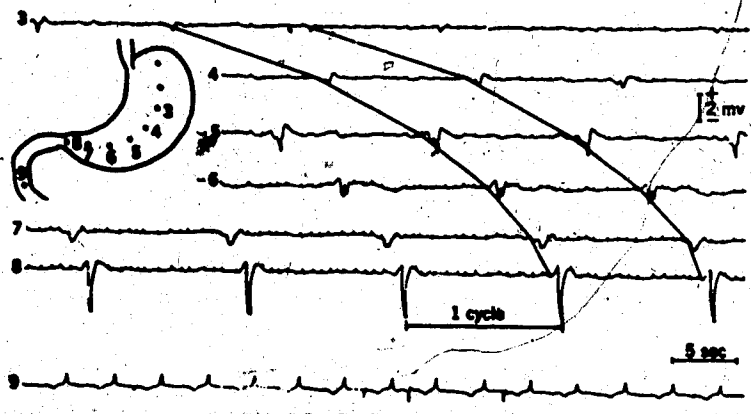
vol. V., pg. 2881-2896, edited by C.F. Code and W. Heidel

usg #19

in my Ph.D. thesis titled "Noninvasive assessment of gastric motility in humans".

I am therefore applying for your permission to use this copyright reserved material. I am willing to abide with the conditions that you may specify in granting such permission. I eagerly await your reply.

Sincerely,



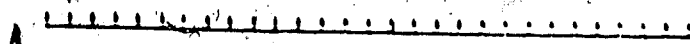
Dept. of Elect. Engineering,
Univ. of Alberta, Edmonton.
April 1, 1986.

Dear Mr. Familoni,

I hereby grant you my permission to use copies of the materials attached, being excerpts from "Measurement and analysis of electrical slow wave activity of the colon", by N.G. Durdle, A Ph.D. Thesis, Univ. of Alberta, 1983 in your thesis titled "Noninvasive assessment of gastric motor function in humans" provided my publication above is credited as the source.

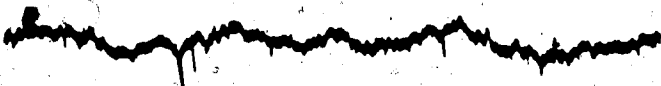
Sincerely,

N.G. Durdle
N.G. Durdle.



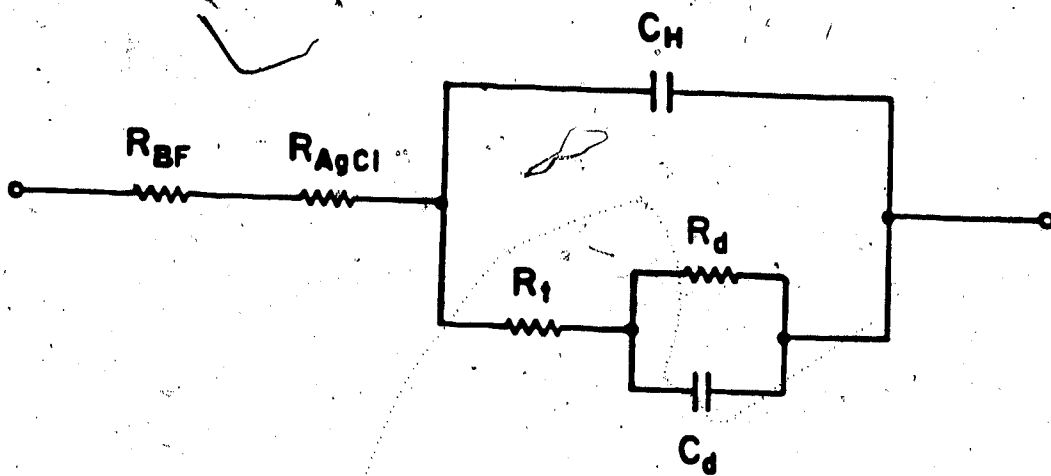
10 μ V

a)



10 μ V

b)



$$R_{BF} = 300 \Omega$$

$$R_{AgCl} = 100 \Omega$$

$$C_H = 15 \times 10^{-9} \text{ farads}$$

$$R_f = 0.72 \Omega$$

$$R_d = 1029 f^{-0.36}$$

$$C_d = 102.1 \times 10^{-6} f^{-0.64}$$

THE UNIVERSITY OF ALBERTA

RELEASE FORM

NAME OF AUTHOR: Babajide Olufemi FAMILONI
TITLE OF THESIS: Ph.D. (Electrical Engineering)
Spring, 1986.

Permission is hereby granted to THE UNIVERSITY OF ALBERTA LIBRARY
to reproduce single copies of this thesis and to lend or sell such
copies for private, scholarly or scientific research purposes only.

The author reserves other publication rights, and neither the
thesis nor extensive extracts from it may be printed or otherwise
reproduced without the author's written permission.

.....
.....

FAMILONI, B.O.

Permanent Address: 4 Adenuga Street

Kongi layout

P.M.B. 5377

Ibadan, Nigeria

April 1986.

THE UNIVERSITY OF ALBERTA

FACULTY OF GRADUATE STUDIES AND RESEARCH

The undersigned certify that they have read, and recommend to the Faculty of Graduate Studies and Research for acceptance a thesis titled "Noninvasive assessment of gastric motor function in humans", submitted by Babajide O. Familoni in partial fulfilment of the requirements for the degree of Ph.D. in Electrical Engineering.

..... *U. King*
Supervisor

..... *Kenneth Jones*

..... *M. L. ...*

..... *B. ...*

..... *J. ...*

Date..... *April 15-86*

"Tire", n'igba a wa l'omode,

"Tire", n'igba a ndagba,

"Tire", n'igba a ba ndarugbo,

Ti aiye wa nbuse.

H.C. 520.

To Enny,

That he may have courage;

Courage enough for the longest day.

O little voice that will not let me go

You fingers of feather that grip me with steel

How long will your wills suffuse my mind?

Even Yahweh of the Jews is saying

"Let my people go".

Babajide.

.....thus sayeth the Lord God of Israel, "Let my people go".....

Exodus 5:1

ABSTRACT

Abnormalities in gastric motor function may be of clinical relevance in a variety of conditions including gastric ulcer, gastroesophageal reflux, gastritis, postvagotomy syndrome, and tachygastric. Methods of monitoring these conditions clinically often involve an assessment of the gastric motor activity and gastric electrical activity (GEA). Unfortunately, established techniques for such measurements are invasive requiring insertion of electrodes during surgical procedures or insertion of an appropriate recording tube through the mouth. Assessment of emptying - the end product of motility - can be done by isotopic emptying studies. However such studies shed very little light on the mechanism for the abnormalities and are therefore, of little use in the development of therapeutic innovations.

Pioneering work in the electrical control of motor activity has established the existence of the one-to-one relationship between myogenic gastric electrical and mechanical activity. It therefore is logical that researchers turn to this link in solving diagnostic problems of the gastrointestinal tract.

Clinically, such information as

- a) the presence and frequency of gastric electrical activity,
- b) the presence of contractions and how often they occur and
- c) the direction of propagation of contractile activity

may be useful in the assessment of gastric motor function and in determining the abnormality involved, if and when they occur.

In this study, an improved method of recording the human electrogastricogram (EGG) is used to obtain the electrical activity noninvasively. An electrical impedance monitoring device is designed and constructed to record the gastric impedance simultaneously and

noninvasively. The relationship between the impedance signal and gastric contractile activity is also established.

To solve the problem indicated in (c) above, the equivalent volume conductor forward problem of the antral electrical activity is developed and solved analytically. In solving the forward problem, a cylindrical quadric surface of revolution is assumed as an approximation to the human torso. The obtained solution is simulated on a digital computer. By allowing the dipole current source representing the myogenic sources to propagate orally and aborally, plots of expected transcutaneous waveforms are obtained. The features peculiar to both cases are noted and used as the basis to discriminate normal from abnormal waveshapes in patient records obtained with electrodes at identical locations to those utilised in the simulations.

Data acquisition and processing software is developed on both an IBM AT personal computer and an amdahl 470/V7 main frame computer.

Reports of measurements on both patients and volunteers are presented.

ACKNOWLEDGEMENTS

I wish to express my profound gratitude to Professor Y.J. Kingma and Dr. K.L. Bowes for their invaluable direction and assistance, and to Dave Rudyk and Ken Cote for their help.

This research was funded in part by a grant from the Alberta Heritage Foundation for Medical Research.

CONTENTS

		Page
1.	INTRODUCTION	1
	1.1 Preamble	1
	1.2 Problem definition	2
2.	MEASUREMENT OF THE BIOELECTRIC EVENT	5
	2.1 Transmembrane Potentials	5
	2.1A Mechanism of the Action Potential and Coordination of Motility	6
	2.2 Recording the Action Potential	15
	2.2A Recording Electrodes	16
	2.2B A Hybrid Electrode	21
	2.2C Sources of Error in Measurements	22
	2.3 Data Acquisition, Processing and Analysis	28
3.	INVASIVE MEASUREMENT SYSTEM DEVELOPMENT	42
	3.1 Electrode Design	42
	3.2 Invasive Measurement in Human	45
4.	NONINVASIVE MEASUREMENT SYSTEM DEVELOPMENT	57
	4.1 Mathematical Model of Gastric Electrical Activity	59
	4.2 Electrical Bioimpedance	83
	4.2A Design of the Gastric Impedance Monitor	87
5.	NONINVASIVE MEASUREMENTS IN HUMAN	100
	5.1 Simultaneous Noninvasive Measurement of Gastric Electrical and Contractile Activity.	100

	Page
5.2 Simultaneous Measurement of Intragastric Pressure and Noninvasive Gastric Electrical and Contractile Activity	107
6. DISCUSSION	116
6.1 Model of Gastric Electrical Activity	116
6.2 Comparison of Extracorporeal and Transmucosal Electrogastrograms	117
6.3 Expansions on this Study	124
6.4 Conclusion	128
REFERENCES	130
APPENDIX	138
A. Setting up the Impedance Monitor	138
A.1 Response Time of the Impedance Monitor	142
A.2 Parts List	144
B. Construction of the Intraluminal Probe	146

LIST OF TABLES

Table		Page
2.1	Ionic Concentrations for Mammalian Skeletal Muscle Cell	8
2.2	Slow Wave Frequencies in Canine and Human GI Tissues	13
4.1	Physical Parameters of Human Tissues	66
4.2	Slope Parameters of GEA.	82
5.1	Results of Transcutaneous Measurement of Gastric Electrical and Contractile Activity	104
5.2	Results of Transcutaneous Impedance and Intragastric Pressure Measurement	114
6.1	Phase Shift in Transmucosal and Extra- corporal EGGs.	122

LIST OF FIGURES

Figure		Page
2.1	Schematic Diagram of Animal Cell Membrane	7
2.2	Circuit Equivalent of Smooth Muscle Cell Membrane	12
2.3	Action Potential	14
2.4	Electrode Impedance Model	18
2.5	Electrode Noise	20
2.6	Electrode Impedance Characteristics	23
	a. Resistance vs. Frequency	
	b. Reactance vs. Frequency	
2.7	Linear Core Conductor Model of an Axon	25
2.8	Variations in Wave Shape of Slow Waves from Cat Jejunum	29
2.9	Variations in Wave Shape of Human Antral Electrical Activity Recorded with a Transmucosal Suction Electrode	30
2.10	Schematic Diagram of Data Acquisition and Signal Processing System	32
2.11	Crosscorrelation Plots	
	a. Ch. 1 by Ch. 2	38
	b. Ch. 2 by Ch. 1	39
2.12	Crosscorrelation Plot Showing Harmonics	40
3.1	Schematic Diagram of Transmucosal Suction Electrode	44
3.2	a. Canine Colonic Electrical Activity	46

	Page
b. 3-D Power Spectrum	47
3.3	
a. Canine Gastric Electrical Activity	48
b. 3-D Power Spectrum	49
3.4	
a. Normal Human Antral Electrical Activity Recorded with Transmucosal Suction Electrode	52
b. 3-D Power Spectrum	53
3.5	
Abnormal Human Antral Electrical Activity Recorded with Transmucosal Suction Electrode	56
4.1	
Record Showing Relative Amplitude of Corpus and Antral Electrical Activity	60
4.2	
Model of Human Torso	62
4.3	
Vector Diagram	64
4.4	
Coupling of GEA	72
4.5	
Transmembrane Potential Approximation	73
4.6	
Simulated Electrogastrograms	
a. Forward Propagation	77
b. Retrograde Propagation	78
4.7	
Measured Electrogastrograms	
a. M_1 and M_2 as in Figure 4.1	80
b. M_1 and M_2 Reversed	81
4.8	
Electrical Impedance of Volume Conductor	85
4.9	
Schematic Diagram of the Impedance Monitor	88

	Page	
4.10	Oscillator and Current Source	90
4.11	Voltage Sensing and Demodulation	91
4.12	Auxilliary Detector	93
4.13	Automatic Gain Control Circuit	94
4.14	Power Supply Scheme	96
4.15	Regualtors and Battery Level Indicator	97
4.16	Battery Charger	98
5.1	Gastric Extracorporal Impedance and Electrical Activity	102
5.2	Power Spectrum	105
a.	GEA	
b.	Gastric Impedance	
5.3		106
a.	Crosscorrelation Coefficient vs. Time Lag	
b.	Absolute Crosscorrelation Coefficient vs. Time lag	
5.4	Electrode Positions	108
5.5	Simultaneous Record of Intragastric Pressure and Extracorporal Impedance and GEA	110
5.6	Correlation Plot	113
6.1	Electrode Positions for Array Calculation	118
6.2	Power in Simulated GEA vs. Electrode Position	119
6.3	Electrode Positions for Intraluminal and	

		Page
	Extracorporeal EGGs	120
6.4	Record of Simultaneous Extracorporeal and Intraluminal EGGs	121
6.5	Power Spectrum	123
	a. Extracorporeal EGG	
	b. Intraluminal EGG	
6.6		
	a. Typical EGG Corrupted by ECG and Respiratory Artifacts	125
	b. Power Spectrum	126
A1	Test Circuit 1	140
A2	Test Circuit 2	140
A3	Test Signal and its Monitor-Delayed Output	143

1. INTRODUCTION

1.1 PREAMBLE

The first recorded use of electrodes is perhaps Galvani's, three frog-muscle contraction experiment in 1800. Interest in electrodes for bioelectric applications has since grown to its present day state of the art.

The present wave of interest is beyond the purely academic. Present clinical applications of bioelectric electrodes include:-

- a) the use of extracorporeal electrodes in electrocardiography (ECG) in the assessment of cardiac conditions;
- b) the use of electrodes in blood flow plethysmography in the diagnosis of peripheral vascular diseases,
- c) the electrical stimulation of various tissues via electrodes in physiotherapy,
- d) and pH and blood gas measurement.

In this work, some knowledge of electrodes and the bioelectric event is pooled to develop a noninvasive technique to assess gastric motor function in humans.

1.2 PROBLEM DEFINITION

The primary functions of the stomach include the retention, mixing and digestion of food materials. In order to perform these functions efficiently, the stomach churns, mixes, and transports food particles in an aboral direction. This capability of the organ is achieved by rhythmical contractions and relaxations of the smooth muscle tissue comprising the organ. It is this ability to move that is termed motility.

Motility may involve the mixing movements which keeps the

intraluminal contents thoroughly mixed at all times and the propulsive movements which transport chyme along the tract.

A pathological condition is said to exist in an organ when it is impaired in the performance of any of its functions. The gastrointestinal tract in disease often exhibit disorders of some sort in motility. Such disorders may manifest themselves in the myoelectrical activity [54,68,69]; since it has been demonstrated that a one-to-one relationship exists between the phasic contractions and the electrical slow wave in those organs [17,60]. Some evidence has been presented to support this position. In 1977, J. Snape et. al. [54] reported a prominent increase in the recorded 3 cycle per minute slow wave activity in tissues from patients of the irritable bowel syndrome. It is also known that nausea, epigastric bloating, gastroesophageal reflux and vomiting occur as a result of disorders in gastric motility. These disorders are often indicated in the electrogastrogram (EGG) as in tachyarrhythmia, and tachygastria [1,68,69].

Diagnostic techniques for such diseases are meanwhile time consuming and often uncomfortable from the patient's perspective. Such diagnosis are still based on

- a) prolonged history of diarrhea
- b) prolonged history of constipation
- c) prolonged history of heartburn
- d) result of sigmoidoscope examinations
- e) result of gastroscope examinations
- f) result of barium meal enemas
- g) result of transit time studies

- h) result of intraluminal pressure studies
- i) result of upper gastrointestinal radiographic studies and/or exclusion of other possibilities.

Substantial improvements in patient comfort, man-hours involved, costs and accuracy may be achieved if reliable and repeatable simultaneous measurements of myogenic electrical and mechanical activity can be obtained from the tissues involved noninvasively.

It is to this objective in the gastric case that this present study addresses itself.

Topics that are fundamental to the understanding of measurements of bioelectric events in general and gastric myogenic electrical and mechanical activity in particular are discussed. Particular attention is paid to how a reliable system to monitor such activities is designed.

As is usually the case in clinical practice, the superior solution should employ a noninvasive method to accomplish its measurement objectives. This however, is often costly in terms of the signal to noise ratio (SNR) of the recorded signal and/or the complexity of the instrumentation required. Hence, pragmatic solutions to measurement problems in human bio-systems often involve some sort of trade-off of accuracy versus noninvasiveness. Thus attempts will be geared towards obtaining

- a) a system that is noninvasive and results in an acceptable SNR, or
- b) a minimally invasive system that realises a good SNR.

A mathematical model and a digital computer simulation that relates the intracellular signal (action potential) to the

extracellular and transcutaneous signal train will be developed.

This will serve to predict such clinically relevant information as frequency and waveshapes as they relate to the direction of propagation of the electrical activity and contraction waves.

A method of analysis that facilitates the identification and therefore classification of the recorded signals will also be developed.

2. THE BIOELECTRIC EVENT

In any quantitative evaluation, it is imperative that an observer understands or, at the very least have a basic idea of the nature of the event to be observed. The following discussion of gastric myogenic electrical and mechanical activity is to this end.

2.1 TRANSMEMBRANE POTENTIALS

The name action potential derives from the electric potential status of a cell when "active" as contrasted with its electric potential status at rest - the resting potential.

An Action potential is generated in living muscle tissue as a result of the depolarization and subsequent repolarization of the tissue cells. The mechanism of activation will be discussed in detail.

There are three basic types of muscle tissue:

- 1) Striated or skeletal muscle tissue,
- 2) Visceral or smooth muscle tissue, and
- 3) Cardiac muscle tissue.

One of the distinguishing factors is the process that leads to the activation of each tissue type.

In skeletal muscle tissue, nervous stimulation of the tissue is under the voluntary control of the animal as contrasted with the case in the smooth muscle in which the control is involuntary. The cardiac pacemaker tissue and other smooth muscle tissues are similar in this respect. Smooth muscles are found around hollow organs in animals.

The electrical activity of the gastrointestinal tract has been determined to be of visceral myogenic origin [9,12,21,22]. The wall of the tissue cells play an important part in the generation of the action potential

2.1A MECHANISM OF THE ACTION POTENTIAL AND COORDINATION OF MOTILITY

The cell membrane of visceral muscle tissue is typically about 70Å thick.

This membrane is composed of assemblies of lipid and protein molecules. The lipid molecules are organized into a bilayer which constitute the basic structure of the membrane. The protein molecules are scattered amongst the lipid molecules and are held in place by noncovalent interactions with the lipid molecules.

The lipid bilayer is essentially water insoluble. Each lipid molecule is composed of a polar head group and a nonpolar tail group as shown in figure 2.1. The head group is made up of three types of lipids: phospholipids, cholesterol and glycolipids. The tail group is usually fatty acids.

This makes the wall essentially dielectric in nature with the capacitance typically of the order of $1 \mu\text{F}/\text{cm}^2$.

The capacitance of a parallel plate capacitor of surface area $A \text{ cm}^2$ and separation $d \text{ cm}$ apart, in microFarads is given by

$$c = 0.0885 \times 10^{-06} A K/d$$

Thus the dielectric constant K of a smooth muscle wall is typically about 8.

This wall enclosing the cytoplasm is semipermeable. The semipermeability is an electric potential controlled inorganic ion selectivity. The wall is in contact on both sides with solutions containing inorganic ions. Some of the more important ones from the point of view of transmembrane potentials include: K^+ , Na^+ , Ca^{++} and Cl^- ions. It is the selective transport of these ions across the cell wall that constitutes the whole basis of transmembrane potentials.

When in equilibrium (with respect to chemical transport), an

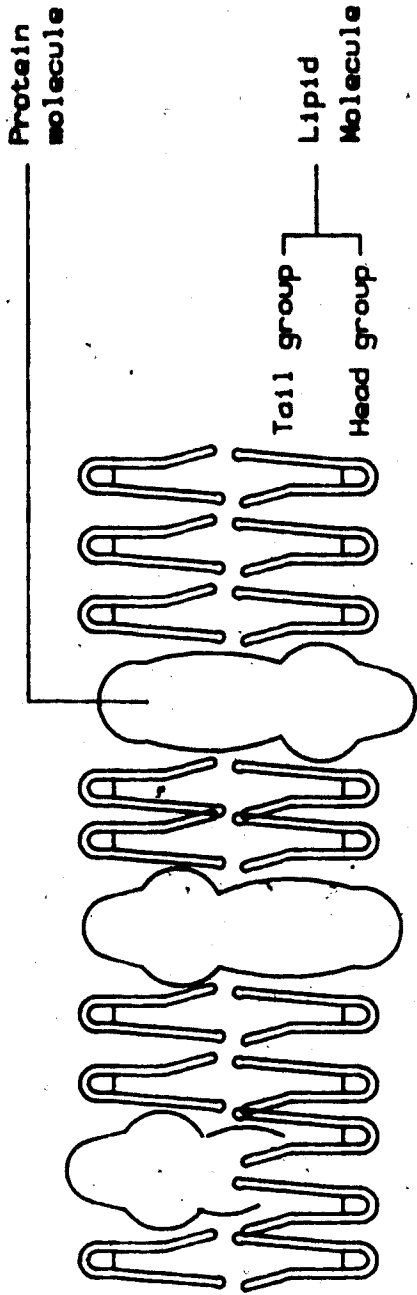


Figure 2.1
Schematic Diagram of Animal Cell Membrane.

ionic charge gradient exists across the cell membrane resulting in a resting membrane potential of about -54 mV. This potential at Donnan equilibrium has been shown to be dependent on the concentration of the ions in and around the cell [53]. This in fact is to be expected if the principle of conservation of energy is to be maintained across the membrane.

TABLE 2.1

IONIC CONCENTRATIONS FOR MAMMALIAN SKELETAL MUSCLE CELL

(Concentrations in mM/l)

Ion	Extracellular Conc.	Intracellular Conc.
K ⁺	4.0	155.0
Na ⁺	145.0	12.0
Cl ⁻	120.0	58.0
Ca ⁺⁺	1.8×10^{-3}	10^{-7}

The energy required to transport an ion x across the membrane is given by

$$W_x = RT \ln \frac{[x]_1}{[x]_0} \tag{2.1}$$

where $[x]_1$, $[x]_0$ are the ionic concentrations inside and outside the cell respectively. R is the universal gas constant and T, the absolute temperature in degrees Kelvin.

It must hold therefore, for an ion of valency z, generating a potential V_{x_0} outside and V_{x_1} inside the cell that

$$\text{energy}_1 = \text{energy}_0$$

which implies that

$$zV_{x1}F + \frac{RT}{zF} \ln \frac{[x]_i}{[x]_0} = zV_{x0}F + \frac{RT}{zF} \ln \frac{[x]_0}{[x]_i} \tag{2.2}$$

The contribution of the x ions to the transmembrane potential is

$$E_x = V_{x1} - V_{x0}$$

therefore from equation 2.2

$$E_x = \frac{RT}{zF} \ln \frac{[x]_i}{[x]_0} \tag{2.3}$$

where F is the Faraday constant.

Equation 2.3 (known as Nernst's equation) assumes

1. a very dilute solution, and
2. no formation of compound ions in the solution so that the

ionic activities are directly proportional to the molar concentrations.

Table 2.1 shows concentrations of some of the more important ions in

solution in and around mammalian cells. The resting membrane potential

E_m may be calculated from the different contributions of the ions in

solution as

$$E_m = \frac{RT}{F} \ln \left\{ \frac{P_K [K]_0 + P_{Na} [Na]_0 + P_{Cl} [Cl]_i}{P_K [K]_i + P_{Na} [Na]_i + P_{Cl} [Cl]_0} \right\} \tag{2.4}$$

where P_x is the membrane permeability of the x ion.

The value of E_m obtained from Goldman's equation is approximately equal to the potassium ion potential calculated by Nernst's equation.

This has led to the conclusion that the resting membrane potential is

essentially the potassium potential. Inomata and Kao [37] confirmed

this by measuring the resting potential in potassium enriched and

potassium deficient environments.

The transmembrane potential of smooth muscle tissues of most of the gastrointestinal tract in general and the distal stomach in particular exhibit spontaneous slow cyclic changes termed slow waves. The exact mechanism responsible for the oscillations is not known, but the ionic basis for transmembrane potentials in general is firmly established [37,53,60]. A typical cycle of slow wave or basal electrical rhythm (BER) or electrical control activity (ECA) comprises of an upstroke potential followed by a plateau with/or without higher frequency activity termed spikes or action potential and a gradual downstroke potential. The frequency of the BER varies from site to site in the gastrointestinal tract. It is however generally lower than 0.5 Hz. Table 2.2 show figures for some sites in the canine and human gastrointestinal tract. It is generally agreed that slow waves largely serve to pace the onset of spike bursts by approaching the threshold potential at which spikes may be generated [17,19,60].

On receiving a supraliminal excitation, say from a nerve, the neuro-transmitter substance acetyl choline released in the postganglionic region causes the Na^+ ion conductivity of the cell to increase rapidly resulting in sodium ion influx into the cell. At the height of the change, the ratio of the K^+ ion conductivity to that of the Na^+ ion would have reversed completely from the situation at rest.

1:0.04 at equilibrium

$g_{\text{K}^+} : g_{\text{Na}^+} =$

1:20 on excitation

The cell wall depolarises rapidly to about +20 mV. The peak of the rise in g_{Na^+} coincides with that of the action potential. As g_{Na^+} starts to fall, g_{K^+} starts to rise. Sodium ions are expelled against the sodium ion gradient and an influx of potassium ions begin. The whole ion exchange process is achieved by an ion pump mechanism brought about by the activation of the membrane-bound ATPase by the Na^+ inside the cell and the K^+ outside it. This active transport process is termed the sodium-potassium pump. The resulting depolarisation and subsequent repolarisation is called the electrical control activity (ECA) or slow wave.

In figure 2.2, contributions of the different ions to the transmembrane potential is represented by batteries and the corresponding membrane conductivities by pure conductances. The sodium and potassium potentials are E_{Na^+} and E_{K^+} respectively. E_r and g_r represent the contribution of the remaining ions in solution. C_m is the transmembrane capacitance.

The relationship between gastric electrical and mechanical activities has been researched extensively [17,19,23,44,68,69]. Various researchers have linked the action potential in a one-to-one relationship to contractions in the gastrointestinal tract [17,19,62]. Hence the names electrical control activity (ECA) for slow waves and electrical response activity (ERA) for spike bursts. This regulation involves varying degrees of myogenic, neural and hormonal influences, all of which are integrated at the cell level to produce the observed coordination of gastrointestinal motility [60].

The action potential is generated throughout the distal stomach as a result of the displacement of the cell from the equilibrium

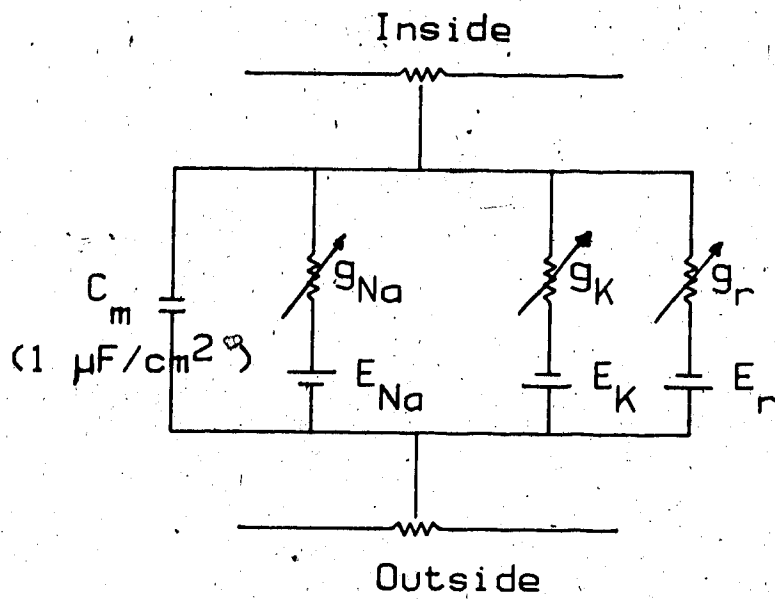


FIGURE 2.2
Circuit Equivalent of Cell Membrane.

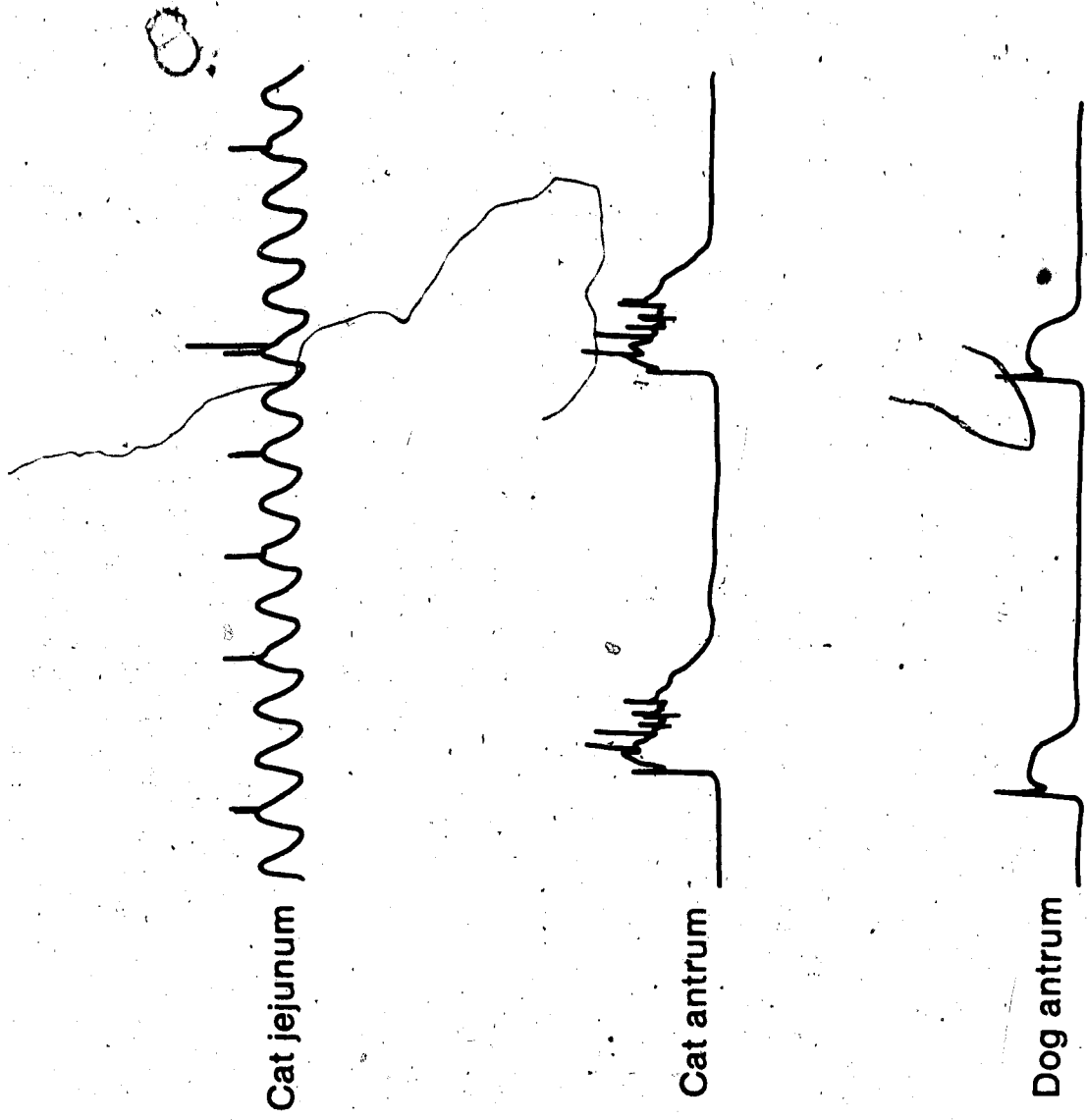
TABLE 2.2

SLOW WAVE FREQUENCIES IN CANINE AND HUMAN GI TISSUES

Tissue	Frequency (CPM)	
	Canine	Human
Small Bowel	12.0 - 19.0	9.0 - 12.0
Stomach	4.0 - 6.0	2.0 - 3.5
Large Bowel	6.0 - 8.0	4.0 - 6.0

state. An excitation that can trigger such a displacement could either be external or of nervous origin. It is worth noting that not all stimuli will cause the cell to "fire". A threshold level whose value is dependent on the potential status of the cell exists. In the so-called inhibition period, a high barrier to excitation exists. This barrier is lowered as the cell potential approaches that at rest. If g_x is the membrane conductance for the x ion at that point t in time, then $g_x = f(E_m, t)$; where E_m is the transmembrane potential.

Inomata and Kao [37] explained the mechanism of the spike activity in terms of the Ca^{++} ion current influx into the cytoplasm through calcium channels in the membrane during the plateau of the slow wave (see figure 2.3). The Ca^{++} ions initiate a series of reactions which allow the myosin to attach to an active site on thin actin filaments thereby causing the muscle tissue to contract. The contraction is maintained until the concentration of the activating Ca^{++} ions drop below 10^{-4} mM/L. Adenosine Triphosphate (ATP) resident on the myosin is hydrolysed to Adenosine Diphosphate (ADP). The energy



30 sec.

Figure 2.3

Action Potential
(Reproduced from Bortoff A. by Permission of University Park Press)

released is converted to muscle shortening.

2.2 RECORDING THE ACTION POTENTIAL

Measurements of biopotentials may be performed in in vitro, in vivo, or ex vivo depending on the accessibility of the tissue involved and the amount of damage that is permissible. When it is possible to isolate the tissue sample, in vitro measurements are the most convenient. The intracellular technique falls in this category. The most accurate way of recording the myogenic electrical activity is to place a recording electrode inside the cell and a reference electrode in the conducting solution surrounding the cell. If one considers that the average size of the cells in question in the human is only about 500 μm by 150 μm , one might begin to appreciate the technical difficulties this entails. Even so, intracellular measurement of myogenic electrical activity is one of the leading methods in the study of the electrical control in the gastrointestinal tract.

Perhaps the commonest intracellular electrode is the glass micropipette which has been in use since 1925 when Ettisch and Peterfi [24] described their heat pulling method. There is also the metal microelectrode. The major advantage of the intracellular method over other in vitro techniques lies in its ability to record the resting membrane potential with fair accuracy, whereas with the other methods (pressure electrodes, sucrose gap, suction electrodes and wire electrodes) this vital information is lost. The sucrose gap method utilises the transmission cable-like properties of smooth muscles to record the transmembrane potential. In all in vitro measurements it is important that the tissue be maintained in an environment as close to

the real system as possible. Thus the tissue is often immersed in a solution that is close to the extracellular solution in composition. Often the solution of choice is Krebs-Ringers solution maintained at about 37°C and irrigated with a mixture of oxygen and carbon dioxide.

In vivo methods include serosal, transmucosal or intraluminal and transcutaneous techniques. The following are the pros and cons of these methods:

- 1) intraluminal and serosal methods are invasive (serosal electrodes require critical surgical invasiveness);
- 2) intraluminal and transcutaneous electrodes are not in direct contact with the tissue of interest thereby resulting in substantial losses in the obtainable SNR.

2.2A RECORDING ELECTRODES

In the measurement of biopotentials, one needs to couple signals originating in a source embedded in an electrolytic medium to an electronic monitoring device with wires and metallic terminals. Thus the measuring arrangement will involve at least two metal-electrolyte interfaces thereby forming a galvanic cell. Such junctions have an electric potential accompanying them as a result of the electrode-electrolyte interface so formed. Sometimes the electromotive force (emf) associated with these junctions could be as large or even larger than the biopotential of interest. It is therefore essential to understand these half-cell potentials so that one can account for, reduce or eliminate their effects in the interpretation of the results.

When an electrode is brought into contact with an electrolyte, an ionic buffer zone is created at the electrode-electrolyte interface. At equilibrium, charge exchange still takes place back and forth between the electrode and the electrolyte. That is to say that the

equilibrium is dynamic. It is this exchange current that is partially responsible for the electrode impedance and the noise level. If there is no net transfer of charge across the interface, the electrode is said to be perfectly polarized.

Helmholtz described the ionic interface in 1879 [33] as a layer of positive ions in contact with another layer made up of negative ions, thereby setting up a charge gradient. Gouy (1910,[29]) and Stern (1924,[56]) suggested modifications that added a diffusion layer to the Helmholtz's layers. When the electrode is connected to form a galvanic cell, an emf that is the difference of the two half cell potentials will result.

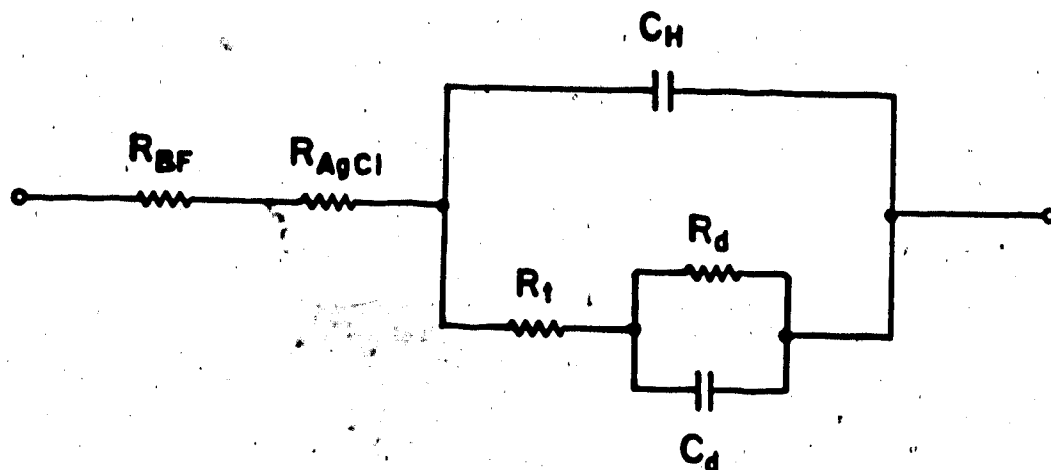
As a result of the interface charge distribution, an impedance can be attributed to the electrode-electrolyte interface. This electrode impedance (Warburg impedance) can be represented as a series combination of a resistance and a capacitance. In 1899 Warburg [63] showed that both the electrode capacitance C_f and resistance R_f are dependent on the frequency f such that

$$R_f = K_1 f^{-a}$$

2.5

$$C_f = K_2 f^{-a}$$

where K_1 , K_2 and $-a$ are constants. Warburg determined the exponent $-a$ experimentally to be about -0.5 . Some modifications have since been made to the Warburg impedance model. Durdle in his work [20] with chlorided silver electrodes reported that the exponent $-a$ was not the same for the resistance and the capacitance. He also reported that the electrode resistance can be split into two distinct components, namely:



$$R_{BF} = 300 \Omega$$

$$R_{AgCl} = 100 \Omega$$

$$C_H = 15 \times 10^{-9} \text{ farads}$$

$$R_t = 0.72 \Omega$$

$$R_d = 1029 f^{-0.36}$$

$$C_d = 102.1 \times 10^{-6} f^{-0.64}$$

Figure 2.4

Electrode Impedance Model
 (Reproduced by Permission of N.G. Durdle [20])

R_{AgCl} , due to the chloride layer and R_{BP} , the bulk Durdle's modified electrode impedance model. C_H is the double layer incremental capacitance and R_t is the charge transfer resistance of the electrode which is given by

$$R_t = \frac{RT}{zFI_0} \quad 2.6$$

where I_0 is the exchange current. By plotting the resistance and reactance of the electrode as a function of frequency he obtained values for the Warburg elements as

$$R_f = 1029 f^{-0.36}$$

$$C_f = 102.1 f^{-0.64}$$

These values show that the major contribution to the electrode impedance is resistive and therefore no significant phase angles should be introduced by the electrode in the range of the physiological frequencies of interest (<100 Hz).

Besides the low electrode impedance advantage, the chlorided silver electrode also has the added advantage of contributing very small thermal noise to the recorded signal. Figure 2.5b is a record of electrode noise for an unchlorided silver electrode while figure 2.5a is that for a chlorided silver electrode. This makes it the electrode of choice in most physiological measurements. The exception being cases requiring long term implantation of electrodes. Its major flaw in this respect is its poor mechanical properties and therefore in such cases, stainless steel electrodes are often preferred. For these

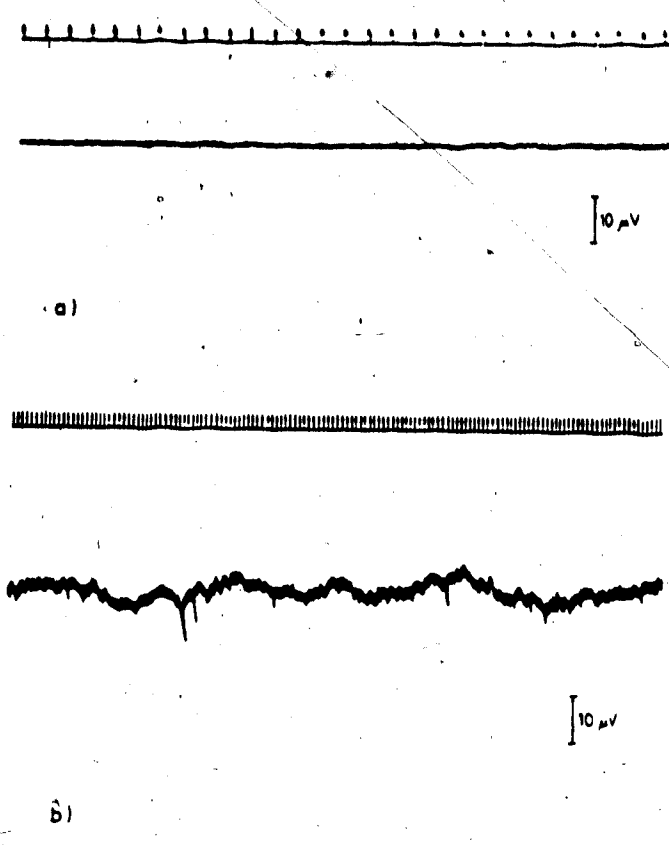


Figure 2.5

Electrode Noise
(Reproduced by Permission of N.G. Durdle [20])

applications one would want an electrode with the electrical properties of the chlorided silver and the mechanical properties of the stainless steel electrode. Such an electrode is described in the following experiment.

2.2B A HYBRID ELECTRODE

Objective: To ascertain if a Ag-AgCl electrode formed on a stainless steel wire base possesses an impedance characteristic similar to that of the Ag-AgCl electrode.

Method: A piece of stainless steel electrode was degreased by soaking in a solution consisting of a mixture of 0.1 molar sodium carbonate and 0.1 molar sodium hydroxide. It was then rinsed in distilled water. To further clean and activate the surface, it was pickled in 10% sulphuric acid and a mixture of 10% nitric acid and 1.5% fluoric acid. The steel electrode was then electrolytically etched in 10% sulphuric acid using a current of 5.4 mA/cm^2 . The electrode was washed in distilled water and transferred into an electrolytic bath containing potassium cyanide solution and silver cyanide dissolved in potassium cyanide. Silver was electrodeposited on the stainless steel electrode (used as the cathode) by passing a 10.76 mA/cm^2 direct current through it for approximately 4 minutes. The steel-silver electrode was again washed in distilled water and then chlorided according to the procedure reported by Kingma et. al. [39]. The impedance of the chlorided steel-silver electrode was measured with a vector impedance meter in normal brine at frequencies ranging from 5 Hz to 600 Hz. The same measurement was also performed for an ordinary stainless steel and an ordinary chlorided silver electrode.

Results: The impedance of all three electrodes varied with frequency in a manner similar to what one expects from the Warburg impedance model as described by equation 2.5. A plot of the impedance versus frequency is shown in figure 2.6.

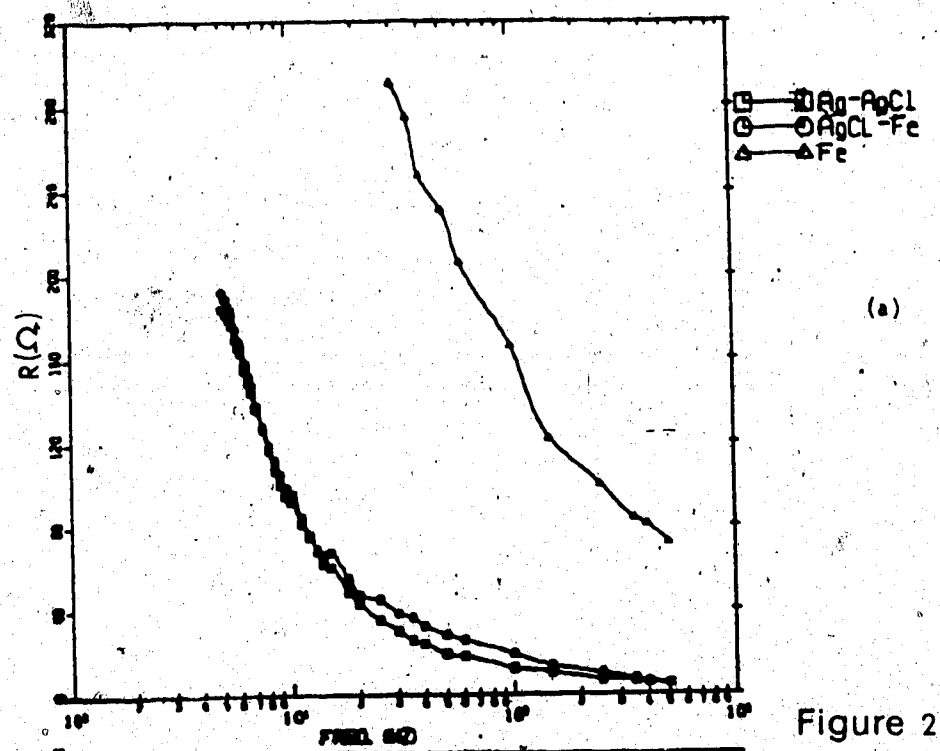
Conclusions:

- 1) The resistance and reactance characteristics of the chlorided silver and silver plated steel electrodes were quite similar.
- 2) The resistance of the ordinary steel electrode was higher than that of the other two at all frequencies investigated by about 60%.
- 3) The reactance of the steel electrode was higher than those of the other two electrodes by about 40% at all frequencies investigated.

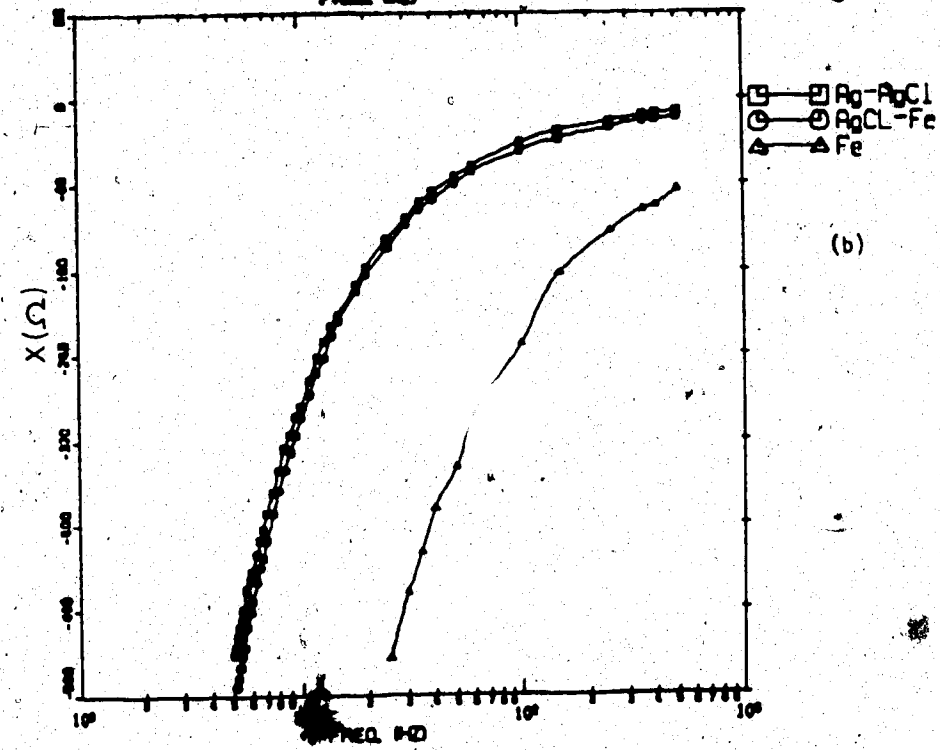
2.2C SOURCES OF ERROR IN PHYSIOLOGICAL MEASUREMENTS

In all forms of measurements, the interpretation of the results play a vital role. Often, this interpretation is made difficult by the disturbances caused in the system due to the measurement process. This is more so in measurements involving biosystems. Take as an example the *in vitro* measurement of myogenic contractile activity with strain or displacement gauges. For these devices to operate properly, an initial tension has to be applied to the tissue. Since stretching the tissue constitutes mechanical stimulation, some controversy exists over the effects of the so called "initial length" on the results of such measurements.

As stated earlier, the electrode potentials of the recording electrodes constitute one of the sources of error in physiological measurements. The term half cell potential is strictly speaking the full cell potential of a galvanic cell composed of the electrode of



(a)



(b)

Figure 2.6

Electrode Impedance Characteristics

- a) Resistance vs. Frequency
- b) Reactance vs. Frequency

interest and a standard hydrogen electrode as reference. The determination of the half cell potential is usually carried out under strictly controlled conditions. It is therefore misleading to use values derived under such conditions to account for electrode potentials in every day measurements in biosystems. Perhaps the closest one can get to accounting for the electrode potentials is to use two similar electrodes in the measurement. The emfs due to both electrodes are similar in value and tend to oppose each other. Even then, a noise problem still exists due to the thermal activity of the ions at the electrode-electrolyte interface.

Another source of error exists as a result of the intrinsic electrical properties of the inactive tissue. It was suggested earlier on that resting membrane potential information is lost in extracellular measurements employing the sucrose gap, pressure electrode and suction electrode techniques. This occurs as a consequence of the transmission cable-like property of the animal tissue when not active. For this reason, experimental investigations of the impedance properties of the cell membrane under sub-threshold conditions often employ a core conductor model of a nerve or muscle fibre. Figure 2.7 shows a linear core conductor model of an axon where V_0 represents the potential across r_0 and V_1 is the potential across r_1 .

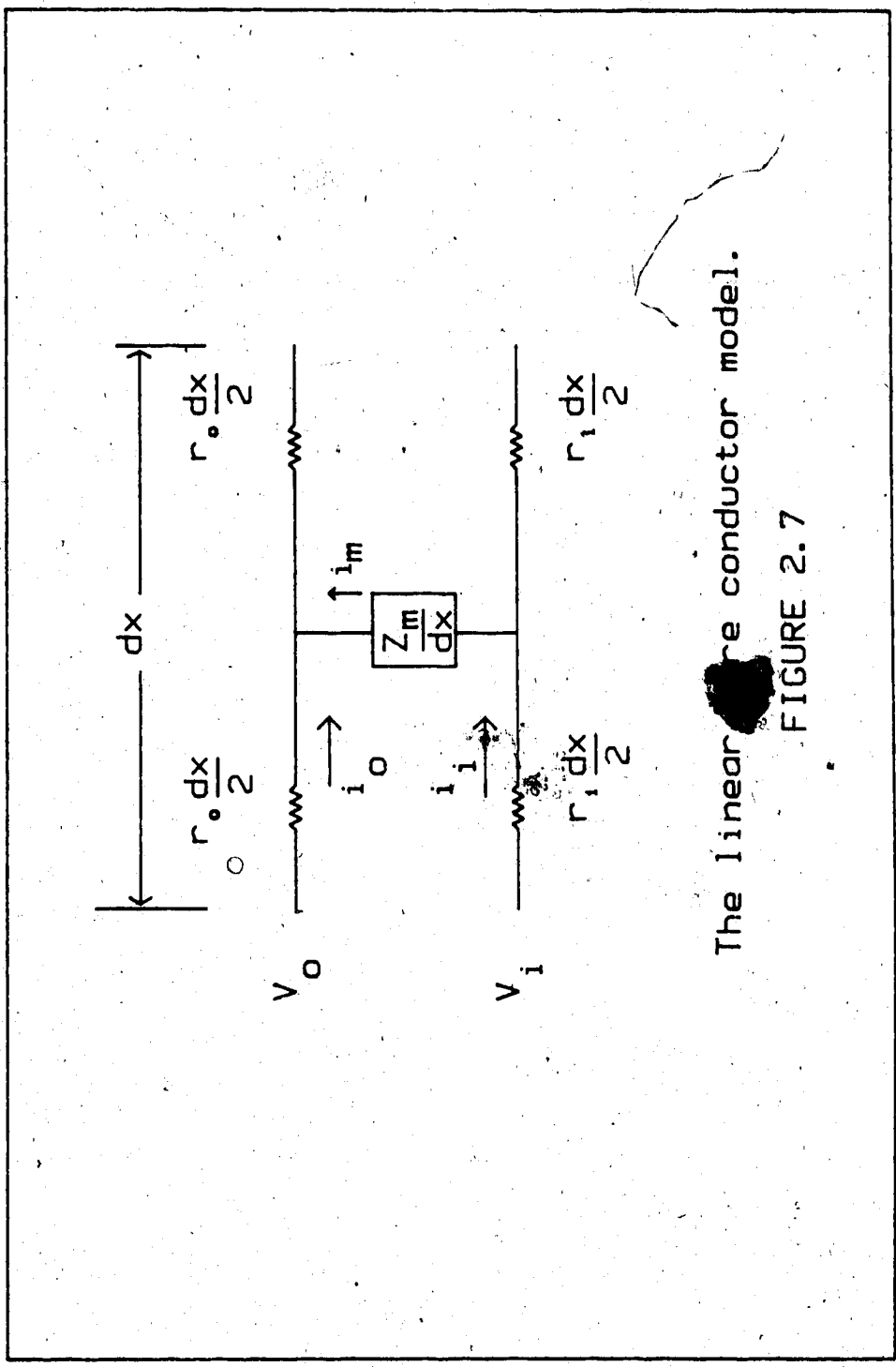
Z_m - membrane impedance

r_0 - resistance per unit length of the external medium

r_1 - resistance per unit length of the axoplasm

i_m - transmembrane current

i_0 - current flow in the environment



The linear core conductor model.

FIGURE 2.7

i_1 - current flow in the axoplasm

ρ - radial distance, and

A - the radius of the axon

The membrane current is given by

$$i_m = \frac{\partial i_o}{\partial x} = - \frac{\partial i_1}{\partial x} \quad 2.7$$

As a result of the current flow, potential gradients exist in both the axoplasm and the interstitial fluids. Clark and Plonsey [15] showed that the potential satisfies Laplace's equation, i.e.

$$\nabla^2 \phi_0 = 0, \rho \geq A \quad 2.8$$

$$\nabla^2 \phi_1 = 0, \rho \leq A$$

and that the linear core conductor model is a good enough approximation for the 3-dimensional system. Therefore the transmembrane potential is

$$V_m = V_1 - V_0 \quad 2.9$$

where $V_1 = \phi_1$ is the axoplasmic potential and $V_0 = \phi_0$ is the interstitial potential. From equations 2.7 and 2.9 one obtains

$$\frac{\partial^2 V_m}{\partial x^2} = \frac{\partial^2 V_1}{\partial x^2} - \frac{\partial^2 V_0}{\partial x^2} = i_m (r_i + r_o) \quad 2.10$$

Since the action potential is propagated as a wave in the inactive tissue, V_m satisfies the wave equation

$$\frac{\partial^2 V_m}{\partial x^2} = \frac{1}{v_0^2} \frac{\partial^2 V_m}{\partial t^2} \quad 2.11$$

Substituting for the 2nd spatial derivative in equation 2.10 from equation 2.11 gives

$$i_m = [v_0^2 (r_i - r_0)]^{-1} \frac{\partial^2 V_m}{\partial t^2} \quad 2.12$$

where v_0 is the propagation velocity of the signal in the inactive tissue. This propagation velocity measured in the squid axon is about 21.2 m/sec. However, it is known to vary proportionally with the diameter of the conducting vessel. Often nerve cells have deposit of Schwann cells called myelin formed on the wall. In such myelinated cells, the membrane capacitance is lower and hence the propagation time constant is shorter. Conduction of impulses from one site (called node of Ranvier) on such a nerve fibre to the other proceed very rapidly. This type of conduction is called saltatory propagation.

Equation 2.12 is a statement of the fact that the recorded membrane current is proportional to the second time derivative of the transmembrane potential.

Hence, bringing a large electrode (large relative to the cell) close to a tissue to measure the myogenic potential often yield results that are not representative of the intracellular potential situation. Due to the deformation of the cell under the electrode and the cable theory in the foregoing, the potential seen by the electrode (termed the injury potential) is usually different from the actual transmembrane potential not only in amplitude but also in its temporal

injury potentials possible when measuring with intracellular, pressure, suction and wick electrodes (figure 2.8). The signal in A in figure 2.8 represents the monophasic transmembrane potential, the wave shape in B is due to the longitudinal current and it is proportional to the first time derivative of the slow wave. The signal in C represents the temporal excursion of the transmembrane current.

Figure 2.9 shows a record of transmucosal antral electrical activity recorded in human with the probe described in section 3.1 and appendix B. In this figure, the wave shapes recorded by the different electrodes are different combinations of the monophasic intracellular action potential, and its first and second time derivatives. The signal seen by the recording electrodes may be represented as

$$v_s = c_1 V_m + c_2 \frac{dV_m}{dt} + c_3 \frac{d^2 V_m}{dt^2} \quad 2.13$$

where c_1 , c_2 and c_3 are some constants whose values depend on the type and amount of contact at the electrode-tissue interface.

In figure 2.9, channel 1 shows more of the monophasic potential than its derivatives. Channel 2 seems to be a sum of the monophasic potential and its second time derivative, and channels 3 and 4 are composed predominantly of the second time derivative.

2.3 DATA ACQUISITION AND SIGNAL PROCESSING

In the previous chapters, we have described at length the type of data involved in this work, its origins and the transducer type employed in monitoring these signals. It is essential to be able to store the received time series events in a form in which they are

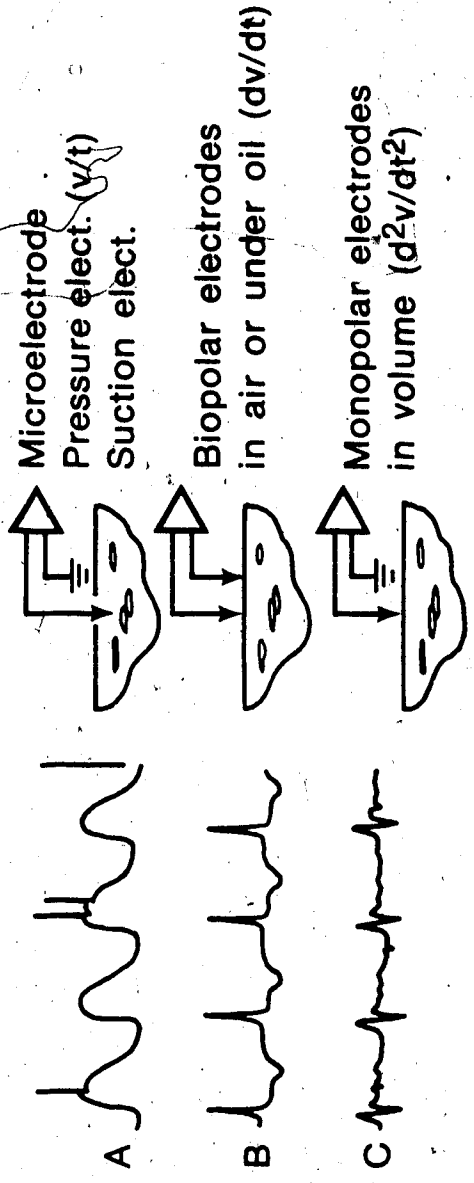


Figure 2.8

Variations in Wave Shape of Slow Waves from Cat Jejunum
(Reproduced from Bortoff [13] by Permission of University Park Press)

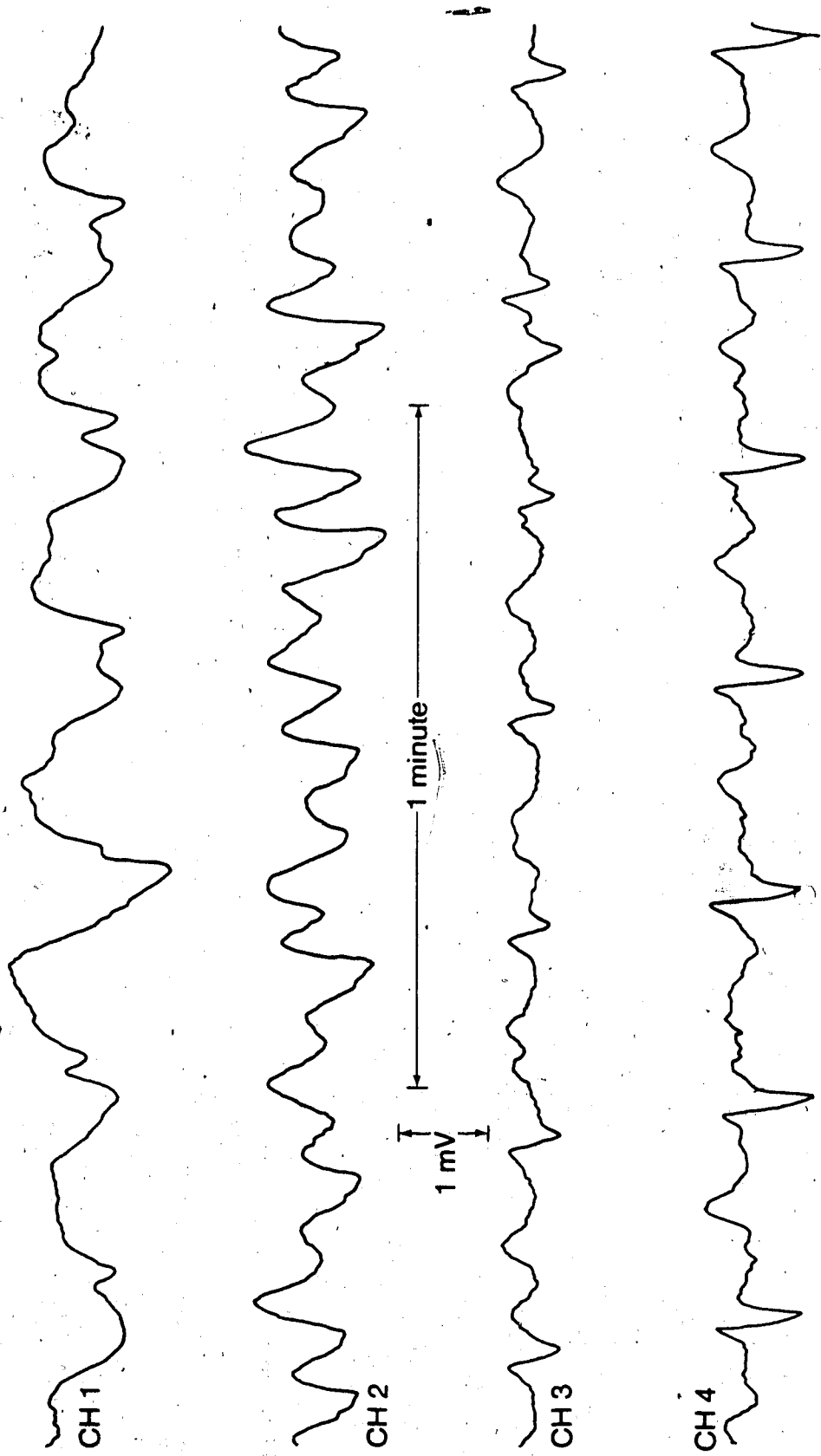


Figure 2.9. Variations in wave shape of Human Antral electrical activity recorded with a transmucosal suction electrode.

easily retrievable to facilitate signal processing. Figure 2.10 shows a schematic diagram of the data acquisition and storage system.

Signals (be it of electrical or mechanical origin) are coupled to a Beckmann polygraph recorder type R611 through input amplifiers. These input amplifiers can either be direct or AC coupled with a time constant variable from 10.0 seconds to 0.03 seconds. The upper cut-off frequency can also be adjusted from 0.08 hertz to 250 hertz. The output signals from these amplifiers can be fed simultaneously to an FM magnetic tape recorder and an IBM AT personal computer through an A to D board. The A to D board is a 12 bit, 8 channel Lab Master^R 200009 manufactured by Scientific Solutions, Inc.

Software exists on the PC to acquire data at variable sampling frequencies. Signals pre-recorded on the FM tape may be played back for storage and processing on the PC.

Data files acquired and stored on the PC can either be processed on it and/or sent through a Gandalf modem to a telephone line for transmission to an Amdahl 470/V7 computer for storage and further processing. The following signal processing options are available on the devices mentioned:-

FM Tape Recorder

- 1) analog signal storage.

IBM AT PC.

- 1) A to D conversion with adjustable sampling rate
- 2) digital signal storage
- 3) 2-D power spectrum analysis of stored data
- 4) auto and crosscorrelation of any given channel(s) in a particular data file

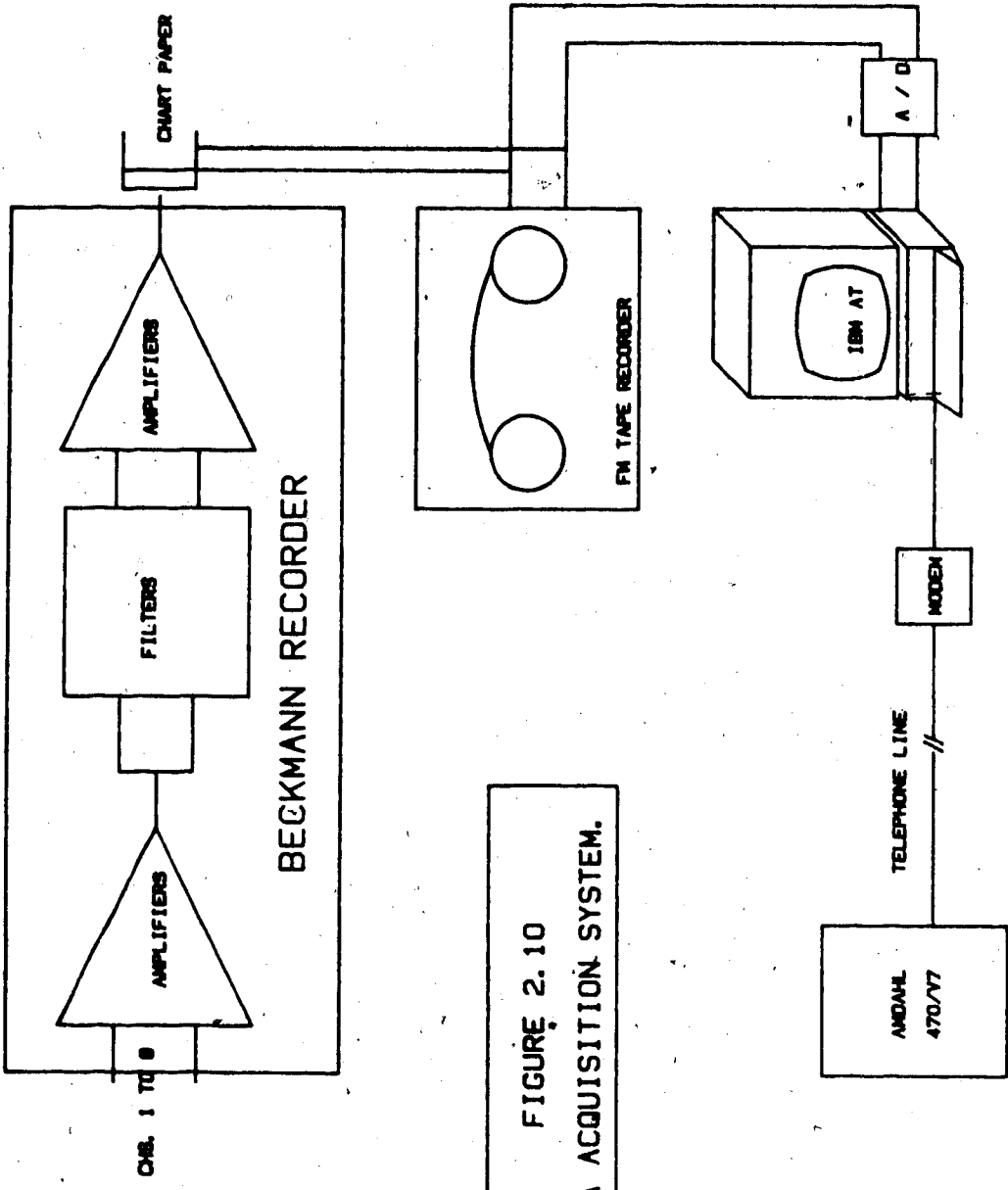


FIGURE 2.10
DATA ACQUISITION SYSTEM.

- 5) data exchange with the Amdahl.
Amdahl Computer.
- 1) digital signal storage,
 - 2) low pass, high pass, band pass and multi-band filtering,
 - 3) 2-D or 3-D power spectrum analysis,
 - 4) auto- and crosscorrelation of any given channel(s) in a particular data file.

A-D CONVERSION

The parameters of data acquisition (sampling rate f_s , calibration values and number of channels) are software controlled. The sampling rate may be varied on the acquisition program resident on the hard disk of the IBM AT from 0.1 Hz to 200 Hz. The system can acquire data from up to 8 different channels simultaneously.

The sampled data is digitized and stored on hard disk from where it can be transferred to a floppy disk or to an Amdahl main frame computer through a modem. Patient files resident on the hard disk can be called from the processing menu for analysis. Such analysis include visual inspection of the raw data, power spectra and auto- and crosscorrelation analysis.

Consider the continuous time series $x(t)$ assumed periodic with a period T seconds. Its Fourier transform can be expressed as

$$X(f) = \int_{-\infty}^{\infty} x(t) e^{-2\pi jft} dt \quad 2.14$$

where f is the continuous frequency variable and $j = \sqrt{-1}$. The equivalent discrete frequency function is

$$X(mF) = \frac{1}{T} \int x(t) e^{-2\pi j m F t} dt \quad 2.15$$

where F is the frequency increment between successive spectra lines. If the input signal is now sampled at $f_s = 1/T_s$ samples per second the discrete frequency transform becomes

$$X(mF) = \sum_n x(nT_s) e^{-2\pi j m n F T_s} \quad 2.16$$

Equation 2.16 often called the discrete Fourier transform (DFT) is usually expressed as

$$X(m) = \sum_{n=0}^{N-1} x(n) W^{mn} \quad 2.17$$

where $N = \frac{1}{F T_s}$ and $W = e^{-\frac{2\pi j}{N}}$

The properties of the DFT and the fact that it takes N^2 complex operations to compute are well known. Equation 2.17 is usually realised through Cooley-Tukey's algorithm known as the fast Fourier transform (FFT) as a consequence of the number of operations required to realise it - $N \log_2 N$, where N is an integer multiple of 2.

The power spectral analysis is performed via the FFT by taking 256 samples at a time. At the sampling frequency mostly employed in this work ($f_s = 2\text{Hz}$), the spectra values are averaged over approximately 2 minutes or 6 cycles of human gastric signals.

On the IBM AT, the spectral components can be plotted out at the frequencies at which they occur. One has the option of choosing from

Hanning, Hamming, and Parzen windowing functions.

The software on the main frame computer takes the spectral analysis one step further. By allowing three quarter overlaps between successive FFT calculations, a 3-dimensional power spectrum is plotted. This three quarter overlap method reported by Hannister in 1980 [6] implies that a 256 sample FFT is calculated every 64 samples into the time series thereby effecting a 192 sample overlap and a better picture of the variations in the signal's spectrum as a function of time.

Software to perform autocorrelation and crosscorrelation also exist on both systems. Correlation plots as a function of time can yield information regarding the frequency of correlation and the time delay between the signals correlated [49]. This analysis is particularly useful in the method proposed in this study for assessing gastric motor function.

Consider a gastric electrical signal $e(t)$ and a mechanical signal $m(t)$ recorded via the impedance monitoring technique described later, both recorded simultaneously. It is known that the electrical signal is always present while contractile activity only occurs part of the time [17]. However, the mechanical activity when it does occur, is always in phase with the electrical activity. Since contraction has not been measured directly, it becomes important to be able to tell if the recorded impedance signal is contractile activity or noise. Therefore, let the two signals be crosscorrelated and define the continuous time correlation function $r(\tau)$ as a function of the time lag

τ as

$$r(\tau) = \lim_{T \rightarrow \infty} \frac{1}{2T} \int_{-T}^T e(t) \cdot m(t+\tau) dt \quad 2.18$$

For the digitized signals, equation 2.18 may be realised as

$$r(k) = \frac{1}{N} \sum_{n=1}^N e(n) \cdot m(n+k) \quad 2.19$$

for sample lags $k = 0, 1, 2, \dots, N-1$. $r(k)$ is zero if there is no correlation between the two signals and it tends to +1 when the signals are perfectly in phase. Hence, if $r(k)$ is plotted as a function of k , maximum value will occur when k/f_s equals the time delay between $e(t)$ and $m(t)$. Figure 2.11 a and b show how phase shift and direction of propagation information is extracted from correlation plots. The plots are for the human intraluminal EGGs shown in figure 2.9 recorded with the multi site electrode described in the next chapter. The crosscorrelation function, $r(k)$ is calculated for 256 samples and plotted against the time lag, k in seconds [49] for

$$-64 \leq k \leq 64$$

This implies that the phase difference θ' obtained via crosscorrelation is averaged over 2.17 minutes.

The phase shift is obtained as

$$\theta' = \frac{-(t_d) * 360^\circ}{\text{Average cycle length}} \quad 2.20$$

where t_d is the time delay indicated on the correlation plot.

The correlation routine is sensitive to the order in which the time series are called up. In figure 2.11a $r(k)$ is plotted for ch. 1

by ch. 2 while figure 2.11a is plotted for ch. 2 by ch. 1 for the same set of data points as figure 2.11a. Figure 2.11a indicates that the first time series leads the 2nd while 2.11b indicates the opposite. The proper order to call the time series of interest is the most proximal channel correlated with the more distal channel, not vice versa. $r(k)$ is also periodic with a frequency equal to that common to both signals.

Figure 2.9 is part of a record of transmucosal EGG in a healthy male. The wave shape of the ECA suggests the presence of peaks at the fundamental and the first 3 harmonic frequencies in the power spectrum [6]. This is often the case in transmucosal measurements. See figures 3.46 and 6.5b. A crosscorrelation plot of CH3 by CH4 from the record in figure 2.9 is shown in figure 2.12. The peaks (a) on the correlation plot are due to the fundamental component of the ECA.

The peaks (b) and (c) represent the first two harmonic frequencies of the signal. Therefore, the distance from any peak (a) to the next peak (a), or any peak (b) to the next peak (b), or any peak (c) to the next peak (c) on the correlation plot is a measure of the period of the electrical activity. In a similar manner, the first two harmonic frequencies can be obtained by inverting the duration from any peak (b) to the next peak (a) and that from any peak (c) to the next peak (b).

With crosscorrelation, information regarding the occurrence of contractions, the frequency of the contractile activity and the duration of the activity can be extracted from a noise corrupted measurement of transcutaneous impedance variations as discussed in subsequent chapters. This information constitutes the bulk of the

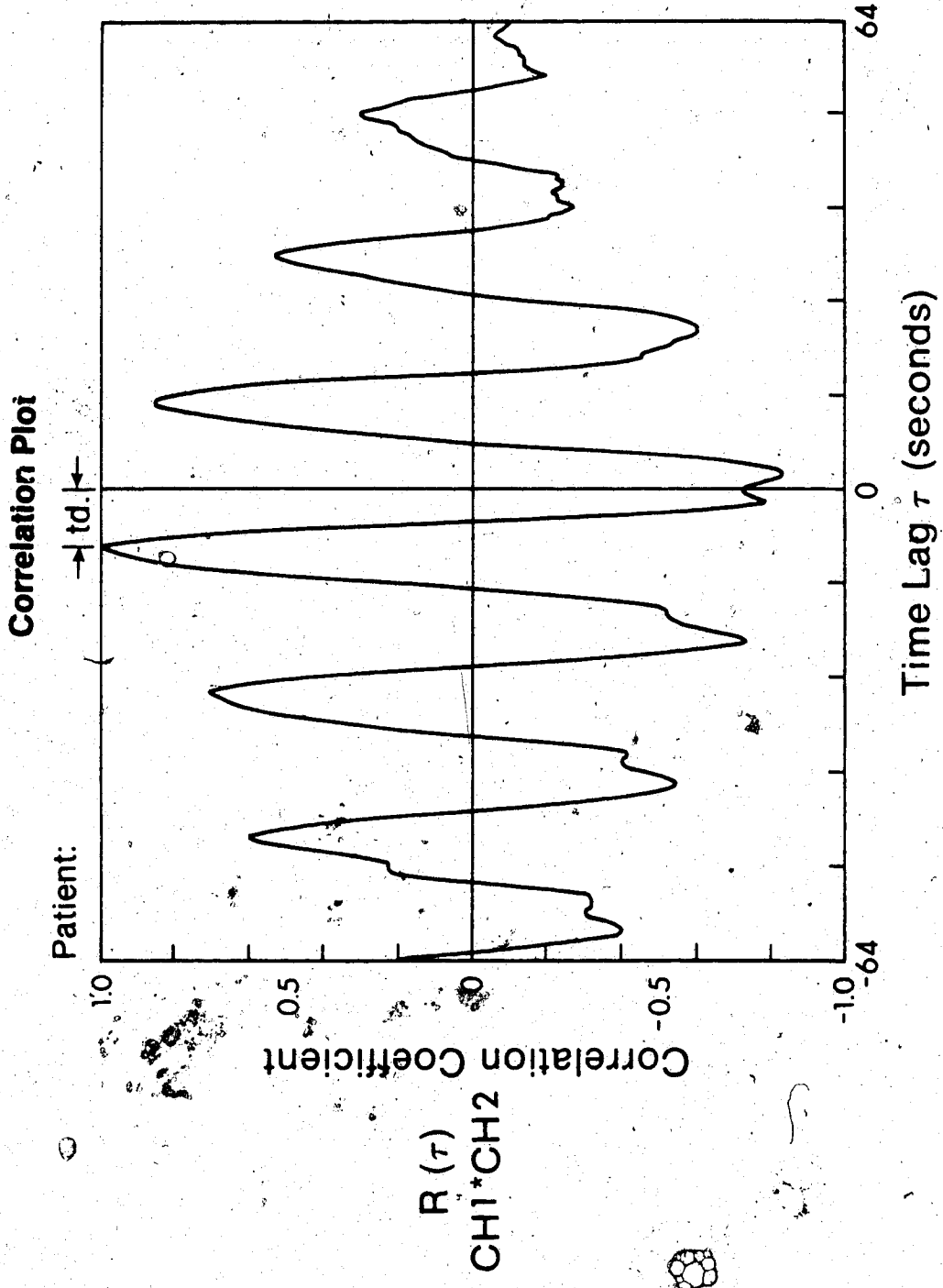


Figure 2.11a

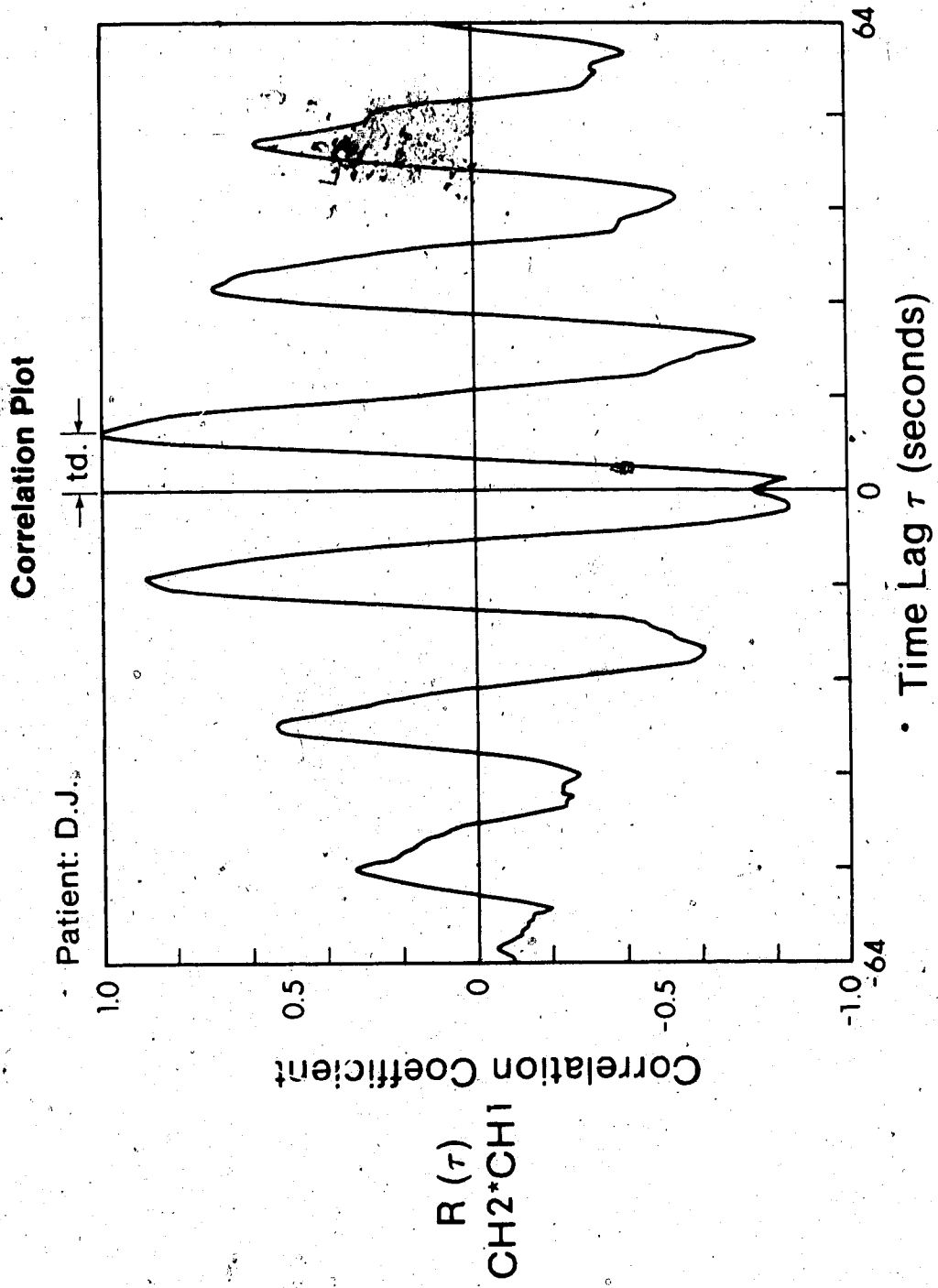


Figure 2.11b

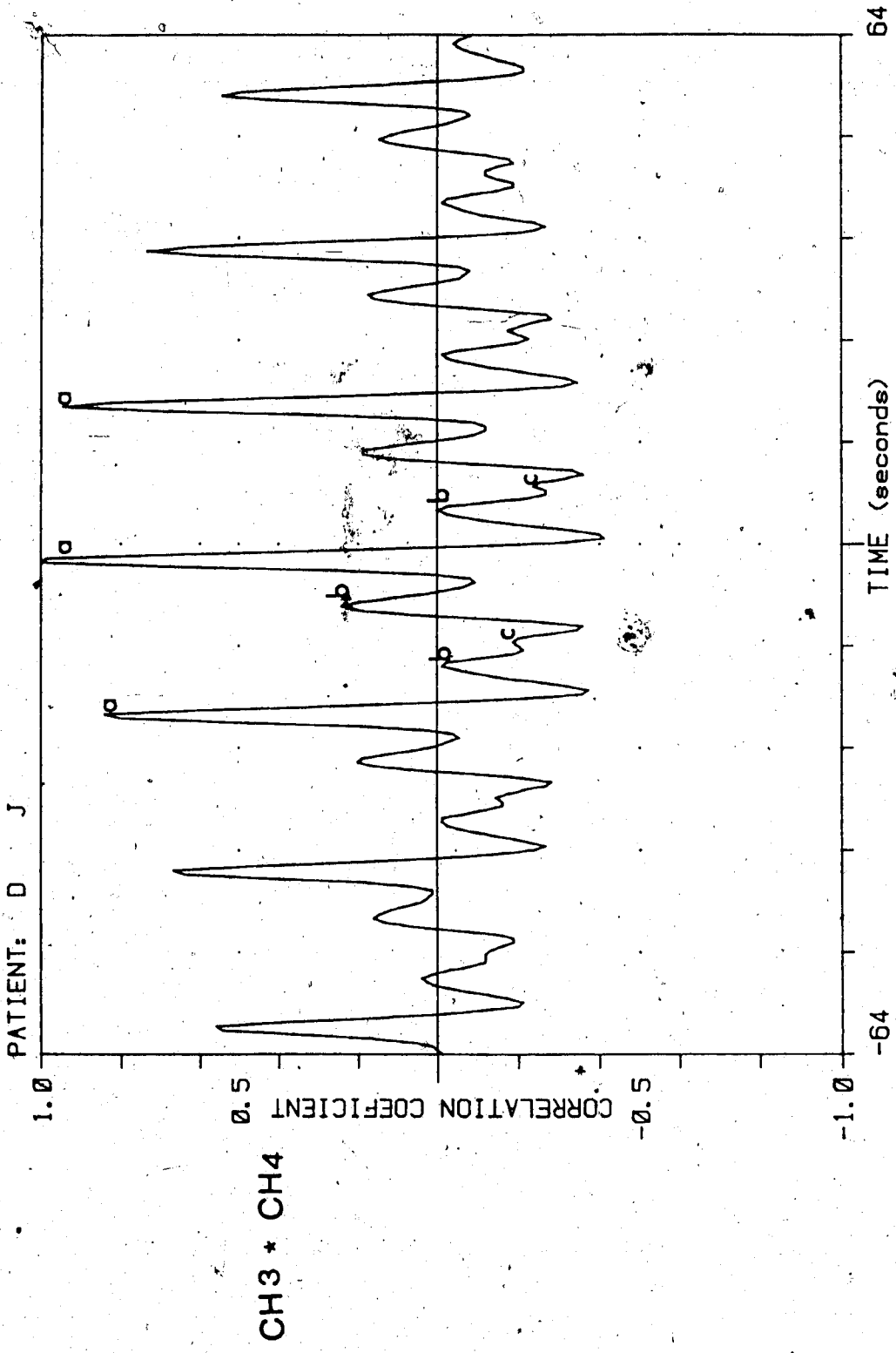


Figure 2.12

Crosscorrelation Plot Showing Harmonics

relevant information in the assessment of gastric motor function.

Output of these signal processing routines are presented throughout this thesis.

3. INVASIVE MEASUREMENT SYSTEM DEVELOPMENT

Invasive measurement of myogenic electrical activity has hitherto been the method of choice in obtaining in vivo human gastrograms. This is largely because of the poor quality of the transcutaneous measurements attempted until recent times. As a result, serosal and intraluminal recording electrodes and techniques have been developed to a level at which confidence exists in their results.

Several authors have reported measurements of the human electrogastrogram both with intraluminal electrodes and with improved noninvasive techniques [1,10,26]. Fioramonti et. al. in 1980 [26] reported their adaptation of this technique to record human colonic slow waves and spike activity. Abel and Malagelada [1] used a magnet held version to record the human electrogastrogram as back-up and check on the recorded transcutaneous signals. These methods provide information about the existence and frequency of gastric electrical activity which may aid in diagnosing tachygastria.

However, none of these methods have provided information regarding the direction and velocity of propagation of GEA. Such information could help isolate such abnormalities as gastroesophageal and antral reflux and gastric stasis.

In order to ascertain the reliability of the extracorporeal measurements, a new electrode assembly was developed. This probe measures GEA through the mucosa in such a way as to yield information regarding the propagation velocity and direction of propagation.

3.1 ELECTRODE DESIGN

Earlier designs of electrodes for use intraluminally sometimes

employed rigid, nondeformable suction cup assemblies to hold the electrodes against the mucosa [10]. The design proposed in this study adapts the pressure electrode that has been so successful in in vitro measurements for mounting on a gastric tube. Figure 3.1 is a schematic diagram of the probe that is designed for use in this work. Appendix B describes the construction of such a probe.

Two features of this device are worth noting.

1) This electrode arrangement incorporates the pressure type electrode in a suction apparatus. The pressure type electrode has been proven repeatedly in bioelectric measurements [11,20,39]. The glass capillary tubing of the pressure electrode [39] is replaced with heat shrinkable tubing for safety reasons. All one need worry about in this application is the consistency of the electrode-tissue interface.

2) Close examination of tissue samples used in in vitro measurements with rigid nondeformable suction devices sometimes show a separation of the mucosa from the tissue (the source of GEA), caused by the suction applied. In such measurements, the electrode sits in the fluid or pocket formed between the tissue and the mucosa, resulting in poor recorded signals.

To get around this problem, part of the suction tube is cut away and replaced with a deformable membrane on which the electrodes are mounted. Thus, on application of suction, the membrane deforms and pushes the electrode towards the tissue thereby maintaining the mucosa-muscle interface intact.

This electrode design was tested in vivo in canine colon and stomach.

The tube was introduced into the sedated animal through the mouth

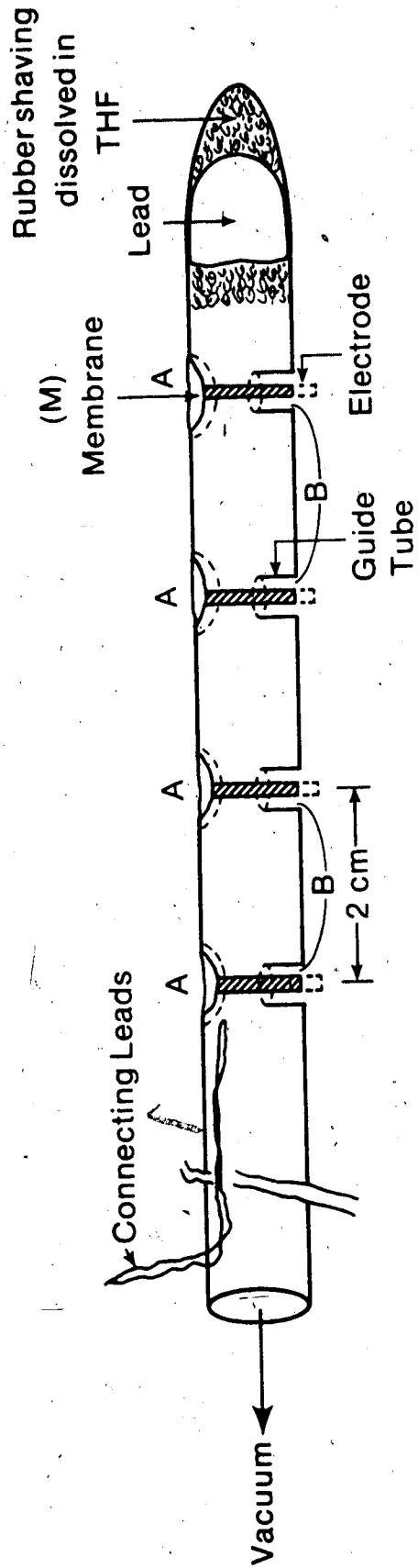


Figure 3.1

Schematic Diagram of Transmucosal Suction Electrode

for GEA measurements and through the anus for measurements of colonic electrical activity. Suction equivalent to 25 cms of water was applied. For monopolar recordings, an ordinary disposable Hewlett Packard ECG electrode type 14445c applied to a shaved part of the animals thigh served as the neutral electrode. Figures 3.2a and b show canine colonic electrical activity recorded with the electrode described and its 3-D power spectrum respectively. Figures 3.3a and b show canine gastric electrical activity recorded with the electrode described in its 3-D power spectrum respectively.

Myogenic electrical activity was recorded in the proximal and distal colon of 13 animals and in the stomach of 18 animals in vivo with the multi site transmucosal suction electrode. Good records of slow waves were obtained in 93% of the total recording time for the stomach experiments and 87% of the total recording time for the colon experiments. The average frequency of the colonic electrical activity recorded was 6.87 ± 0.5 cpm and that of the GEA was 4.71 ± 0.3 cpm.

3.4 INVASIVE MEASUREMENTS IN HUMAN

Gastric electrical activity was recorded in both healthy volunteers and patients with gastric disorders. All experimentation on humans described throughout this study were approved by the Ethics Committee of the University of Alberta Hospital, and prior written consent was obtained from all participants in the studies.

Subjects were fasted for at least 8 hours before the experiment started.

The mouth and the back of the throat of the subject was first sprayed with a xylocain mist. The local anaesthetic effect reduced the

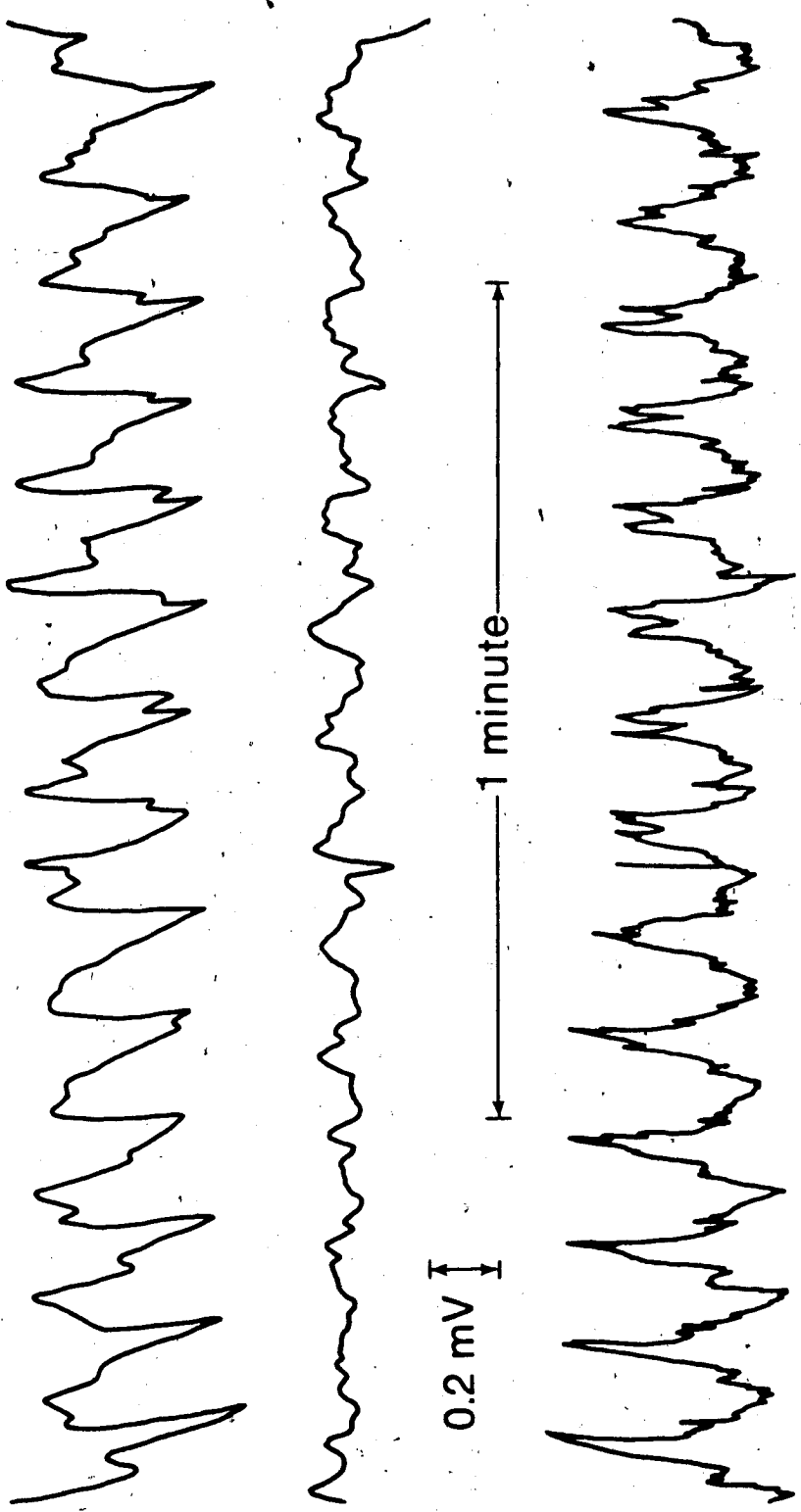


Figure 3.2. Canine colonic electrical activity obtained with the transmucosal suction electrode.
Figure 3.2a.

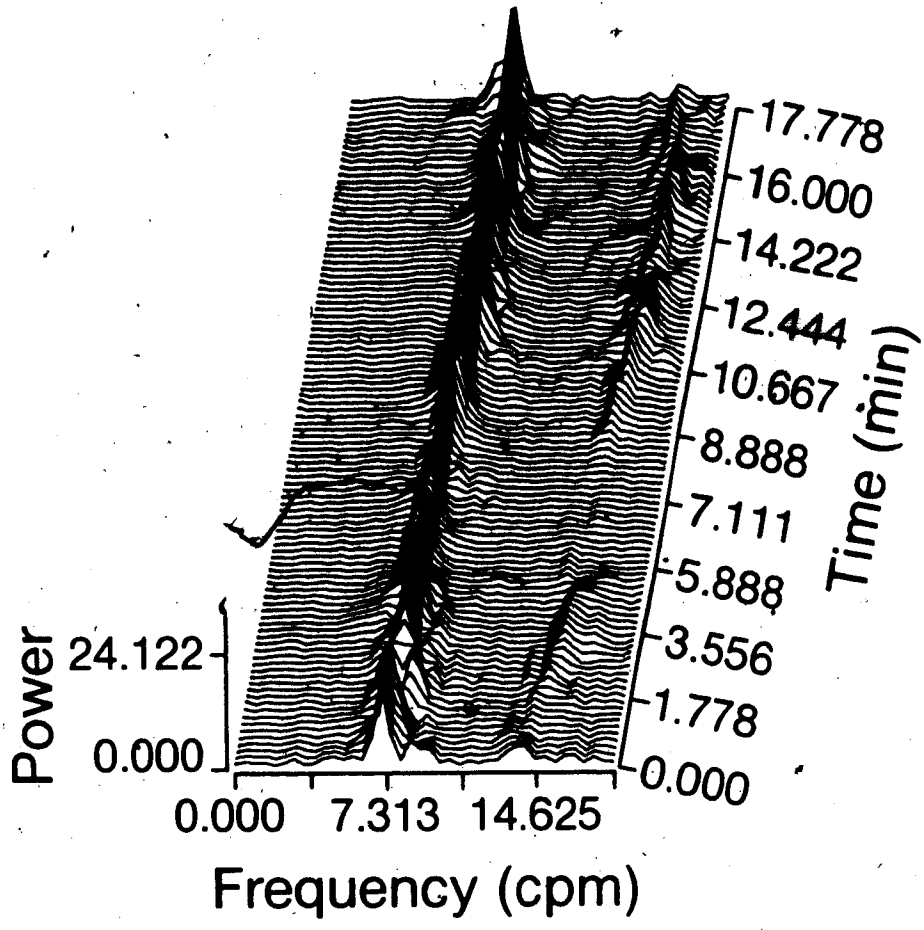


Figure 3.2b.

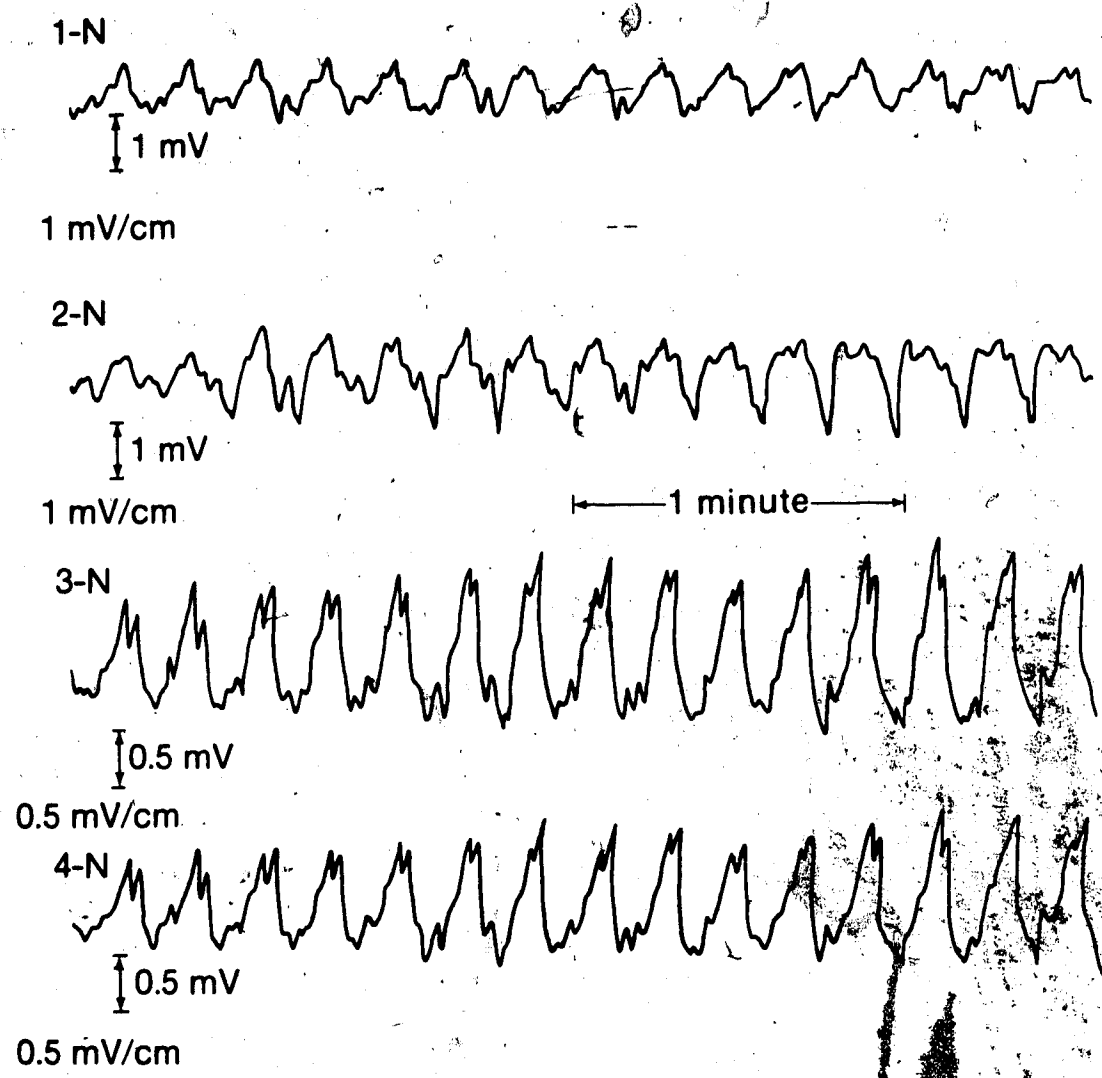


Figure 3.3. a) Canine gastric electrical activity obtained with the transmucosal suction electrode. b) and its 3-D power spectrum.

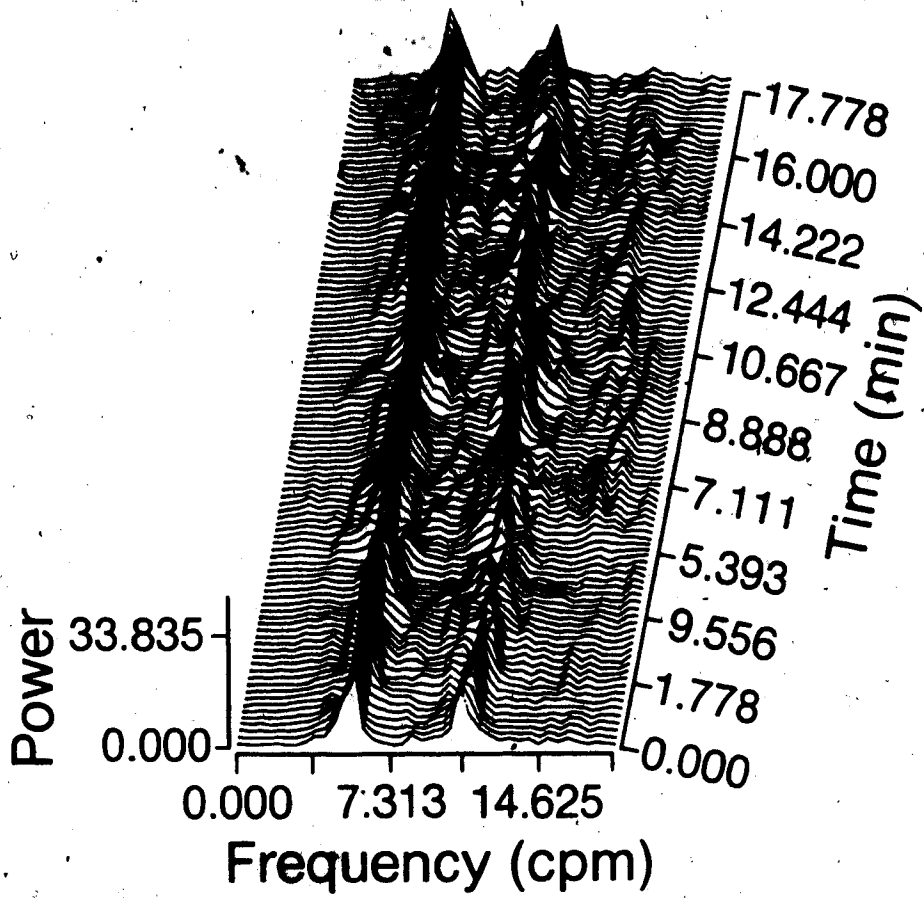


Fig. 3.3b.

subject's gagging reflex. After a few minutes, the throat region was numb enough for intubation to proceed. The position of the tube was then verified by fluoroscopy. The tube was positioned such that all four electrodes lie in the antrum parallel to the antral axis. Suction equivalent to 25 cms of water was then applied to hold the tube and electrodes in this position. An ordinary ECG electrode attached to the lower abdomen served as the neutral electrode. The subjects were then made to lie supine and move as little as possible while the measurement proceeded. Recordings were made for periods of 45 to 90 minutes.

The signals were AC coupled to a Beckmann R611 polygraph with a time constant of 10s for all channels. The high frequency filters were set at 0.3 Hz.

The recorded signals were sampled at a rate of 2 Hz and digitized as described in section 2.3. Power spectra were generated and crosscorrelation analysis were performed on the IBM AT personal computer and an Amdahl 470/V7 main frame computer. Crosscorrelation was performed to ascertain phase shifts between channels and power spectra analysis was performed to ascertain the dominant frequencies. Results of intraluminal measurements performed in this study serve as a basis for some of the modelling and experiments reported in chapter 4.

Results and Discussions:

a)

Transmucosal GEA was recorded in 14 normal volunteers and 4 patients. Good records of intraluminal EGG were obtained in 47 out of 56 channels on the healthy volunteers and 7 out of 16 channels on the patients at least 50% of the recording duration. This recording duration included an initial period of anywhere from 5 to 15 minutes

which the system takes to settle down.

b)

The average amplitude of the slow wave in the normal volunteers was 1.2 ± 0.4 mV and the average frequency was 2.95 ± 0.22 cpm.

The frequency of the activity was ascertained by inspection, FFT derived power spectrum analysis and crosscorrelation. Figure 3.4a shows a typical record of transmucosal antral electrical activity in a normal subject.

The power spectrum analysis for channel 4 of the record is shown in figure 3.4b. The frequency of the fundamental is 2.81 cpm.

c)

It is easy to see the repetitive nature of the slow waves in figure 3.4a. The fact that they are phase locked and propagating in an aboral direction can be verified by constructing lines from a particular point on a slow wave in channel one to the corresponding point on another slow wave in channel two as shown in the figure. The numbers between the traces indicate the phase shift between the upper and lower channels calculated as

$$\theta = \frac{(\text{delay}) * 360^\circ}{(\text{average period of upper and lower cycles})} \quad 3.1$$

In this way, the phase lags can be shown to be constant between a given pair of channels within some tolerance limits.

The phase lag in the normal subjects ranged from $25^\circ/\text{cm}$ to $75^\circ/\text{cm}$ depending on the location of the electrodes in the antrum. It remained approximately constant for a given pair of channels over considerable lengths of time. Its mean deviation staying within 10% of the average

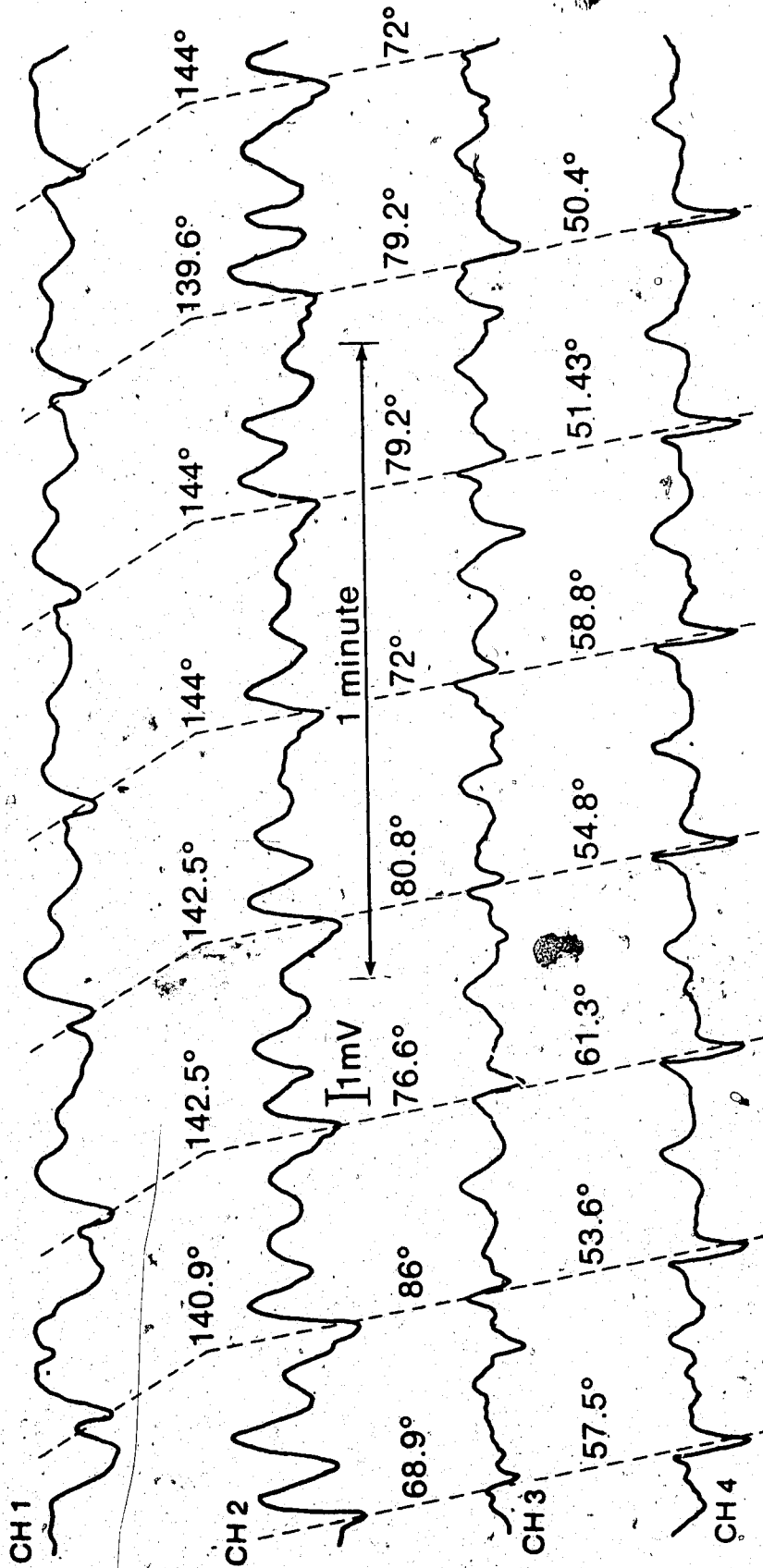


Figure 3.4a

a) Normal Human Antral Electrical Activity Recorded with Transmucosal Suction Electrode

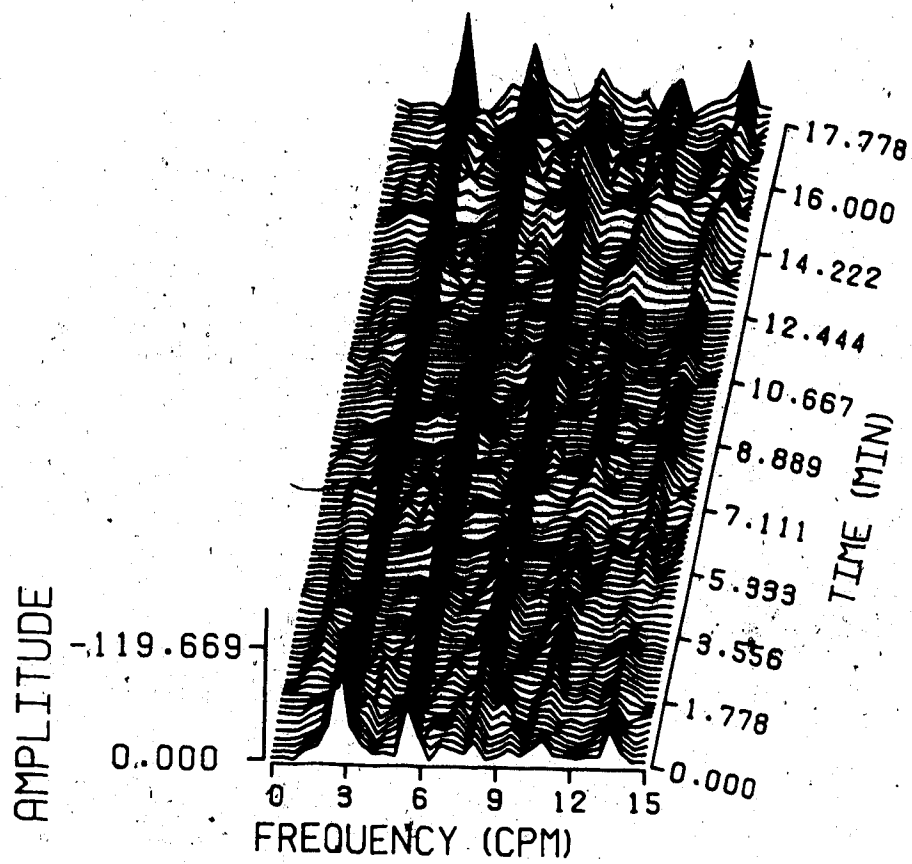


Figure 3.4b

3-D Power Spectrum

over 10 minute intervals.

The average phase lag between sites 1 and 2 in this record by inspection is $71.3^\circ/\text{cm}$, $38.4^\circ/\text{cm}$ between sites 2 and 3 and $27.7^\circ/\text{cm}$ between sites 3 and 4.

From a plot of the crosscorrelation coefficient as a function of the time lag performed on the IBM AT computer, the average phase lag θ' (averaged over 256 samples) obtained from the correlation plots is $70.0^\circ/\text{cm}$ between electrodes 1 and 2, $43.3^\circ/\text{cm}$ between electrodes 2 and 3 and 25.0° between electrodes 3 and 4.

d)

The velocity of propagation of GEA increases from 0.1 cm/s in the proximal corpus to 4 cm/s in the distal antrum [18]. The velocity of propagation v_0 is given by

$$v_0 = \frac{360^\circ \cdot d}{T} \quad 3.2$$

where T is the average period of the activity and d is the electrode spacing - 2 cm in this case,

This implies that the velocity of the GEA in figure 3.4a increases from 0.22 cm/s between the 1st and 2nd electrodes to 0.68 cm/s between the 3rd and 4th electrodes.

e)

In figure 3.4a, the wave shape varies from electrode to electrode. Channels 1 and 2 appear to be composed largely of a sum of the 1st and 3rd terms in equation 2.13, while channels 3 and 4 are almost purely the 2nd time derivative of the transmembrane potential. The shapes of the slow waves can be attributed in part to the

longitudinal current in the mucosa which is proportional to the 2nd time derivative of the transmembrane potential, V_m [15] as discussed in section 2.2 and described by equation 2.13.

f)

Figure 3.5 is an intraluminal EGG from a female patient with gastric disorders. The average period of the slow wave remains approximately constant at 20 seconds. However, the average phase shift between channels 2 and 3 is only 12.8° and that between channels 3 and 4 only 6.5° . This is one type of abnormality observed in the group with gastric complaints. The others include a wide variation in the cycle-to-cycle period of the slow wave (up to 50%), lack of coupling between recording sites and tachygastria as described by previous authors [1,10,68].

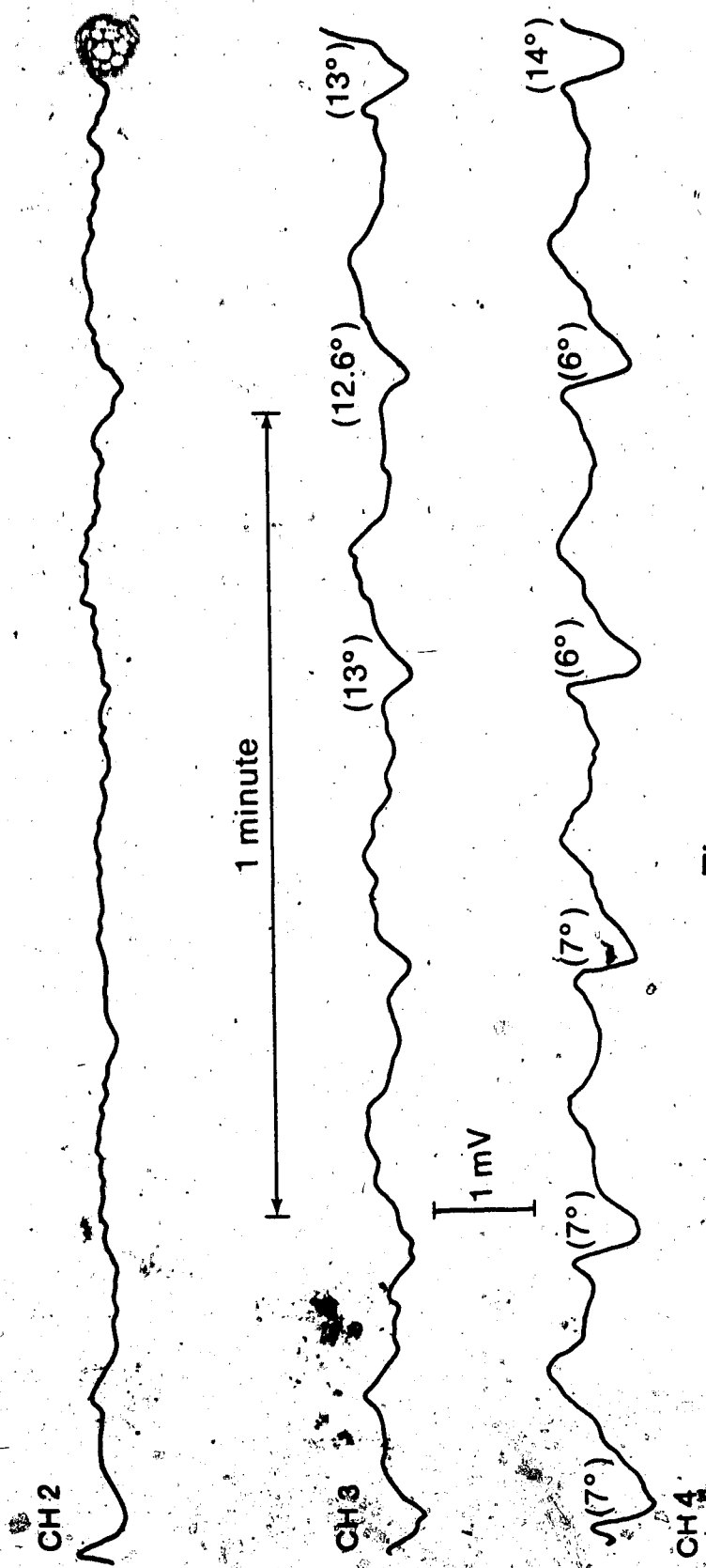


Figure 3.5
Abnormal Human Atrial Electrical Activity Recorded
with Transmucosal Suction Electrode

4. NONINVASIVE MEASUREMENT SYSTEM DEVELOPMENT

Noninvasive measurement of electrogastrography was first reported by Alvarez in 1921 [3]. Major advancements have since been made in the development of better skin electrodes which has enhanced the attainable SNR in transcutaneous recordings. A number of authors [1,10,32,43] have since reported improvements in the recorded electrogastrogram. Mirrizi et. al. [43] reported in 1983 that the best electrode arrangement to record the human gastrogram is one in which a pair of electrodes is lined up above the antral axis.

All of these activities has resulted in records good enough to enhance the clinical application potential of the electrogastrogram. Abel and Malagelada [1] reported being able to detect glucagon evoked gastric dysrhythmias in volunteers by evaluating their electrogastrograms.

To extract more information from the electrogastrogram, it is essential to be able to predict its features for normal and abnormal slow waves in the gastric muscle. In particular, it is desirable to be able to tell the direction of propagation of the myogenic contractile waves from the wave shape of the gastrogram.

The shapes of the recorded signals can be predicted by mathematically modelling the antral electrical activity. Such mathematical modelling (both the forward and the inverse volume conductor problems) have been studied extensively in the cardiac cases [4,5,7,8,51]. In general, the forward problem is concerned with predicting the potential anywhere in a medium and at its boundary due to a source embedded somewhere within those boundaries. On the other hand, the inverse problem determines the strength and location of a

source inside a medium from values of potentials due to this source at some locations inside or on the boundaries. The source types often employed include the single dipole SD, the single moving dipole SMD, and multipoles current sources and epicardia charge distributions.

In this study, we shall concern ourselves with the SD and SMD approximations to the myogenic generators of interest.

The SD and SMD are based on the intuitive notion that a dipole moment can be made to represent the electrical activity in a locale of active tissue or what Kingma et. al. [40] described as an oscillating region. We now know that calculations from such models can be 80% to 95% accurate in some regions on the torso when compared with the amplitude of actual measurements [5,8]. To obtain a high accuracy in the forward problem, one needs to determine the dipole moment and the location of the dipole that best describes the active tissue of interest. This can be obtained by solving the inverse problem for a number of potential measurements made at different locations on the boundary. The optimal dipole moment and location is that source term with the least quadrupole amplitude in it. On the other hand, a variable dipole moment and location can be used in the forward problem and the dipole moment and location iteratively fitted by minimizing the sum of the squared deviations of actual potential measurements from the calculated values [38]. In the mathematical model developed in this study, the latter approach is utilised.

The gastric case has some characteristics differentiating it from the cardiac case. We will take advantage of the following differences to simplify the model.

- a) Code et. al. [17] reported that the strongest coupling and

amplitudes of gastric electrical activity occur in the distal and mid antrum. In figure 4.1, the signal at site 3 in the corpus is only about 10% of that in the antrum. Thus one may locate the sources in the antrum without any serious loss of accuracy.

b) This study, is more concerned with the direction of propagation and the relative amplitudes of the signal rather than the absolute values. Hence, all we need to do is ensure that the source function resembles the monophasic transmembrane potential.

The information gathered from this modelling will serve to predict the features of transcutaneous EGG. An electrical impedance technique is employed to monitor the gastric impedance which is a function of gastric contractions. Morris et. al. [44] simultaneously recorded canine intestinal and colonic electrical and mechanical activity from implanted electrodes via a similar system in 1982.

A noninvasive method for monitoring GEA is used in conjunction with a noninvasive electrical impedance monitoring device to measure gastric electrical and contractile activity simultaneously.

4.1 A MATHEMATICAL MODEL OF THE TRANSCUTANEOUS GASTRIC ELECTRICAL ACTIVITY

Several authors have dealt with the solutions of the appropriate integro-differential equations to determine the scalar potentials due to current sources embedded in conducting mediums [4,7,35,47,51]. Often the emphasis is on the relative signal strength at near and far fields. The mathematical modelling proposed here is different in the sense that it is aimed at predicting the temporal features of the transcutaneous EGG. The essential steps include:

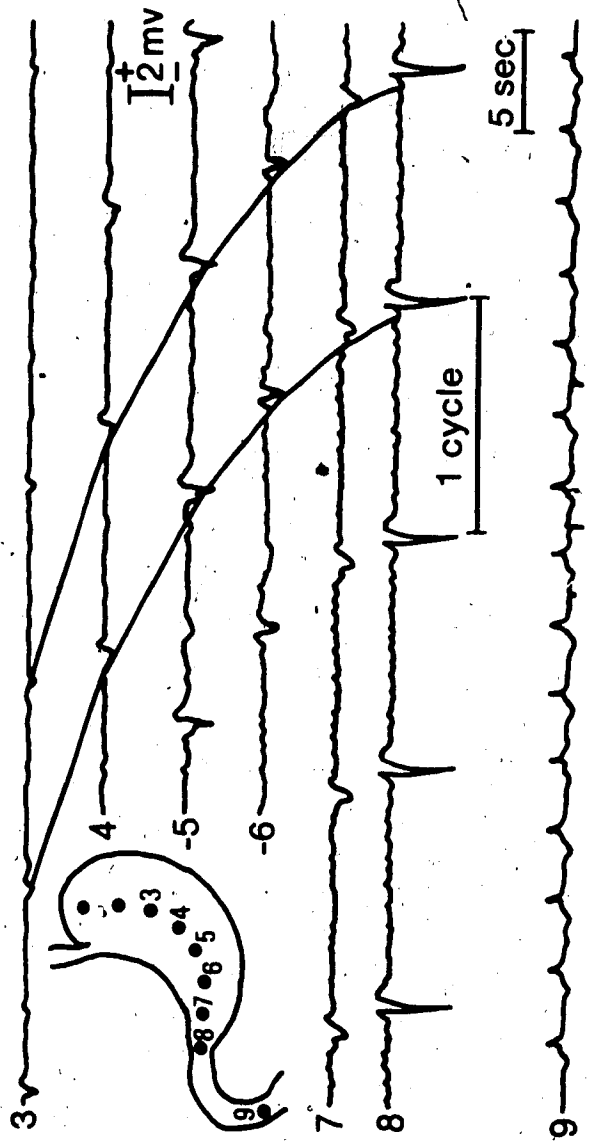


Figure 4.1

Record Showing Relative Amplitude of Corpus and Antral

Electrical Activity

(Reproduced from Code C.F. [17] by Permission of the American Physiological Association)

- 1) developing an approximation to the human gastric system,
- 2) formulating an adequate integro-differential equation,
- 3) solving this equation,
- 4) and simulating the solution on a digital computer.

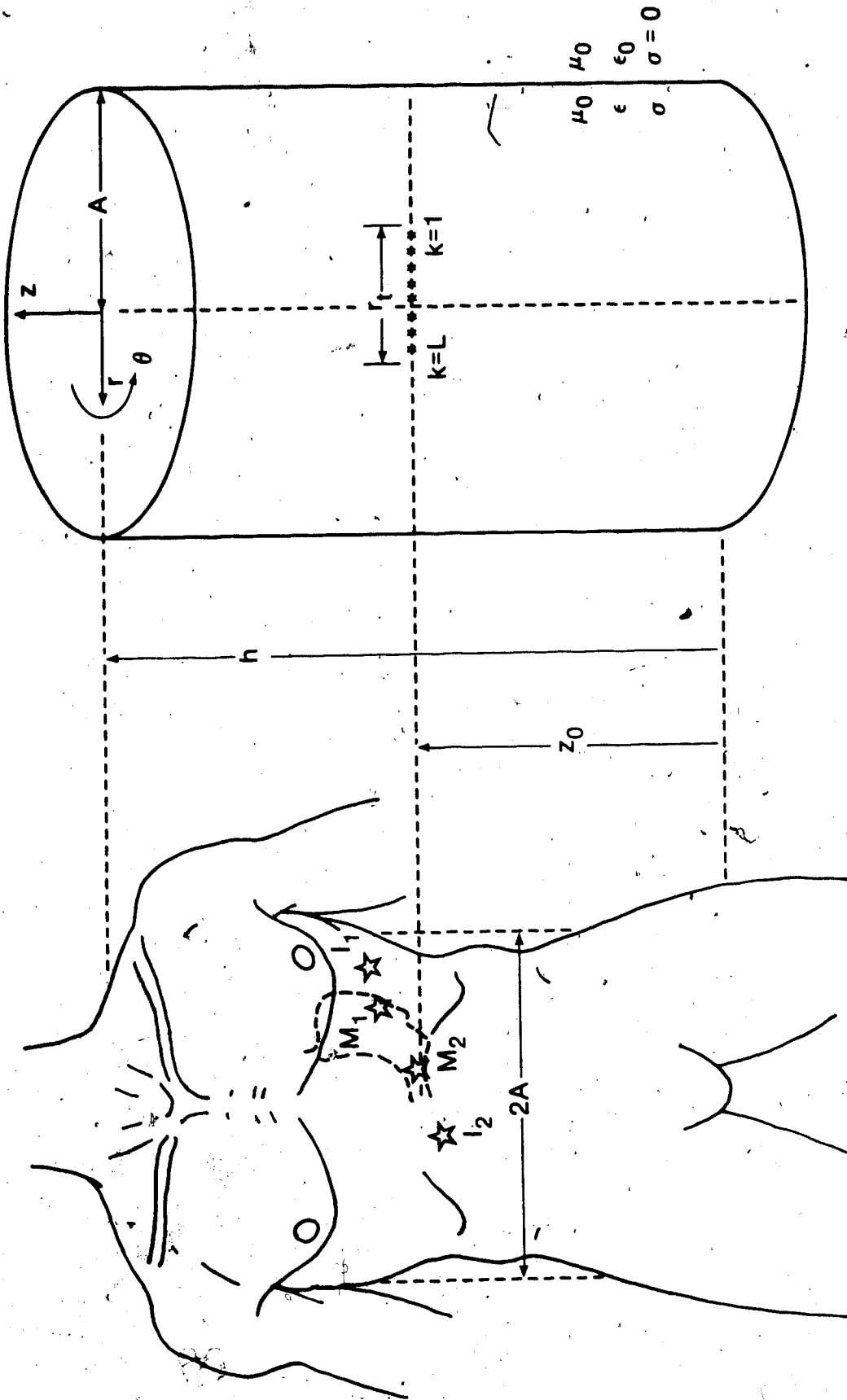
In the approximation that follows, we will work with a finite length cylinder representation of the human torso. Such representation though simplistic, is adequate not only because of the geometric similarities but also because of the accuracies attainable. Okada [47] calculated the scalar potential produced by an eccentric current dipole in a metal cylinder filled with a conducting solution and reported an accuracy of 95% compared with experimentally measured values.

Formulation of a precise equation involves consideration of the following:-

- a) a moving source in the torso whose source strength I resembles figure 2.3 in its temporal excursions,
- b) the path of motion is along the wall of the antrum at a propagation velocity v_0 m/sec ($0.1 < v_0$ cm/sec < 4 [18]),
- c) the medium ($r < A$ in figure 4.2) is inhomogeneous and nonisotropic,
- d) the medium has both conductive and dielectric properties,
- e) and the solution is subject to the boundary conditions at the skin-air interface.

The potential $\phi(\underline{r}, t)$ due to such a myogenic current source may be represented by [45, 48]

$$\nabla^2 \phi(\underline{r}, t) + K^2 \phi(\underline{r}, t) = - \frac{I \delta(\underline{r} - \underline{v}_0 t)}{\sigma + j\omega\epsilon} \quad 4.1$$



Finite Cylinder Approximation

FIGURE 4.2

Human Torso

Model of Human Torso

where $\phi(\underline{r}, t)$ - electric potential at the observation point,
 $\underline{r}(r, \theta, z)$ - observation point vector,
 $\underline{r}_0(r_0, \theta_0, z_0)$ - source point vector,
 σ - conductivity of the volume conductor in mho/m,
 ϵ - permittivity of the volume conductor in Farad/m,
 μ - permeability of the volume conductor in Henry/m,
 ω - angular frequency of the signal emitted by the source, and the wave number K is defined by

$$K^2 = -j\omega\mu\sigma \quad 4.2a$$

$$\sigma_c = \sigma \left(1 + \frac{j\omega\epsilon}{\sigma}\right) \text{ complex conductivity} \quad 4.2b$$

Morse and Feschbach [45] define this potential as the retarded scalar potential such that a signal emitted at the retarded time t_0 by the source arrives at the observation point \underline{r} (see figure 4.3) at time t . An exact solution under these circumstances will be at least tedious if not downright impossible to simulate. To simplify situations, we start by assuming a stationary current source approximation of the myogenic sources.

The reduced equation is therefore

$$\nabla^2 \phi + K^2 \phi = \frac{-I}{\sigma + j\omega\epsilon} \quad 4.3$$

We assume this equation and use its solution to justify our approximation of the real system.

A solution of equation 4.3 in an infinite medium is

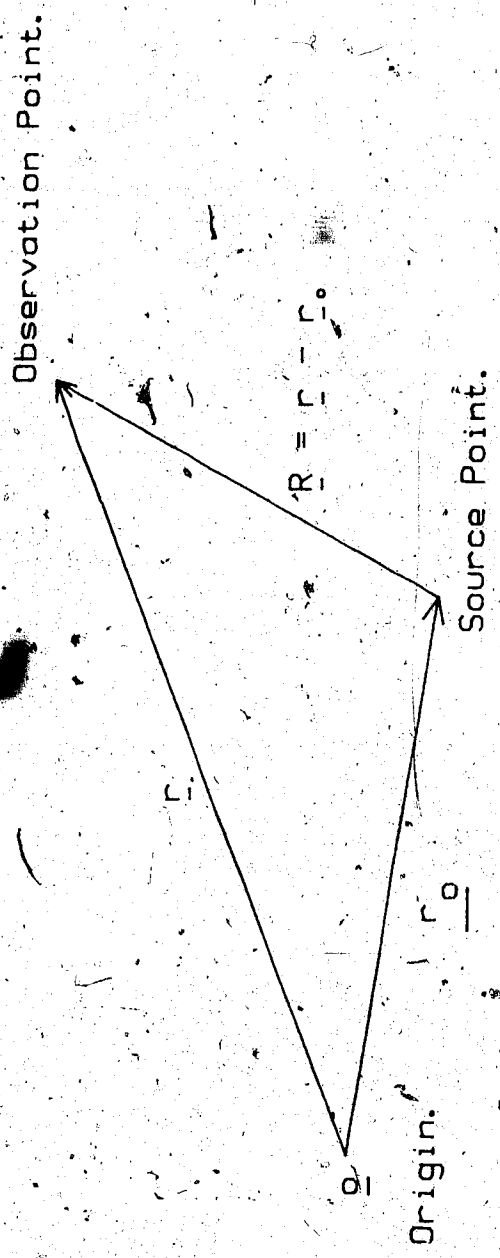


FIGURE 4.3
VECTOR DIAGRAM.

$$\phi_{\infty} = \frac{1}{4\pi\sigma c} \int_V \frac{I_{\text{ex}}}{R} e^{-jKR} dV \quad 4.4$$

where $R = |\underline{R}| = |\underline{r} - \underline{r}_0|$ and e^{-jKR} is the propagation delay.

As previously stated, the medium composed of the torso has both conductive and dielectric properties. If one is to take these properties into consideration, any change in the signal at a given point in time will take a finite time to register at far field. Since the system is nonisotropic, a single change in a field quantity may arrive at the same observation point with different time delays depending on the number of signal paths available. Therefore, the system is not synchronized in its temporal responses. The following consideration of equation 4.4 shows that in fact a synchronized system exists that is a good approximation of the real system.

First, we note that no magnetic materials exist in biological systems. Hence, it is reasonable to approximate the magnetic susceptibility of the torso by that of free space ($4\pi \times 10^7$ Henry/m).

It is also known that no significant signals exist in the biological system of interest above 1 KHz. In fact, in the gastrointestinal tract which is of interest here, cut-off at 10 Hz is reasonable. In an average human being $R_{\text{max}} = 1$ m. These extreme values are assumed in the following evaluation of the approximate system.

Plonsey [48] shows that the capacitive inductive and propagation effects can be neglected without a great loss in accuracy. These effects are neglected with the following arguments

a) Capacitive effect:

The limits of conductivity in man from table 4.1 is

$$0.04 \text{ mho/m} \leq \sigma \leq 0.67 \text{ mho/m}$$

(in fat) (in blood)

and the ratio of the displacement current to the conduction current is

$$\frac{\omega \epsilon}{\sigma} < 0.2 \text{ at } f = 10 \text{ Hz.}$$

TABLE 4.1

PHYSICAL PARAMETERS OF HUMAN TISSUES

Tissue	σ (mhos/m) (S. Rush et. al.)	$\frac{\omega \epsilon}{\sigma}$ at $f=10$ Hz. (Schwann and Kay)
Blood	0.67	-
Torso	0.21	-
Liver	0.14	0.2
Lung	0.5	0.15
Fatty Tissue	0.04	-
Heart Muscle	-	0.1

Therefore, an approximate system that does not take the displacement current into consideration can achieve 80% accuracy.

b) Propagation effect:

Phase propagation delay can be expanded into a power series as

$$e^{-jKR} = 1 - jKR - \frac{(KR)^2}{2!} - \frac{(KR)^3}{3!}$$

therefore for $KR \ll 1$, $e^{-jKR} \approx 1$. From equation 4.2,

$$KR_{\max} = 0.039 (1-j)$$

Hence, propagation effects can be neglected.

c) Inductive effect:

The vector electric field \underline{E} is a function of the scalar potential ϕ and the vector potential \underline{A} ;

$$\underline{E} = j\omega\underline{A} - \nabla\phi$$

Plonsey [48] showed that the ratio

$$\frac{|j\omega\underline{A}|}{|\nabla\phi|} = |KR|^2$$

Since propagation effects can be neglected implying that $|KR| < 1$, so can inductive effects.

The system, therefore is described by Poisson's equation

$$\nabla^2\phi = -\frac{I}{\sigma}$$

4.5

subject to the boundary conditions

- 1) ϕ is finite inside the volume, and
- 2) Neumann's boundary condition

$$\frac{\partial\phi}{\partial\underline{n}} \Big|_s = 0 \quad (\underline{n}, \text{ normal vector at the surface } s)$$

It is synchronized with respect to time for all field quantities and quasi static. This idea of the system being quasi static plays an important role in this simulation. Since transient effects can be ignored, it is easy to perform sampling in time and space. Sampling in time allows us to obtain the system solution at each sample instant and

by superposition simulate the time dependency of the system. A solution of equation 4.5 in infinite space is

$$\phi_{\infty} = \frac{I}{4\pi\sigma} \cdot \frac{1}{R} \quad 4.6$$

where

$$R^2 = \rho^2 + (z-z_0)^2, \quad \text{for } \rho^2 = r^2 + r_0^2 - 2r_0 \cos(\theta-\theta_0)$$

adding $\frac{1}{R}$ so that the expression converges for $r > r_0$ gives

$$\frac{1}{R} = \frac{2}{\pi} \int_0^{\infty} \cos \xi (z-z_0) K_0(\xi \rho) d\xi$$

(Gray and Mathews [31])

where

$$K_0(\xi \rho) = \sum_{m=0}^{\infty} \epsilon_m \cos m(\theta-\theta_0)$$

$$I_m(\xi r_0) K_m(\xi r), \quad r > r_0$$

$$I_m(\xi r) K_m(\xi r_0), \quad r < r_0$$

$$1, \quad m=0$$

and

$$2, \quad m \geq 1$$

I_m and K_m are the modified Bessel functions of order m of the first and second kind respectively.

Hence equation 4.7 becomes

$$\phi_{\infty} = \frac{1}{2\pi\sigma} \int_0^{\infty} I \cos \xi (z-z_0) \cdot \sum_{m=0}^{\infty} \epsilon_m \cos m(\theta-\theta_0) \cdot I_m(\xi r_0) \cdot K_m(\xi r) d\xi \quad 4.8$$

If we now replace the current source by a SD of dipole moment \underline{P} , the equivalent of equation 4.8 may be obtained by differentiating ϕ_∞ with respect to the direction of the dipole moment. By assuming a homogeneous conducting medium [7], we impose a linearity on the medium in all directions. The dipole moment may then be resolved into its r, θ and z components as

$$\underline{P} = P(P_r, P_\theta, P_z)^T$$

Hence, the surface potential is calculated as

$$\phi = \phi_r + \phi_\theta + \phi_z \quad 4.9$$

The solution for a single current dipole of dipole moment $\underline{P}(0,0,P_z)^T$ is obtained by differentiating 4.8 with respect to Z and replacing I with P_z . Therefore,

$$\phi_\infty = \frac{P_z}{2\pi^2\sigma} \int_0^\infty \xi \sin\xi(z-z_0) \sum_{m=0}^\infty \epsilon_m K_m(\xi r) \cdot I_m(\xi r_0) \cdot \cos m(\theta-\theta_0) d\xi$$

The finite volume solution can be obtained by the method of images [45]. Okada [47] obtained the same solution by inserting terms satisfying Laplace's equation and containing no poles within the boundary under the integral sign and then forcing the expression to satisfy $\frac{\partial\phi}{\partial r} \Big|_{r=A} = 0$ i.e.

$$\frac{\partial\phi}{\partial r} = \frac{\partial}{\partial r} \left[\frac{P_z}{2\pi^2\sigma} \int_0^\infty \xi \sin(z-z_0) \sum_{m=0}^\infty \epsilon_m [K_m(r\xi) + c_2 I_m(\xi r)] \right]$$

$$I_m(\xi r_0) \cos m(\theta - \theta_0) d\xi \Big|_{r=A} = 0$$

where $c_1 = I(h, \xi)$

$$c_2 = - \frac{K'_m(\xi A)}{I'_m(\xi A)}$$

The primes denote differentiation with respect to the argument.

By imposing the other boundary conditions $\frac{\partial \phi}{\partial z} \Big|_{z=0, h} = 0$, c_1 is evaluated to be a periodic impulse function of strength

$$\frac{2\pi}{h} \text{ at } \xi = \frac{n\pi}{h}; \quad n=0, 1, 2, \dots$$

therefore

$$\phi_z(z, \theta) \Big|_{r=A} = \frac{-2P}{\pi Ah \sigma} \sum_{n=0}^{\infty} \sin \frac{n\pi z_0}{h} \cos \frac{n\pi z}{h}$$

$$\sum_{m=0}^{\infty} \epsilon_m \frac{I_m\left(\frac{n\pi r_0}{h}\right) \cos m(\theta - \theta_0)}{I_{m-1}\left(\frac{n\pi A}{h}\right) + I_{m+1}\left(\frac{n\pi A}{h}\right)} \quad 4.10$$

Equation 4.10 is what we need to evaluate ϕ_z at the time and space sample points chosen for the z component of the SD,

In a similar manner, solutions can be obtained for ϕ_r and ϕ_θ as

$$\phi_r = \frac{2P_r}{\pi Ah \sigma} \sum_{n=0}^{\infty} \cos\left(\frac{n\pi z_0}{h}\right) \cos\left(\frac{n\pi z}{h}\right) \sum_{m=0}^{\infty} \epsilon_m 0.5 \frac{\{I_{m-1}\left(\frac{n\pi r_0}{h}\right) + I_{m+1}\left(\frac{n\pi r_0}{h}\right)\}}{I_{m-1}\left(\frac{n\pi A}{h}\right) + I_{m+1}\left(\frac{n\pi A}{h}\right)} \cos m(\theta - \theta_0) \quad 4.11$$

and

$$\phi_{\theta} = \frac{2P_{\theta}}{\pi Ah\sigma} \sum_{n=0}^{\infty} \cos\left(\frac{n\pi z_0}{h}\right) \cos\left(\frac{n\pi z}{h}\right) \\ \sum_{m=0}^{\infty} \epsilon_m^{0.5} \frac{\{I_{m-1}\left(\frac{n\pi r_0}{h}\right) - I_{m+1}\left(\frac{n\pi r_0}{h}\right)\}}{I_{m-1}\left(\frac{n\pi A}{h}\right) + I_{m+1}\left(\frac{n\pi A}{h}\right)} \sin m(\theta - \theta_0) \quad 4.12$$

SIMULATION

Savard et al. [46] suggested that the SD representation is not very accurate in describing migrating cardiac electrical activity because of the system's intrinsic multiple wavefronts. GEA, on the other hand, possess a single wavefront that normally migrates distally in the antrum. As a result of this and the strong electrical coupling in the antrum, we may represent the oscillating regions in the antrum by several discrete SDs $K = 1, 2, \dots, L$ spaced at $\frac{r_t}{L-1}$ cm apart; where r_t cm is the length of the antrum.

Figure 4.4 shows the tight electrical coupling in human antrum as recorded by the multisite electrode.

The average phase angles of antral electrical activity obtained in this study is $45.5^\circ/\text{cm}$.

Let the dipole moment at each oscillating region be defined by figure 4.5. The amplitude of the dipole moment was determined via the inverse volume conductor problem. This procedure is discussed in greater detail later in this chapter; and we shall not concern ourselves with the amplitude at this point. It is however important to define a figure of merit for the leading and trailing edges of the wave form. Let the leading slope be defined as $\left.\frac{dV}{dt}\right|_l$ mV/s and the trailing edge as $\left.\frac{dV}{dt}\right|_t$ mV/s. Also, let the ratio

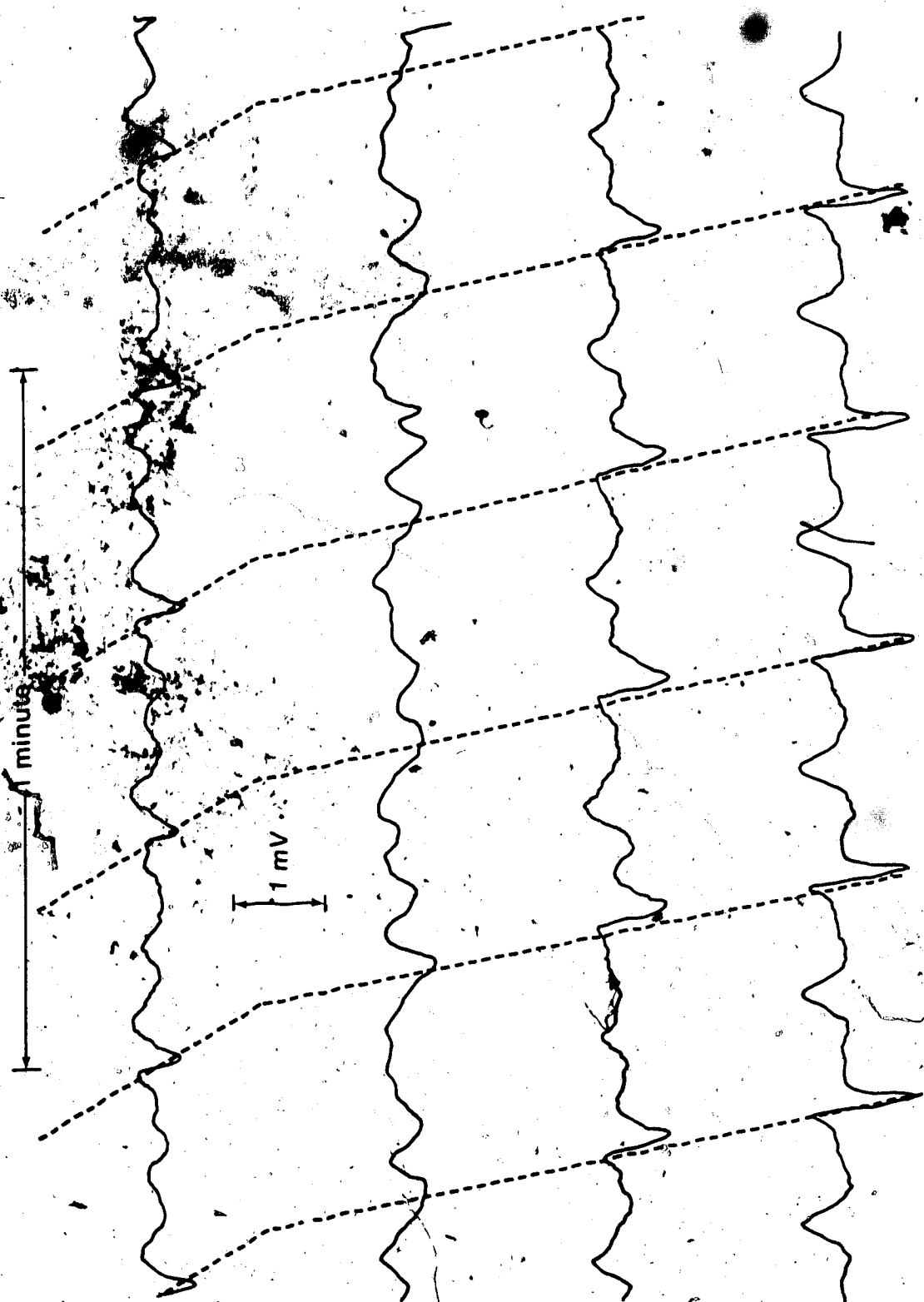
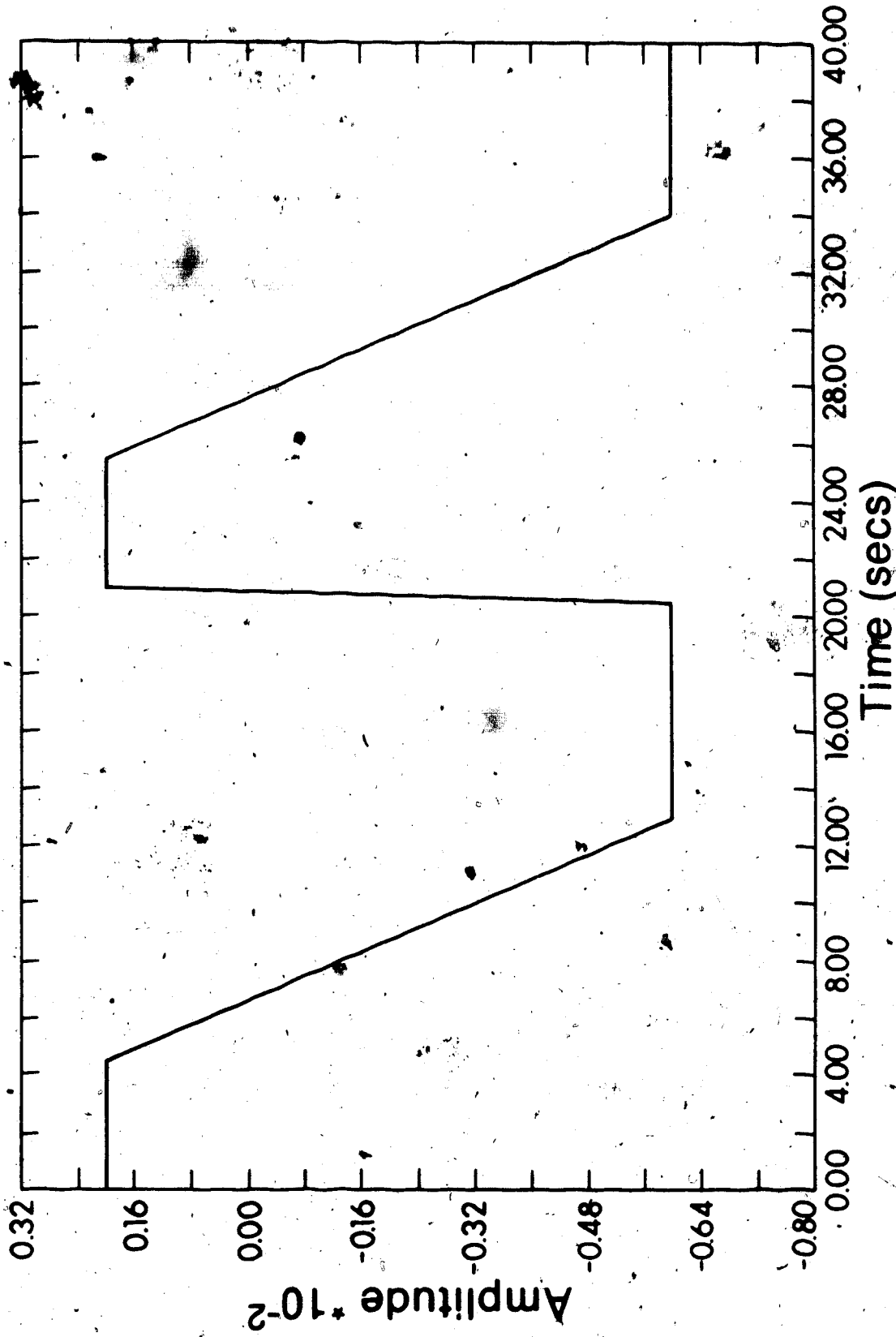


FIGURE 4-4 Coupling of GEA



Transmembrane Potential Approximation

FIGURE 4.5

$$\left| \frac{\frac{dV}{dt}|_1}{\frac{dV}{dt}|_t} \right| = \gamma$$

Previous investigators have reported values for some of these parameters.

In their intracellular work on gastric smooth muscle, El-Sharkawy et. al. [22] obtained $\frac{dV}{dt}|_1$ for canine and human antral ECA as 1400 ± 50 mV/s and 600 ± 700 mV/s respectively. They however, did not report values for $\frac{dV}{dt}|_t$. From their records, an estimate of $\frac{dV}{dt}|_t$ in human antral tissue is -29.69 mV/s and -38.14 mV/s in canine antral tissue. These imply that γ is 20.21 and 36.71 in human and canine antral tissue respectively. γ for the idealized ECA shown in figure 4.5 is 12.97.

Let each source function may be sampled at a rate $f_s = 1/T_s$ to produce the discrete dipole moment $P(1T_s)$, $1 = 0, 1, 2, \dots$. Let the propagation velocity of GEA in the antrum be v_0 . The effective dipole moment at the K^{th} oscillating region at the sample instant $1T_s$ is $P(1, T_s)$ where

$$1T_s + f_s(L-K), \text{ for forward propagation}$$

$i_K =$

4.13

$$1T_s + f_s(K-1), \text{ for retrograde propagation}$$

and the total antral length is

$$r_t = v_0 T = \frac{360^\circ}{\delta} \tag{4.14}$$

The potential on the skin at the $1T_s$ sample instant is thus

$$\phi(1T_s) = \sum_{K=1}^L \phi_z(1T_s) + \phi_r(1T_s) + \phi_\theta(1T_s) \tag{4.15}$$

For the SD representation to have a reasonable accuracy on a macro scale, the dipole moments P_r , P_z and P_θ and their position z_0 have to be optimized.

To pick these values; we revert to the inverse problem [4,38].

Nine electrodes are placed on a subject at known locations $p_j(A, z_j, \theta_j)$ $j=1,2,\dots,9$. One of these electrodes is designated as neutral and an 8 channel 30 minute record of GEA $y_j(t)$ $j=1,2,\dots,8$ is made. The same locations are then substituted into equations 4.10, 4.11 and 4.12 to obtain ϕ_j values according to equation 4.9, using an estimate of P_r , P_θ , P_z and Z_0 . The sum of the squared deviations $f_j = (y_j - \phi_j)^2$, $j=1,2,\dots,8$ are then minimized using a finite difference Levenberg-Marquardt algorithm routine. The best fit values so obtained for P_r , P_θ , P_z and Z_0 are the values used in the model defined by equations 4.10, 4.11, 4.12 and 4.15.

In this model we have assumed $\sigma = 0.2$ mho/m (Rush et. al. 1963 [50]), $v_0 = 0.5$ cm/sec and $T = 20.5$ secs. therefore $\delta = 34.29^\circ/\text{cm}$; all values typical of GEA.

RESULTS

Figure 4.6a and b show the wave shapes calculated at the same electrode position for forward and retrograde propagation of the SD in the model.

70

The following values were utilised in the model to calculate figures 4.6a and b with electrodes positioned at $M_1(A, 160^\circ, 0.3)$ and $M_2(A, 60^\circ, 0.292)$.

Parameters measured on the subject:

$$h = 0.6 \text{ m}, A = 0.13 \text{ m}.$$

Parameters of the model:

$$r_t = 0.105 \text{ m}, L = 22, T = 20.5 \text{ secs and } f_s = 2 \text{ Hz};$$

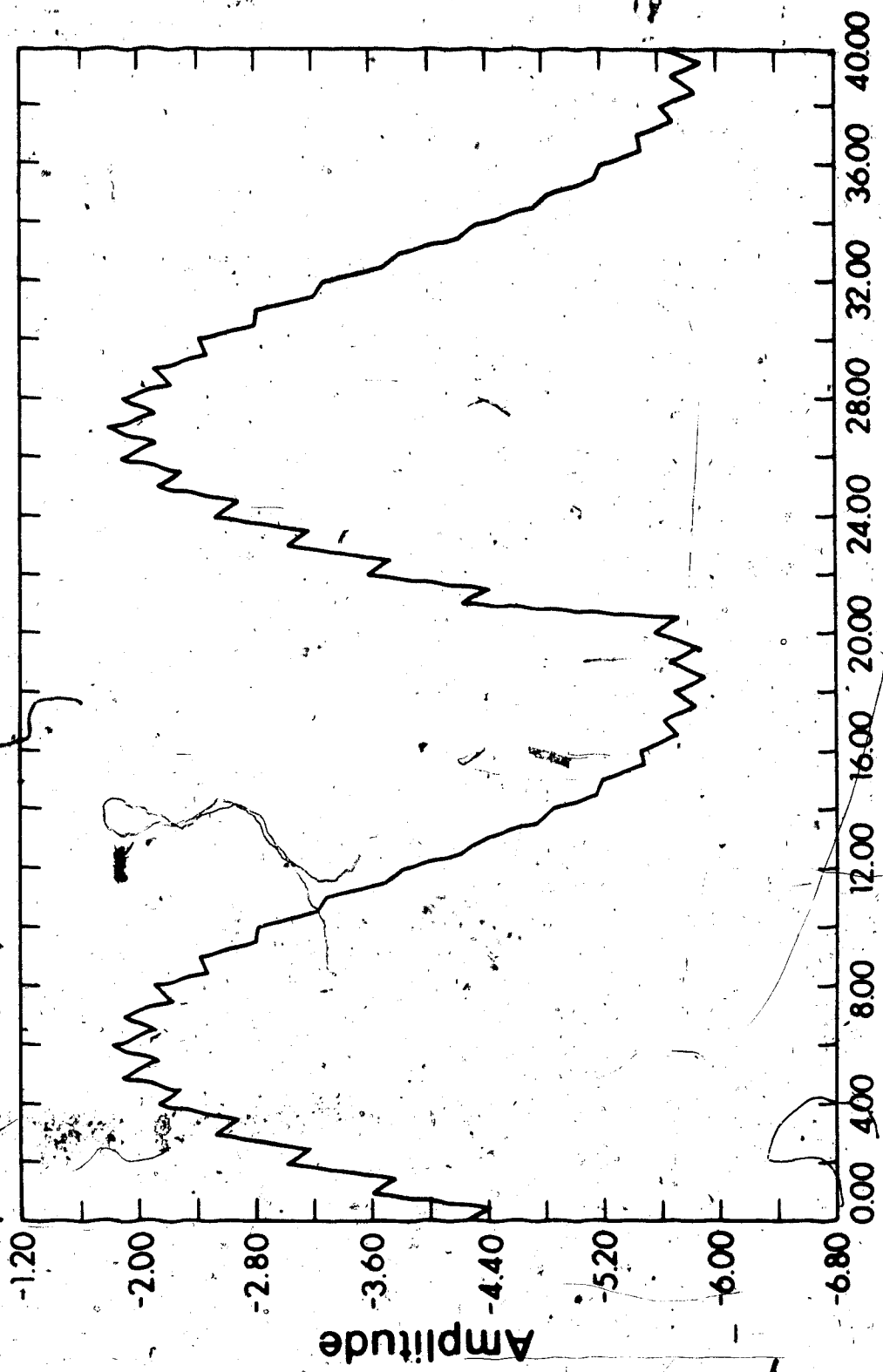
$$\underline{P} = (1.0736, -0.2379, -0.6921)^T * P(t) \text{ (P(t) is shown in figure 4.5) and } r_m = 0.285 \text{ m}.$$

$$n = 0, 1, \dots, 6, m = 0, 1, \dots, 6$$

Perhaps the most important information gathered from the simulated waveforms is the fact that the rising slope of the signal in figure 4.6a (forward propagation) is steeper than the slope of the trailing edge. Figure 4.6b (retrograde propagation) shows the converse - the slope of the trailing edge of the signal is steeper than that of the leading edge.

The figure of merit γ for the calculated EGG in figure 4.6a is 2.4 and 0.47 for figure 4.6b. Hence, the slope ratio γ is greater than 1 for EGGs calculated for forward propagation and lesser than 1 for retrograde propagation.

Extracorporeal measurements of GEA were made for comparison. The measurements were made with two ordinary ECG electrodes positioned approximately above and lined up with the antral axis of the subjects stomach according to the method reported by Mirrizi and Scafoglieri [43]. The subject was then allowed to lie supine for the duration of the recording (30 to 45 minutes).



Time (secs) Simulated Electrograms

FIGURE 4-6 a

Forward Propagation



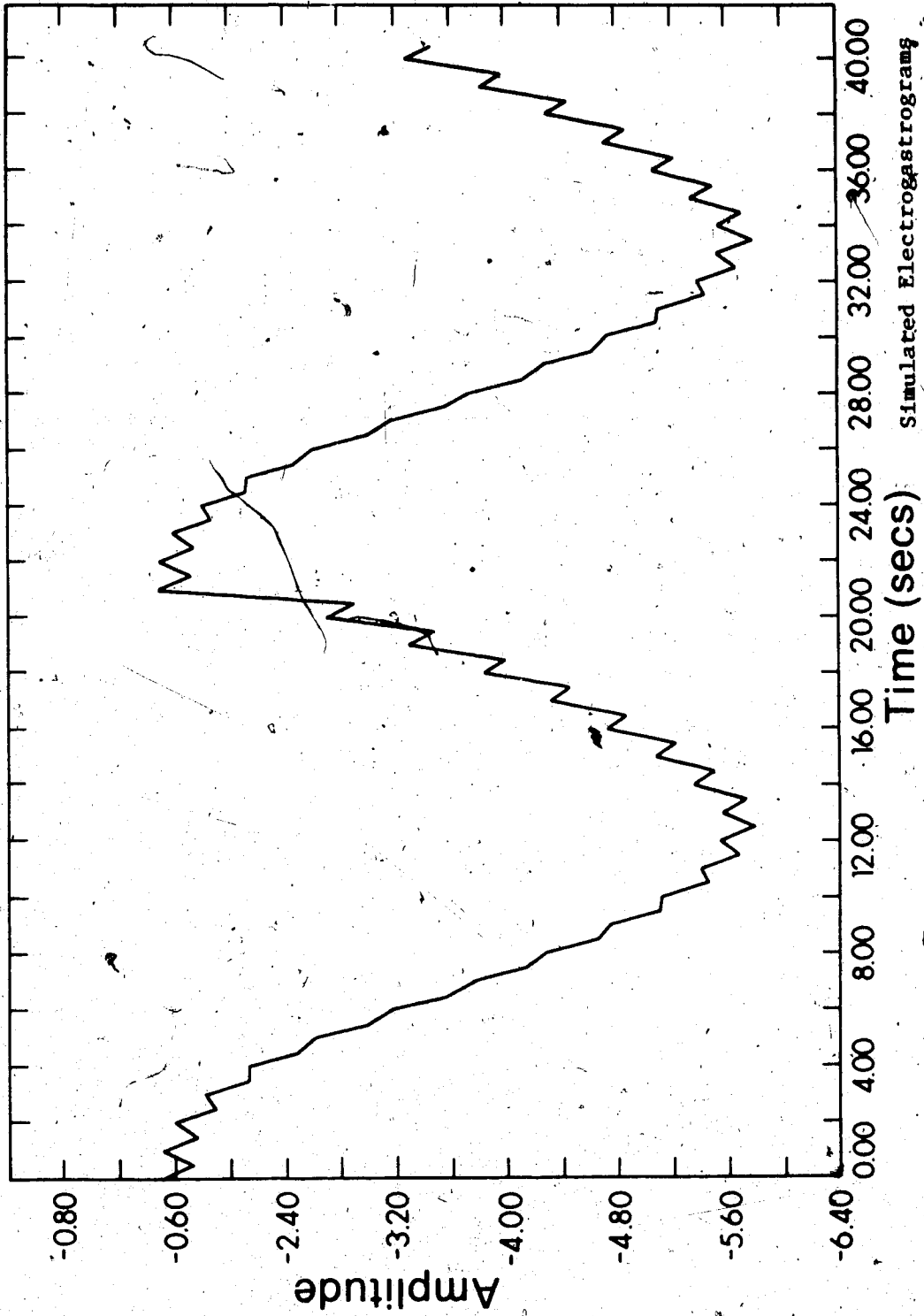


FIGURE 4.6b
Retrograde Propagation
Simulated Electrograms

In 26 out of 28 channels on 28 healthy volunteers and in 10 out of 12 channels on 4 patients, excellent records of the transcutaneous GEA were obtained.

Figure 4.7a shows a human EGG recorded in a male with no known gastric disorders with the neutral electrode M_2 in the region above the distal antrum and M_1 in the region above the proximal antrum as in figure 4.1. The rising edge of the signal is steeper than the falling edge. Using figures 4.6a and b as reference, one concludes that the antral electrical activity in the subject of figure 4.7a propagates in the forward direction.

To simulate reverse propagation, the relative positions of the electrodes were reversed to record figure 4.7b in a subject with no known gastric disorders. Since the relative slope of the edges of the signal are similar to that in figure 4.6b, one might conclude that propagation in this case is orad. However, the order of the electrodes were reversed for the measurement. Hence, propagation of antral electrical activity in this subject is also aborad.

GEA was monitored in a total of 17 subjects with the electrode M_2 distal to M_1 along the projection of the antral axis on the stomach. The mean value of $\frac{dV}{dt}|_1$ was 46.09 ± 29.53 mV/s and the mean value of $\frac{dV}{dt}|_t$ was -14.47 ± 9.49 . These parameters were evaluated only on slow wave cycles that were reasonably free of ECG, respiratory and motion artifacts. The average value of γ obtained was 3.4 ± 1.93 .

A total of 11 records were made with the relative position of M_1 and M_2 reversed as described for figure 4.6b and 4.7b. The values of $\frac{dV}{dt}|_1$, $\frac{dV}{dt}|_t$ and γ obtained in these experiments were 14.95 ± 4.98 mV/s, -34.62 ± 16.19 mV/s and 0.47 ± 0.15 respectively. These results

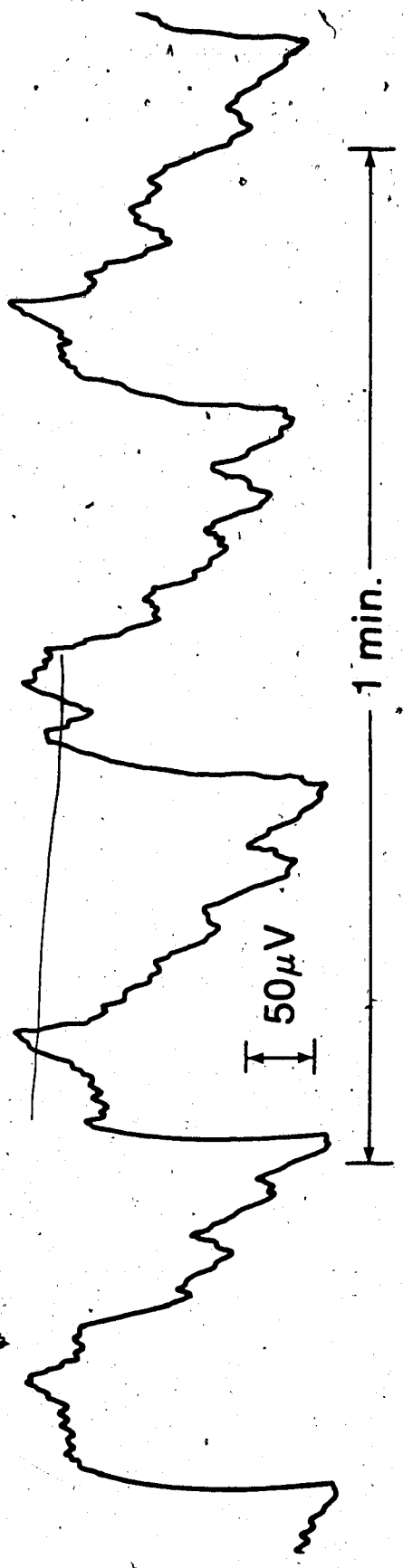


Figure 4-7a

Measured Electrogastrograms
M₁ and M₂ as in Figure 4.1

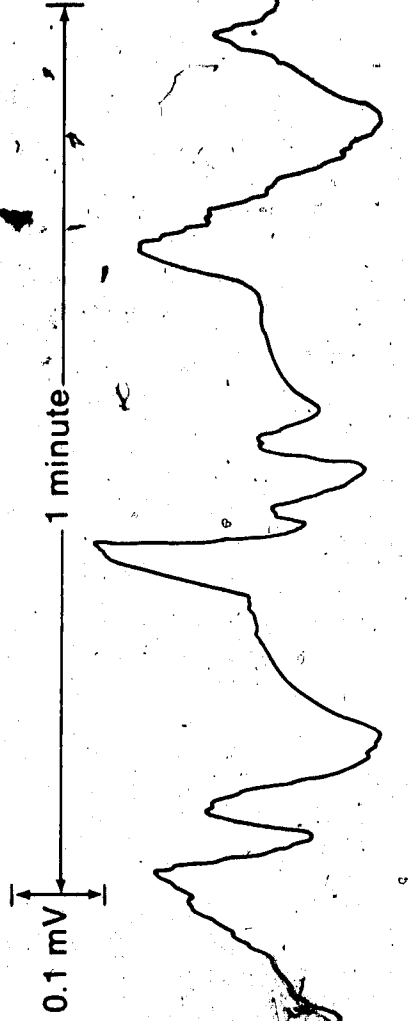


Figure 4.7 b

Measured Electrograms

M₁ and M₂ Reversed

Table 4.2

SLOPE PARAMETERS OF GEA

	Subjects	Successes	$\frac{dV}{dt} _t$ (mV/s)	$\frac{dV}{dt} _t$ (mV/s)	γ
From El-Sharkawy et.al.[21]	-	-	600±700	-29.69*	20.21*
Transmembrane Potential (Fig.4.5)	-	-	0.012†	-0.001†	12.97
From Model					
EGG; M ₁ -M ₂ (Fig.4.6a)	-	-	0.825†	-0.344†	2.4
EGG; M ₂ -M ₁ (Fig.4.6b)	-	-	0.236†	-0.502†	0.47
From Experiments					
EGG; M ₁ -M ₂	17	16	46.09±29.53	-14.47±9.49	3.40±1.93
EGG; M ₂ -M ₁	11	10	14.95±4.98	-34.62±16.19	0.47±0.15

*These values were not calculated by El-Sharkawy et.al. in their study [22]. These estimates were made from their results.

†Relative units/S.

are presented in table 4.2.

4.2 ELECTRICAL BIOIMPEDANCE

The basic idea of electrical impedance plethysmography is that of a source that generates energy waves which are made to interact with the internal organs. The result of such interactions are measured and interpreted to extract information regarding the changes of interest in the living body. Sources of energy that have been used in this manner include X-rays and radioisotopes in X-ray imaging and fluoroscopy, ultrasound in ultrasound imaging, and microwaves [61] and electrical energy in impedance plethysmography [42,44].

In this particular study, electrical impedance has a definite advantage over the rest. It permits simultaneous measurement of the electrical and contractile activities of the torso without the sophisticated instrumentation of the other techniques.

The method was first developed by J. Nyboer in 1940 [46] to monitor variations in thoracic impedance as a measure of cardiac output. It has since been used in

- a) monitoring cardiac output and flowrate,
- b) monitoring pulse volume and blood flow in the clinical evaluation of vascular effects in arteriography,
- c) vertebral artery studies in the clinical evaluation of vertigo patients,
- d) diagnosis of peripheral vascular diseases,
- e) studying blood perfusion in organs and tissues,
- f) respiration rate and lung volume measurement in pneumography and more recently,

g) in the monitoring of gastric emptying [25,42].

Electrical impedance plethysmography is superior to other plethysmographic techniques (strain gauge and air) because its application is not limited by the shape of the segment of interest.

The whole basis of the method is Ohm's law

$$V = IZ$$

where V volts is the potential drop across a segment whose electrical impedance is Z ohms when the impressed current is I amperes.

There are two electrode configurations that are generally employed:- the bipolar and the tetra polar electrode configurations. The tetra polar electrode configuration has the advantage of eliminating the dependency of the system's performance on the skin-to-electrode contact impedance.

Consider the volume conductor shown in figure 4.8 in a tetrapolar electrode configuration scheme. If a current I_{AB} is impressed at time t at the terminals A and B, let the resulting current density be J_1 , the resulting potential distribution throughout the volume be ϕ_1 and the conductivity g_1 . At the same time t , let the corresponding parameters at electrodes C and D be J_2 , ϕ_2 and g_2 . The divergence theorem states that

$$\int_V \nabla \cdot A \, dv = \int_S A \cdot ds \quad 4.16$$

If A is replaced by $\phi_2 J_1$ in equation 4.16, equation 4.17 results

$$\int_V \nabla \cdot (\phi_2 J_1) \, dv = \int_V \phi_2 (\nabla \cdot J_1) + J_1 \cdot \nabla \phi_2 \, dv = \int_S \phi_2 J_1 \cdot ds \quad 4.17$$

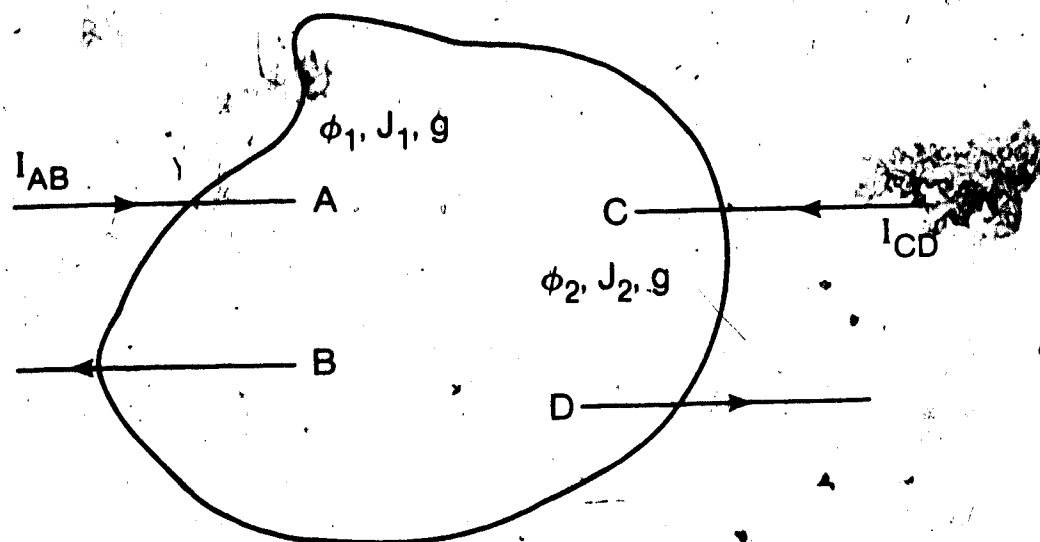


Figure 4.8. Volume Conductor with a tetrapolar electrode configuration

Since there are no current sources within the volume $\nabla \cdot J_1 = 0$ and

$$\int_V J_1 \cdot \nabla \phi_2 dv = \int_S \phi_2 J_1 \cdot ds \quad 4.18a$$

In the same way

$$\int_V J_2 \cdot \nabla \phi_1 = \int_S \phi_1 J_2 \cdot ds \quad 4.18b$$

From 4.18a and b one obtains

$$\int_V (g_2 - g_1) \nabla \phi_1 \cdot \nabla \phi_2 dv = \int_S (\phi_2 J_1 - \phi_1 J_2) \cdot ds \quad 4.19$$

now $g_2 = g_1 = g$

Therefore

$$\int_S (\phi_2 J_1 - \phi_1 J_2) \cdot ds = 0 \quad 4.20$$

Equation 4.20 is essentially a statement of the reciprocity theorem.

By considering a different time t' at electrodes A and B, Lehr [41]

showed that

$$\int_V -\Delta g (\nabla \phi_1' \cdot \nabla \phi_2) dv = -\Delta \phi_{CD} (-I_{CD}) \quad 4.21$$

where $\Delta g = g - g'$ and $\Delta \phi_{CD} = \phi_2 - \phi_2'$.

Dividing both sides of equation 4.21 by $I_{AB} \cdot I_{CD}$ gives

$$-\int_V \Delta g \cdot \frac{\nabla \phi_1'}{I_{AB}} \cdot \frac{\nabla \phi_2}{I_{CD}} dv = \frac{\Delta \phi_{CD}}{I_{CD}} = \frac{\Delta \phi}{\Delta a} \quad 4.22$$

Equation 4.22 known as Geselowitz's equation [28] essentially states that the impedance change, z within the volume conductor is proportional to the change in potential $\Delta\phi_{CD}$ at the measuring electrodes CD when the current is kept constant. This is the basis of the application of the electrical impedance technique.

4.2A DESIGN OF THE GASTRIC IMPEDANCE MONITOR

Gastric impedance, like all bioimpedance is composed of two parts, namely: a basal impedance, Z_0 and a time varying component, $Z(t)$. The basal impedance is typically about 1000 times or more the value of the time varying component. Even though the basal impedance is labelled as the DC component, it is worth noting that its value does drift with time in such a manner that it might play havoc with the proper functioning of an impedance monitor if it is not paid due attention in the design of the equipment.

The major components of the instrument are the power supply, the oscillator and current source, the voltage sensing amplifiers, the synchronous detector and the output circuit. A block diagram of the arrangement is shown in figure 4.9. A brief description of the system follows.

A constant current of between 0 and 2 mA rms at 100 KHz is supplied to the current electrodes I_1 and I_2 from a stable amplitude sine wave oscillator through a constant current source. A second pair of electrodes M_1 , M_2 monitors the potential difference on the torso. The input stage of the device is tuned to the oscillation frequency f_0 . This signal is amplified and detected synchronously with the carrier to give $Z_0 + Z(t)$.

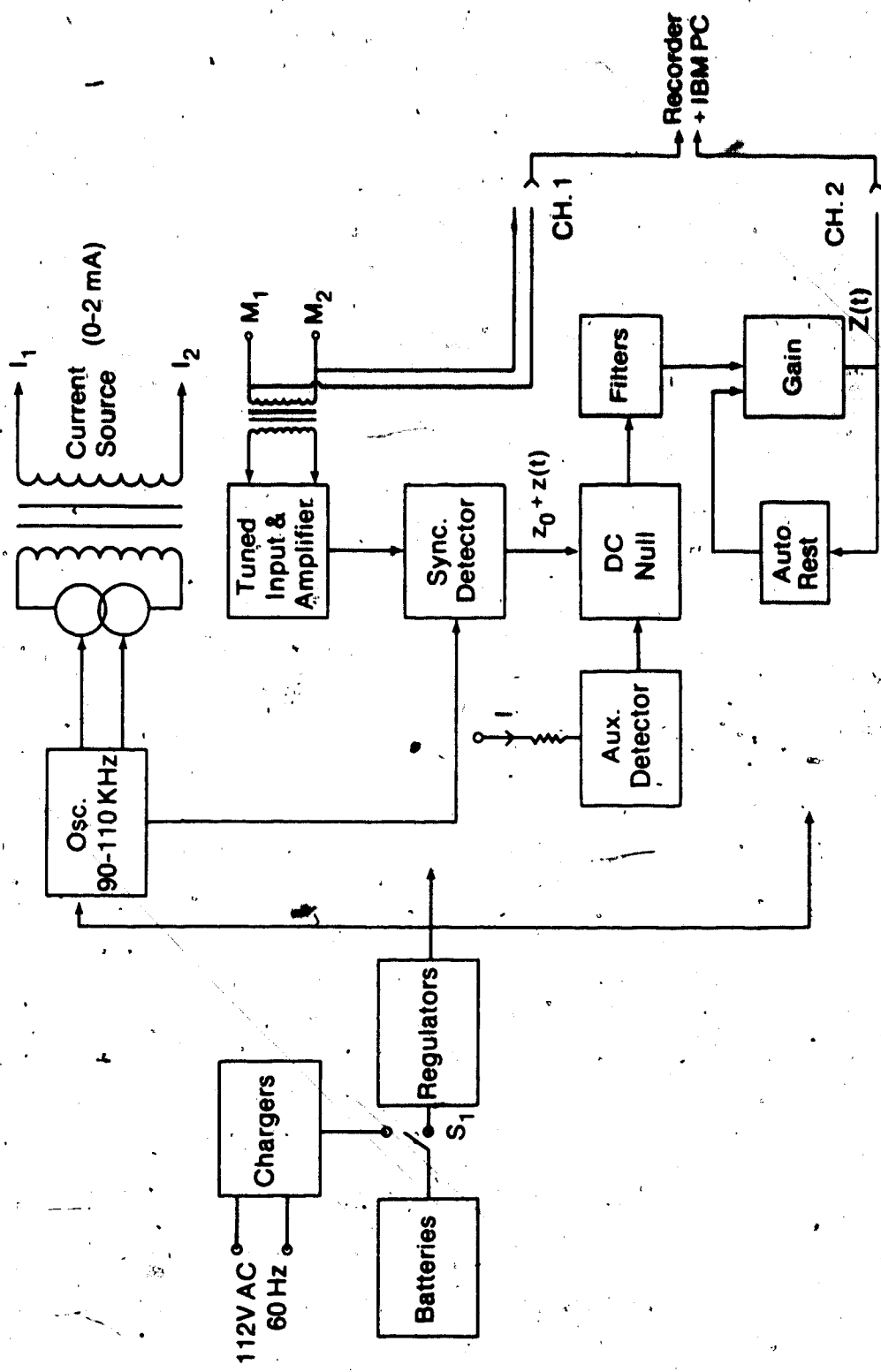


Figure 4.9 Schematic Diagram of the Impedance Monitor

The basal impedance Z_0 is nulled out by a DC level derived from the current source and an auxiliary demodulator that is identical to the one producing $Z_0 + Z(t)$. This arrangement ensures that any drifts in the demodulated signal due to amplitude drifts in the oscillator and/or current source is eliminated alongside Z_0 .

At this juncture, it is useful to remember that $Z(t)$ comprises of impedance variations due to

- 1) blood flow in the region under the electrodes,
- 2) volume variations due to respiration,
- 3) gastric contractile activity, and
- 4) motion artifacts.

The first two are eliminated by low pass filtering at 15 cpm. Motion artifacts can be reduced by ensuring that the subject remains as still as possible during the course of the measurement. What is left is a signal that is proportional to gastric contractile activity. This signal is amplified by an automatic gain control (AGC) section and sent to the recording devices.

OSCILLATOR AND CURRENT SOURCE:

The oscillator is a Wien bridge sine wave generator. The circuit will oscillate at that frequency f_0 where the phase of the signal at the output of A1 equals that at A2. This frequency is given by

$$f_0 = 2\pi(R_1.R_2.C_1.C_2)^{-0.5} \quad 4.23$$

Oscillation will be sustained if the positive feedback through R_1 , R_2 , C_1 and C_2 is exactly equal to the forward gain. This is satisfied if $R_2=R_3=R_4=R_5$ and $C_1=C_2$; in practice, $R_3 = 1.1R_2$, R_4 and R_5 . In this

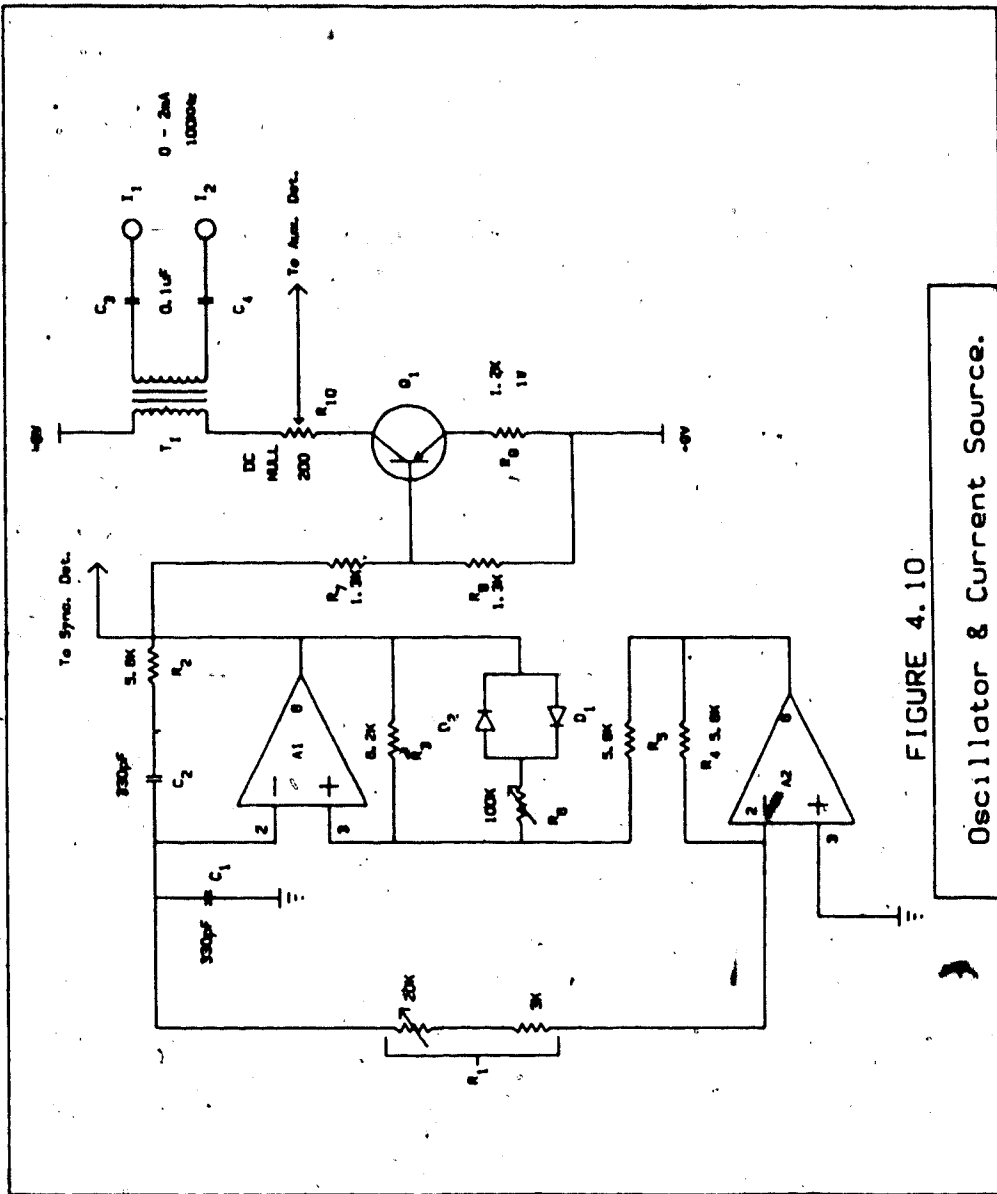


FIGURE 4.10
Oscillator & Current Source.

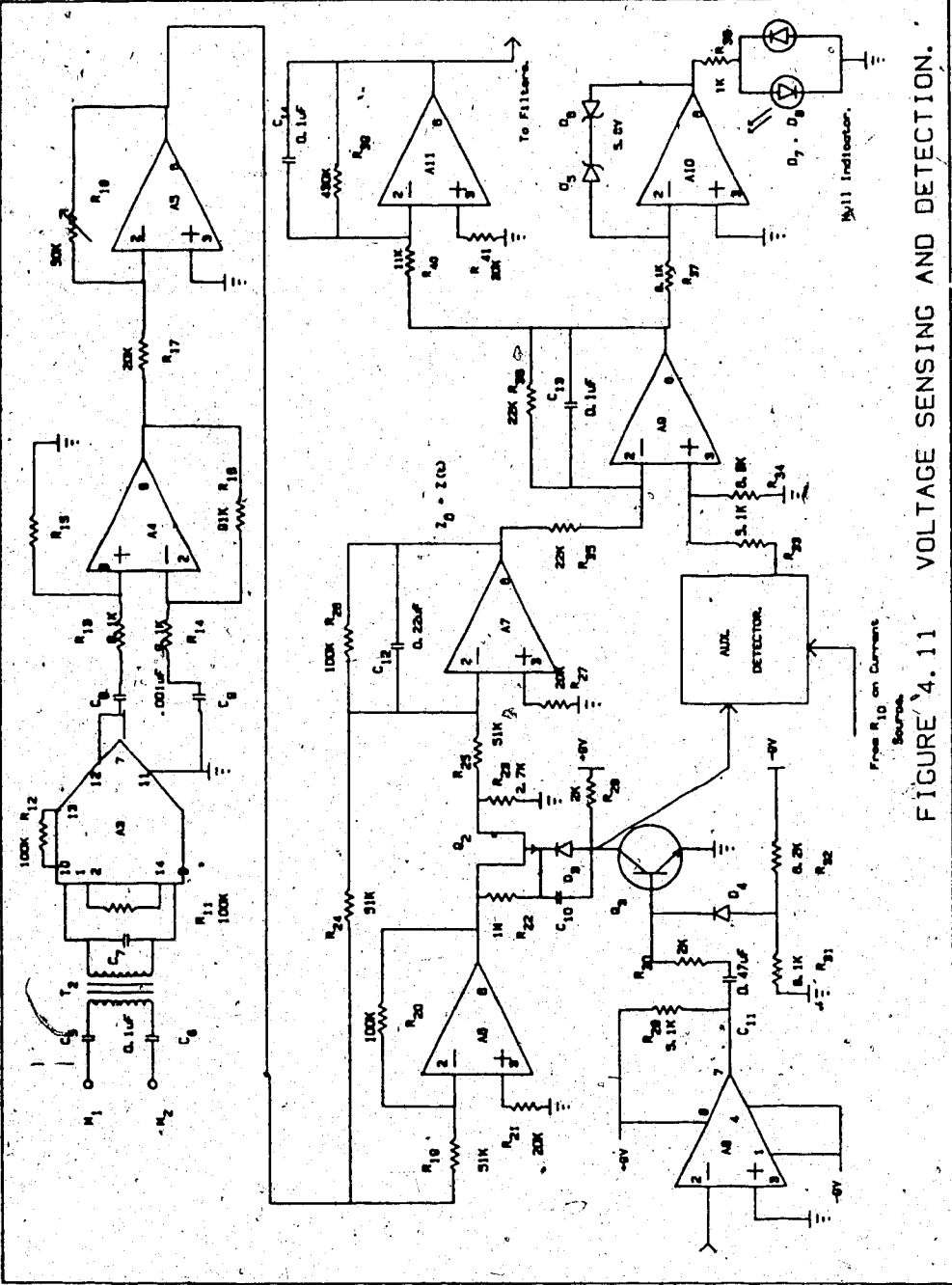


FIGURE 4.11 VOLTAGE SENSING AND DETECTION.

From R₁₀ on Current Source.

design the frequency can be varied from 90 KHz to 110 KHz with the 20K pot included in R1. See figure 4.10.

The collector current of the transistor T1 is transformer coupled to the current electrodes. The transformer provides patient isolation and load matching. The current is variable from zero to 5mA rms by adjusting pots R6 and R10.

VOLTAGE SENSING AND DETECTION

The input stage comprises of a transformer T2 and an instrumentation amplifier, A3. The transformer T2 and the capacitor C7 form a tuned stage rejecting signals outside of the 90KHz to 110KHz operating band. A4 and A5 provide further gain and amplitude control through R18. A6, A7, A8 and Q2 and Q3 constitute the detector.

The oscillator's output is fed to the comparator A8 which drives an NPN transistor (Q3). The collector of Q3 provides the gating signal to the P-channel FET switches Q2 and Q2' (in the auxiliary detector).

For proper operation of the detector, the overall gain of the half wave rectified signal through A6, Q2 and A7 should be twice that of the gain of the input signal through A7. That is

$$\frac{R20}{R19} \cdot \frac{R26}{R25} = 2 \cdot \frac{R26}{R24}$$

The sum of the two signals at A7 is a full wave rectified signal that is filtered by R26 and C12 to give $Z_0 + Z(t)$. Z_0 is nulled out by adjusting the amplitude of the input into the auxiliary detector. Balanced condition is indicated when both the yellow and red LEDs, D7 and D8 are reduced to a dull glow or turn on and off alternately.

A12 to A15 provide a 2-stage 2nd order low pass filtering at 15

cpm and a 2-stage 2nd order high pass filtering at 0.1 cpm.

It is important to note that this bank of filters coupled with the AGC cause a delay of a few seconds in the output. An estimate of this delay is made in section A.1.

A16 to A20 provide further gain and AGC of the signal. If the signal at the output gets larger than a level determined by the 1M pot R58, the signal fed back to the comparators A19 and A20 cause the FET switch Q4 to turn on and thereby turning on the integrator A17. A17 continues to integrate until the output falls below the threshold value. R62 and C26 reset the integrator.

POWER SUPPLY

The power supply scheme is shown in figures 4.14 to 4.16. Power is derived from two ELPOWER gel type 12V, 2.6AH batteries. When switch S1 is in the ON position, the batteries are connected across the terminals of the voltage regulators, A21 and A22 which supply the +9V and -9V rails. The emf of the batteries are continuously monitored by the battery level indicator which turns LED D21 on if either of the emfs fall below a threshold level set by the zener diodes D15 and D16 and the potential dividers R69, R72 and R73, R76. Note that in this position, the mains input terminals are interrupted by S1.

To charge the batteries, S1 has to be in the Charge position and the 112V receptacle connected to a mains outlet. The charging circuit (figure 4.16) is a float type charger. It provides the manufacturer specified charging current when the battery is low and maintains a float current when the battery is fully charged.

Two units of the gastric impedance monitor were constructed -

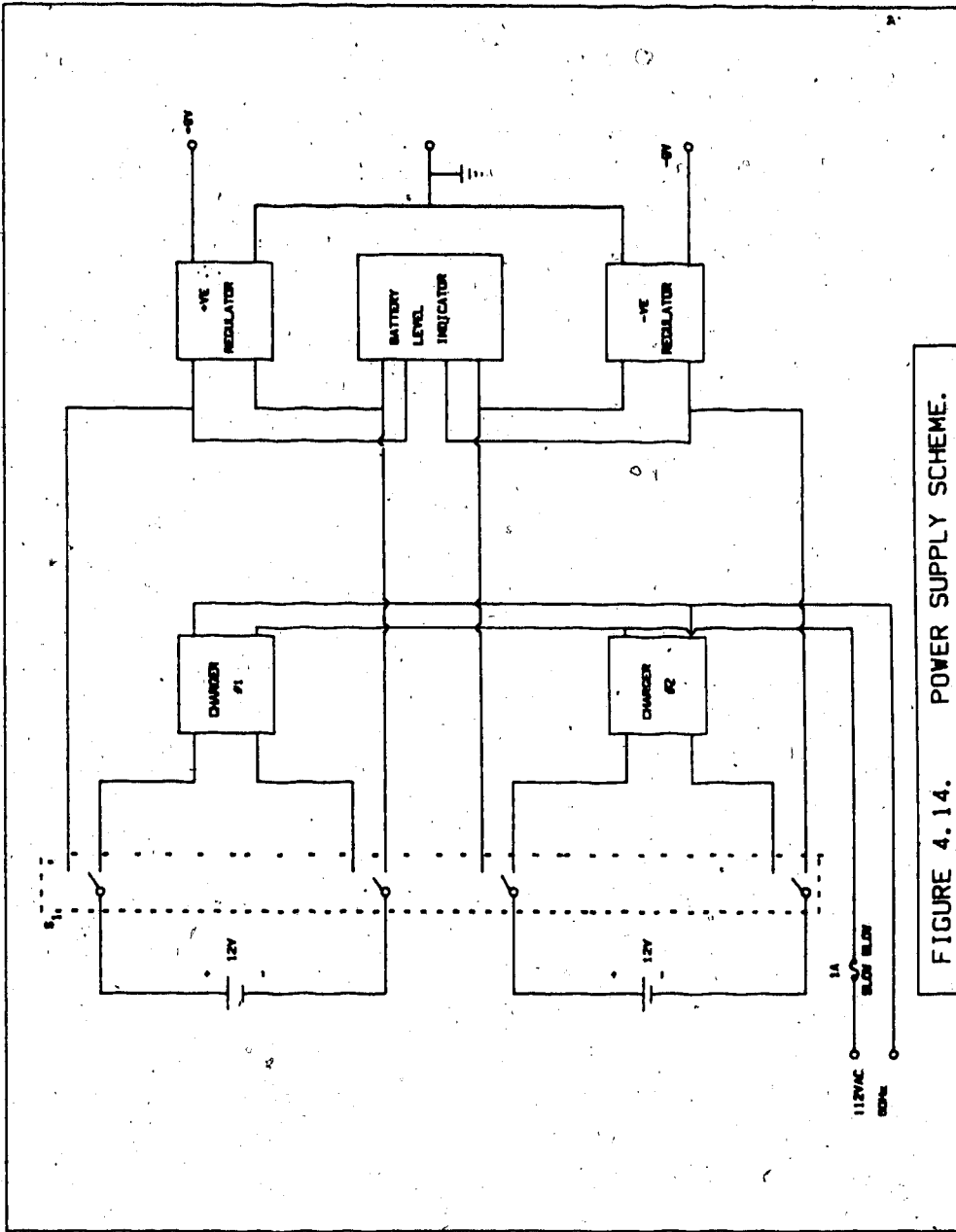


FIGURE 4.14. POWER SUPPLY SCHEME.

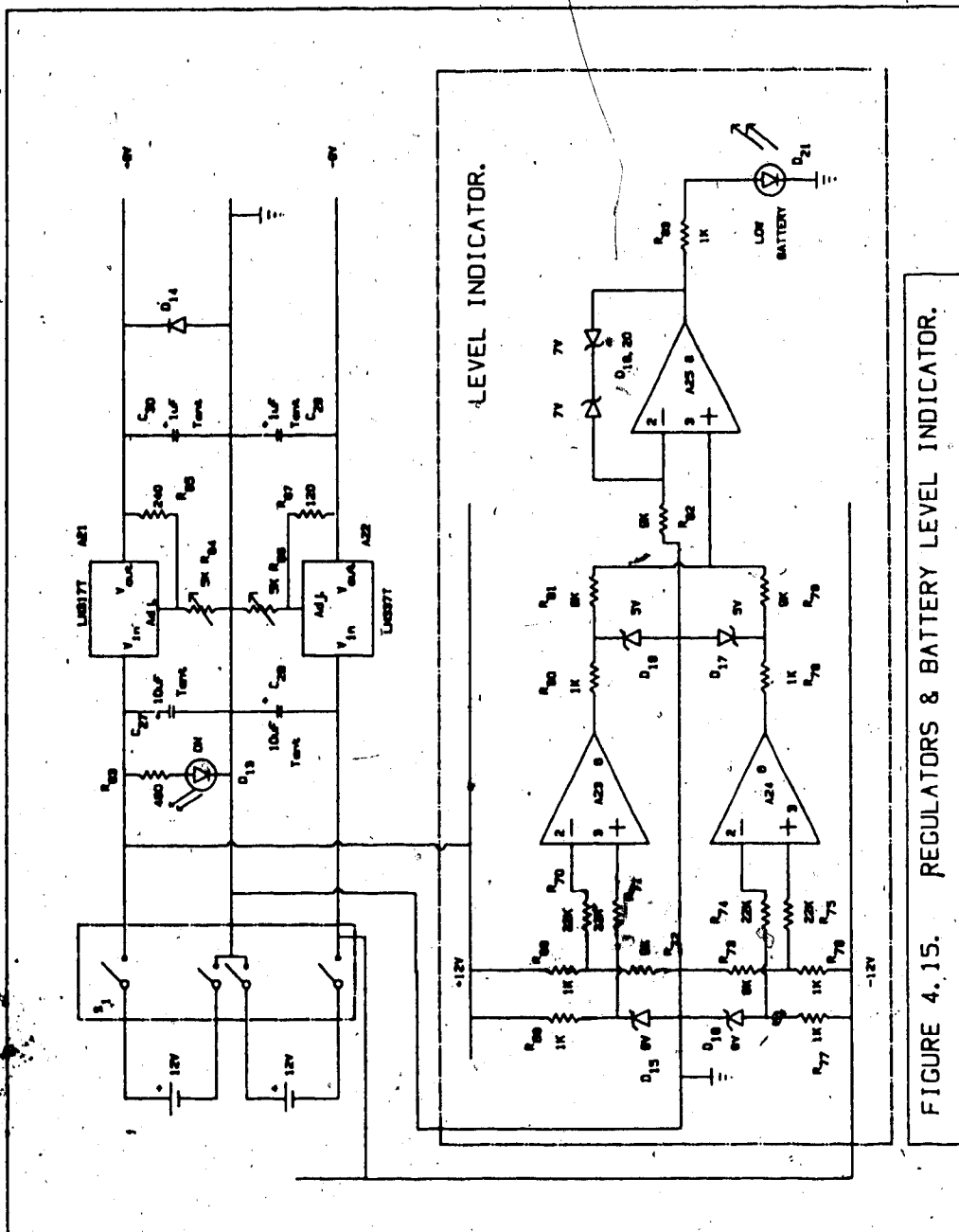


FIGURE 4.15. REGULATORS & BATTERY LEVEL INDICATOR.

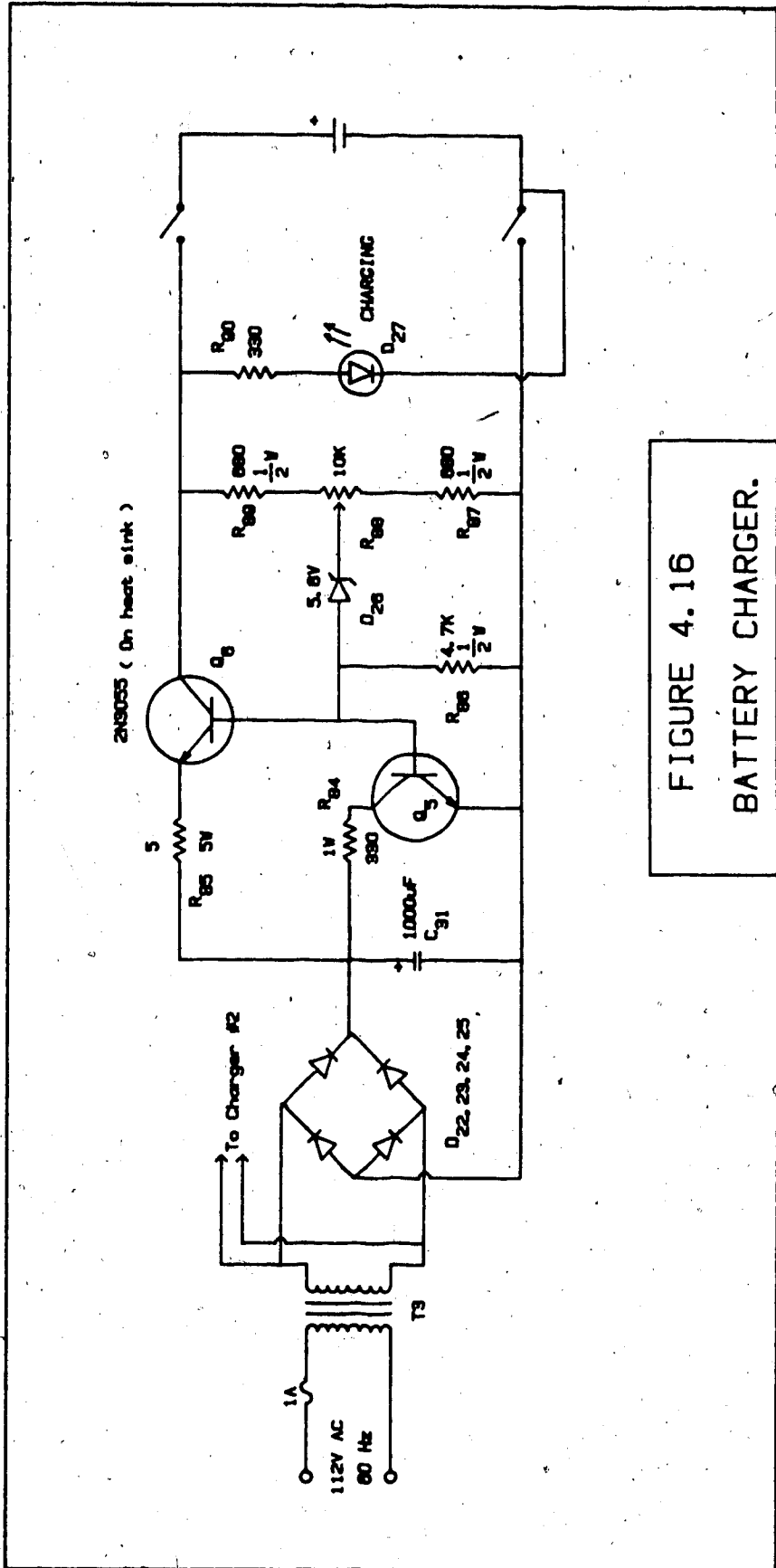


FIGURE 4.16
BATTERY CHARGER.

model #GIM1, serial #001 and model #GIM2, serial #002. Both units are certified by the Canadian Standards Association, the Alberta Electrical Protection Branch and the University of Alberta Hospital as a risk class 2 patient monitoring device (CSA file #A34-893-E1).

See appendix A for further details and the parts list.

5. IN VIVO MEASUREMENT IN HUMANS

5.1 SIMULTANEOUS NONINVASIVE MEASUREMENT OF GASTRIC ELECTRICAL AND CONTRACTILE ACTIVITY

To obtain information regarding gastric contractile activity, the impedance variations in the region above the stomach is simultaneously recorded with GEA.

METHODS

Four disposable Hewlett Packard electrocardiography (ECG) electrodes (type 14445C) are placed on the subjects torso just above the gastric antrum as shown in figure 4.1. A 2 mA rms 100 KHz current is injected into the skin above the stomach via the two outer ECG electrodes. The current is supplied from the battery operated constant current source that is transformer coupled to the electrodes. See section 4.2A. The other pair of ECG electrodes is used to record the potential drop on the skin. This potential drop has the following components:

- 1) GEA
- 2) $A(t)\cos\omega t$, where $\omega=2\pi(10^5)$ Rad/sec and $A(t)$ depends on (amongst others) the contractile state of the antrum.
- 3) ECG

The potential seen at the monitoring electrodes M_1, M_2 is processed as follows.

a) Low pass filtering at a cut off frequency of 0.159 Hz yields the GEA. This reduces ECG and respiratory artifacts without removing possible incidences of tachygastria.

b) The 100 KHz signal is synchronously demodulated to obtain the basal impedance Z_0 and the time varying impedance $Z(t)$. The basal

impedance is nulled out by adjusting the NULL knob on the Gastric Impedance Monitor.

Both the GEA and $Z(t)$ are sampled at a rate of 2 Hz and digitized on an IBM AT personal computer through a Lab Master^R 200009 12 bit, 8 channel A-to-D converter manufactured by Scientific Solutions Inc. The two channels are analysed on the IBM and an Amdahl 470/V7 main frame computer. Three dimensional power spectra are generated and crosscorrelation analysis is performed.

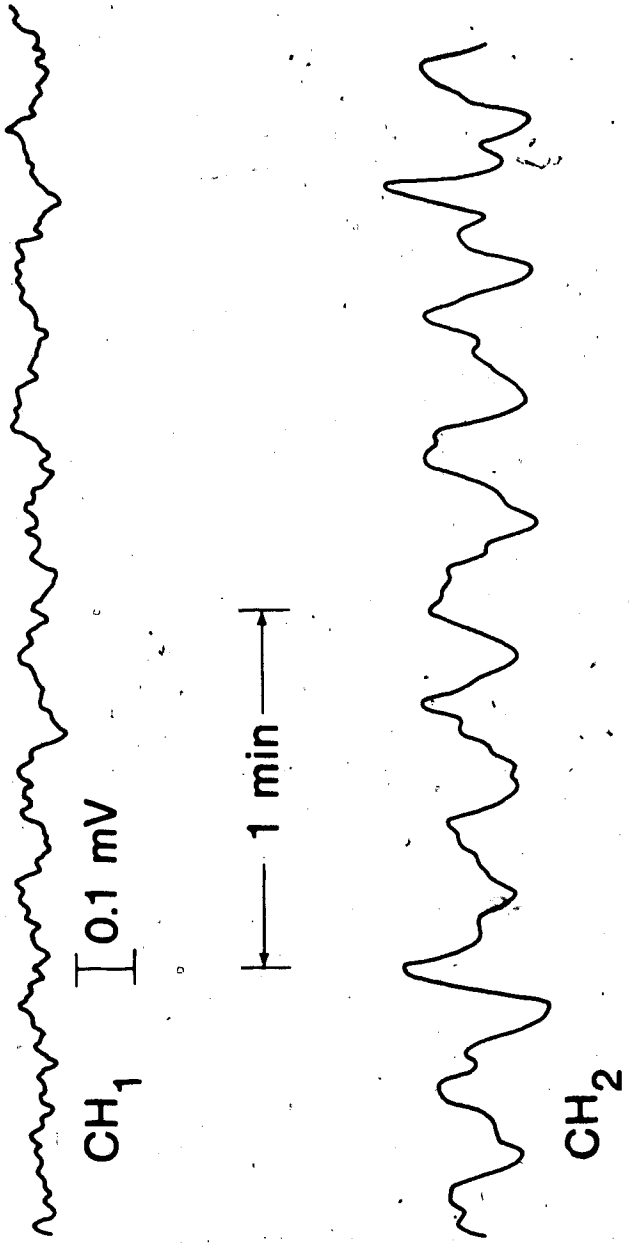
RESULTS

In 25 out of 27 channels on 27 healthy volunteers and in 10 out of 12 channels on 4 patients, excellent records of the transcutaneous GEA were obtained.

In 21 out of 27 healthy volunteers and in 1 out of 2 patients, good records of the impedance signal were obtained. These results are tabulated in table 5.1. A record is presumed "good" if GEA can be detected by visual inspection in 50% of the time constituting the total recording duration. Examples are shown in figures 5.1a and b. Figures 5.1a and b show strong phasic contractions (CH2) accompany each cycle of the ECA (CH1). This and the fact that both records were made in fasted subjects suggest that the records were excerpts from the phase III of a migrating motor complex (MMC) [60]

In figure 5.1b, the phase shift between channels 1 and 2 is clearly not zero. This is because the impedance signal is delayed an average of 10.55 ± 3.39 seconds.

The electrical activity is recorded at an average frequency of 2.9 ± 0.22 cpm about 78.75% of the time and the impedance signal at the same frequency occurs only during part of the time depending on the



CH #1 - Electrogram
CH #2 - Impedance Signal (Relative Units)

Figure 5.1a

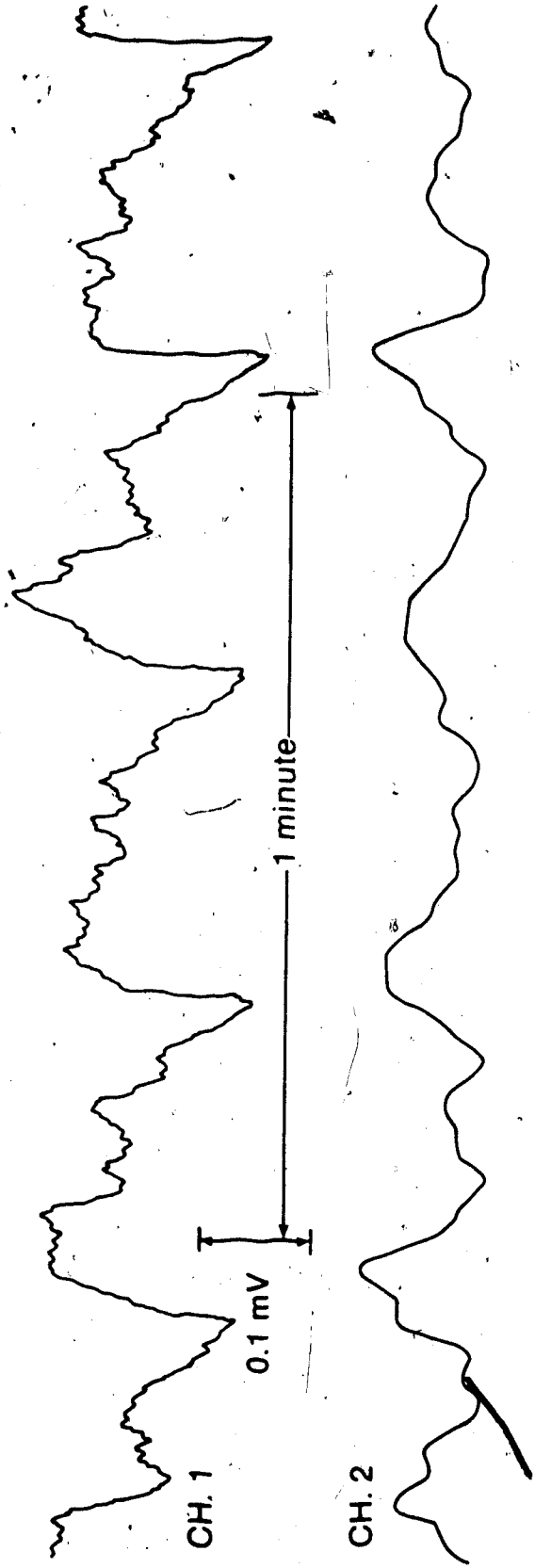


Figure 5.1b

patient. The mean frequency indicated for the impedance signal in table 5.1 is calculated for those periods with at least 3 cycles of contractile activity following each other. Figures 5.2a and b show typical power spectral of the GEA and impedance signals respectively.

The cross-correlation of the impedance of the impedance and the electrical signals is shown in figure 5.3. The correlation coefficient of two noise corrupted signals is always less than unity depending on their SNR's. If we assume for instance that a coefficient of 0.3 implies contractile activity, then there are contractions 49.5% of the time in the record shown in figure 5.3b.

TABLE 5.1

RESULTS OF TRANSCUTANEOUS MEASUREMENT OF GASTRIC ELECTRICAL
AND CONTRACTILE ACTIVITY

ACTIVITY	# ₀	#	%	T ₀	T	T%	f _{mean} (cpm)
				(Minutes)			
ELECTRICAL	26	24	92.3	1685	1327	78.75	2.95 ± 0.22
IMPEDANCE	26	20	76.9	1122	401.5	35.78	2.91 ± 0.4

#₀ - Total number of participants

- Number of successes

T₀ - Total recording duration in minutes

T - Duration with GEA in minutes

$$\% \text{ } - \frac{\#}{\#_0} \cdot 100\%$$

$$T\% - \frac{T}{T_0} \cdot 100\%$$

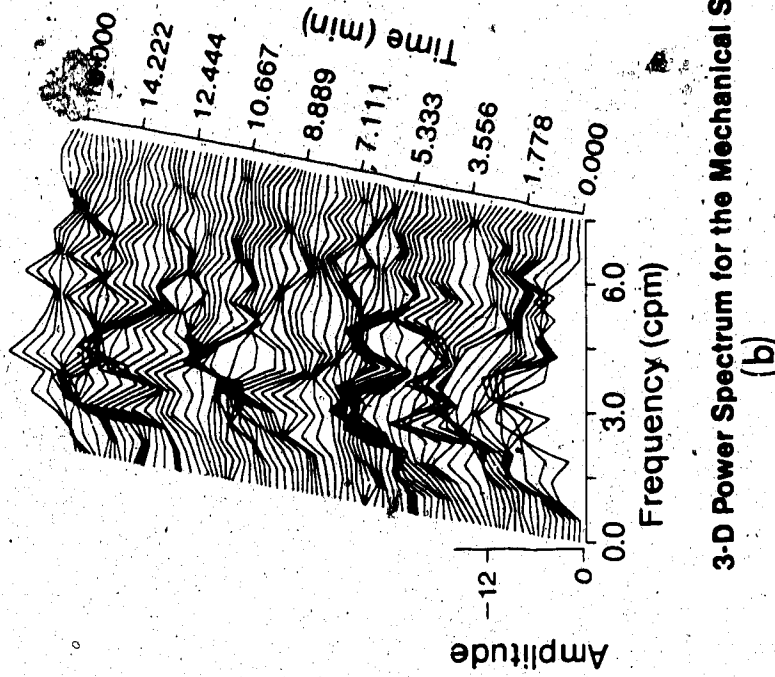
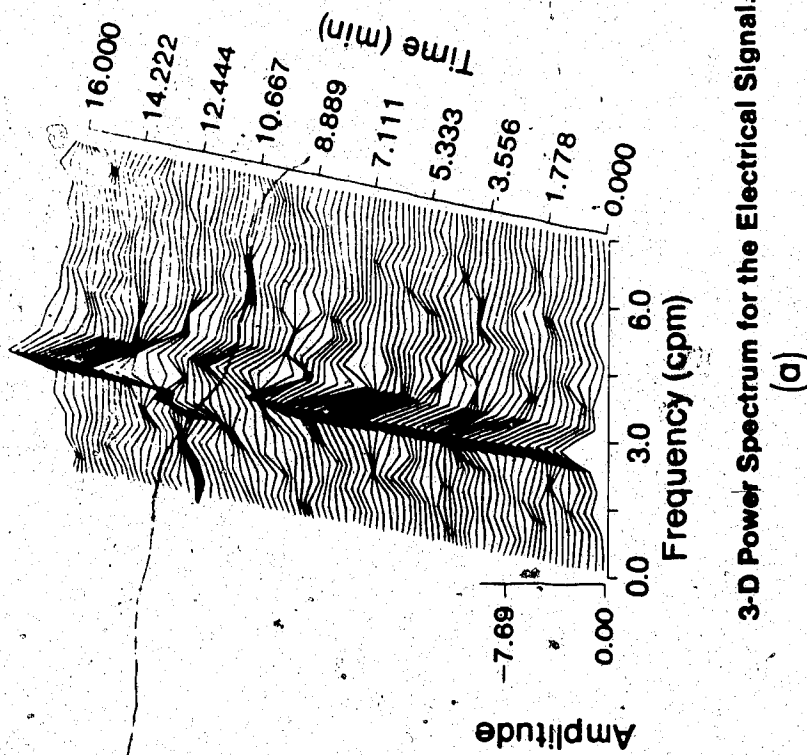
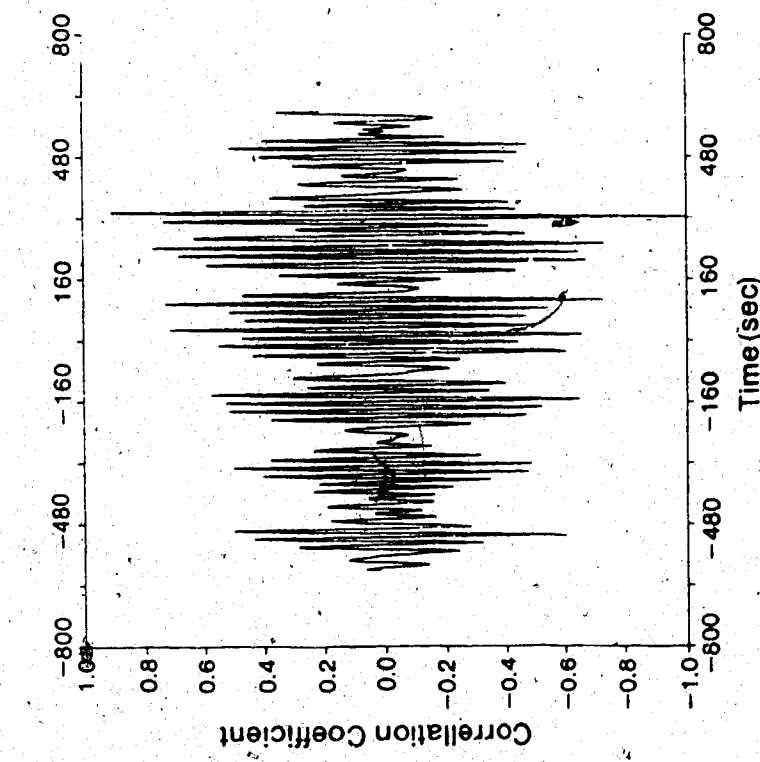
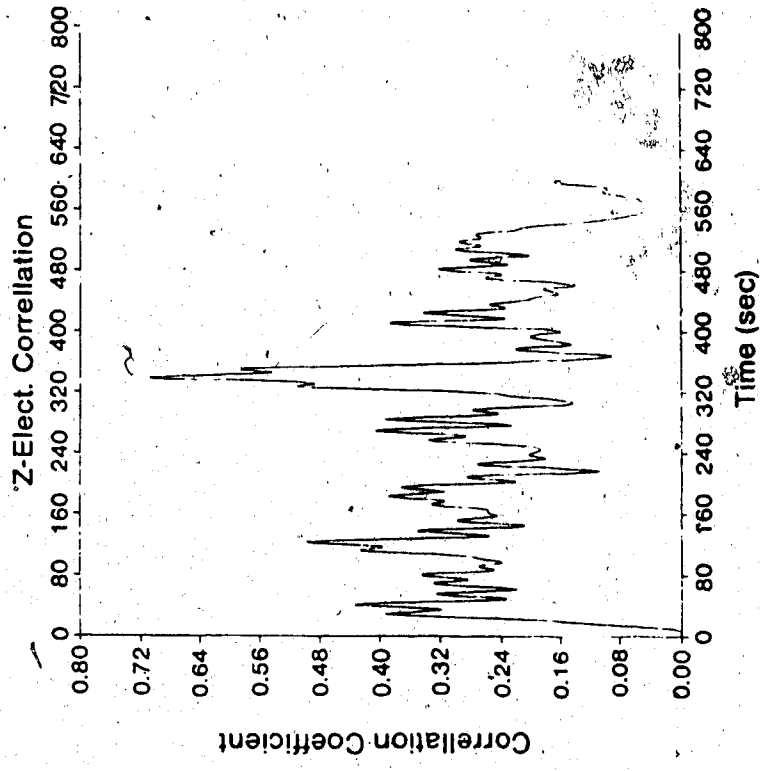


FIGURE 5-2



Electrical/Contractile Correlation vs Time Delay.
(a)

Z-Elect. Correlation vs Time
(b)

FIGURE 5-3

5.2 SIMULTANEOUS MEASUREMENT OF INTRAGASTRIC PRESSURE AND NONINVASIVE GASTRIC ELECTRICAL AND CONTRACTILE ACTIVITY

OBJECTIVE:

To compare intragastric luminal pressure measurements with variations in gastric electrical impedance measured from the torso surface.

METHOD AND MATERIALS:

Measurements were made on 9 healthy male and female volunteers ranging in age from 19 to 30 years old. Potentially pregnant females were excluded from the study.

Subjects were fasted for 8 to 12 hours prior to commencement of the experiment. The back of the subjects throat was sprayed with a xylocaine mist to reduce the gagging reflex. After the throat was numb, the transmucosal electrode described in section 3.1 with a PE-60 #7416 Intramedic^R polyethylene tubing manufactured by Clay Adams taped to its side was introduced into the stomach through the mouth. The assembly was positioned in the antrum by fluoroscopy.

The PE-60 tubing was connected to a manometry pump to monitor the intraluminal pressure. The device forces water at a trickle pace into the stomach through the opening at the end of the tubing. The pressure required to keep the water flowing at a slow but steady rate was recorded through a Beckmann R611 recorder.

The leads from the intraluminal electrodes were also connected to different channels on the same recorder.

Four ordinary Hewlett Packard ECG electrodes, type 14445C were attached to the surface of the subjects torso as shown in figure 5.4. The electrodes were arranged to be approximately colinear above the

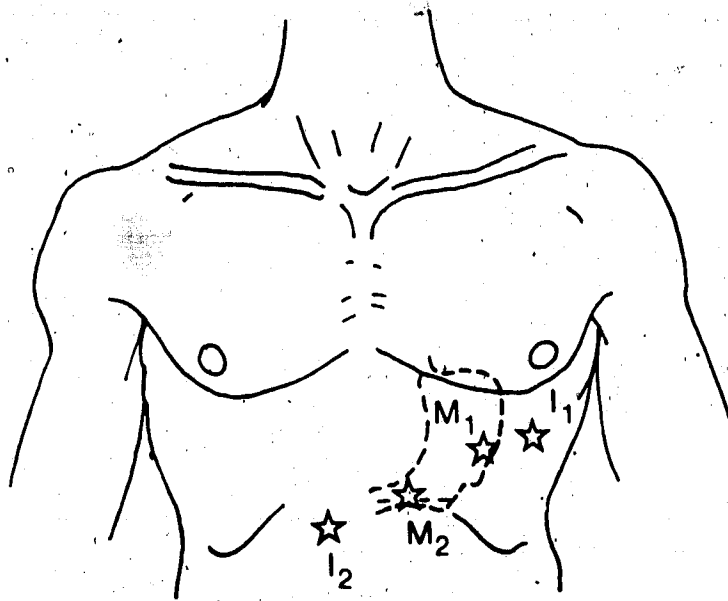


Figure 5.4 Electrode Positions.

projection of the antral axis on the skin [43] and spaced about 8 to 12 cm² apart. These tetrapolar electrical impedance electrodes were connected to the proper terminals on the gastric impedance monitor. See figures 4.1 and 4.9. Switch S1 on the device was flipped to the ON position. After about 60 seconds, the basal impedance was nulled out with the NULL knob on the front panel. The subject was instructed to lie as still as possible while measurement proceeded for about 30 to 45 minutes. The impedance variations were recorded on the Beckmann recorder.

The output of the Beckmann recorder was also coupled to the digital signal acquisition system described in section 2.3.

RESULTS AND DISCUSSION:

Figure 5.5a, b and c, show the transcutaneous GEA (ch. 1), the impedance signal (ch. 2) and the intraluminal pressure (ch. 3) signals in three different records.

The EGG occurs at a frequency of 2.9 cpm in figure 5.5a and 3.0 cpm in figure 5.5b. As has been shown in section 5.1, there is correlation between the GEA and the impedance signal. Visual inspection of channels 2 and 3 also suggest that there is correlation between the intraluminal pressure and the impedance derived contractile activity. In figure 5.5c, correlation between the intragastric pressure recorded and the extracorporal impedance may be visually verified over an 8 minute period. Figure 5.6 shows the correlation plot for channels 2 and 3 for a typical record. The two signals are correlated in the region of 3 cpm in this plot.

Table 5.2 shows the results of these experiments in tabular form.

T_{Pz} indicates in minutes, how often contractile activity is detected on

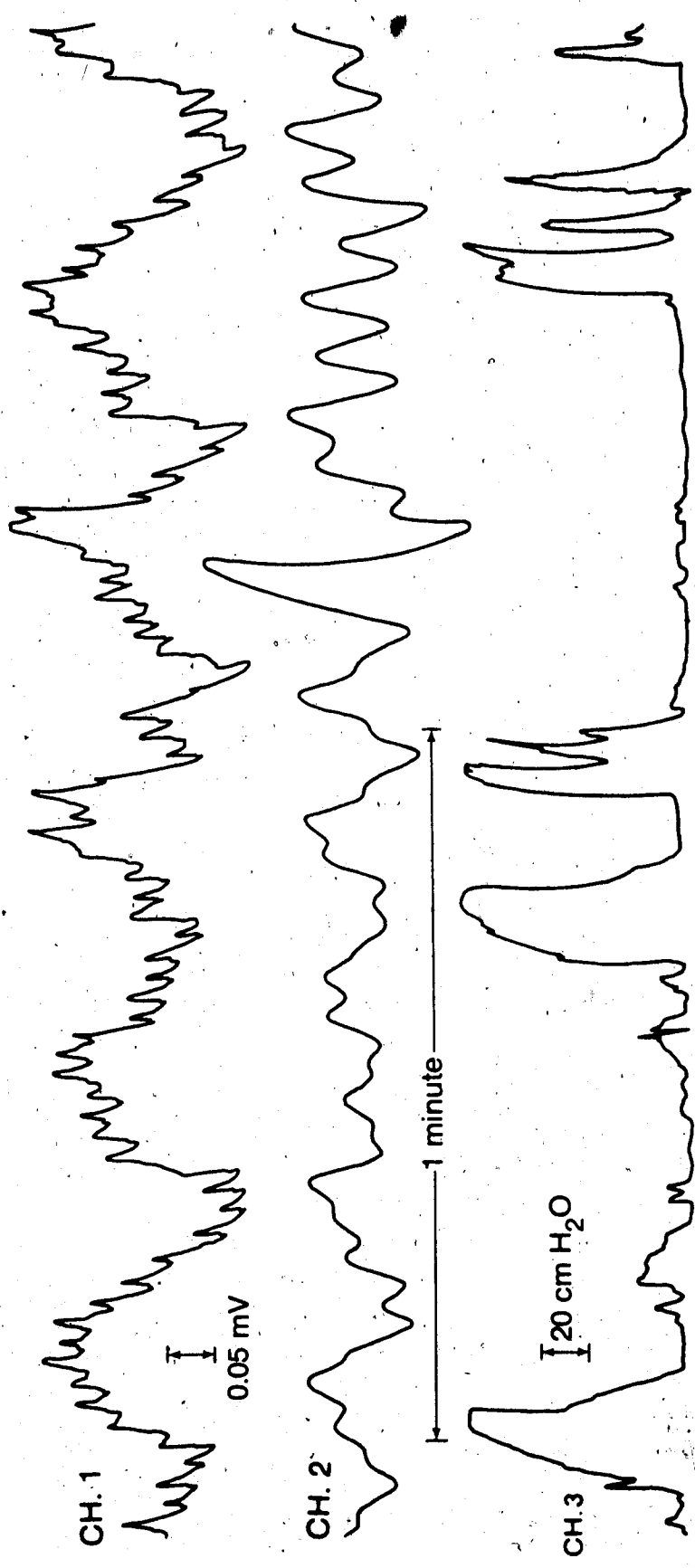


Figure 5.5 (a)

Simultaneous Record of Intra-gastric Pressure and
Extracorporal Impedance and GEA

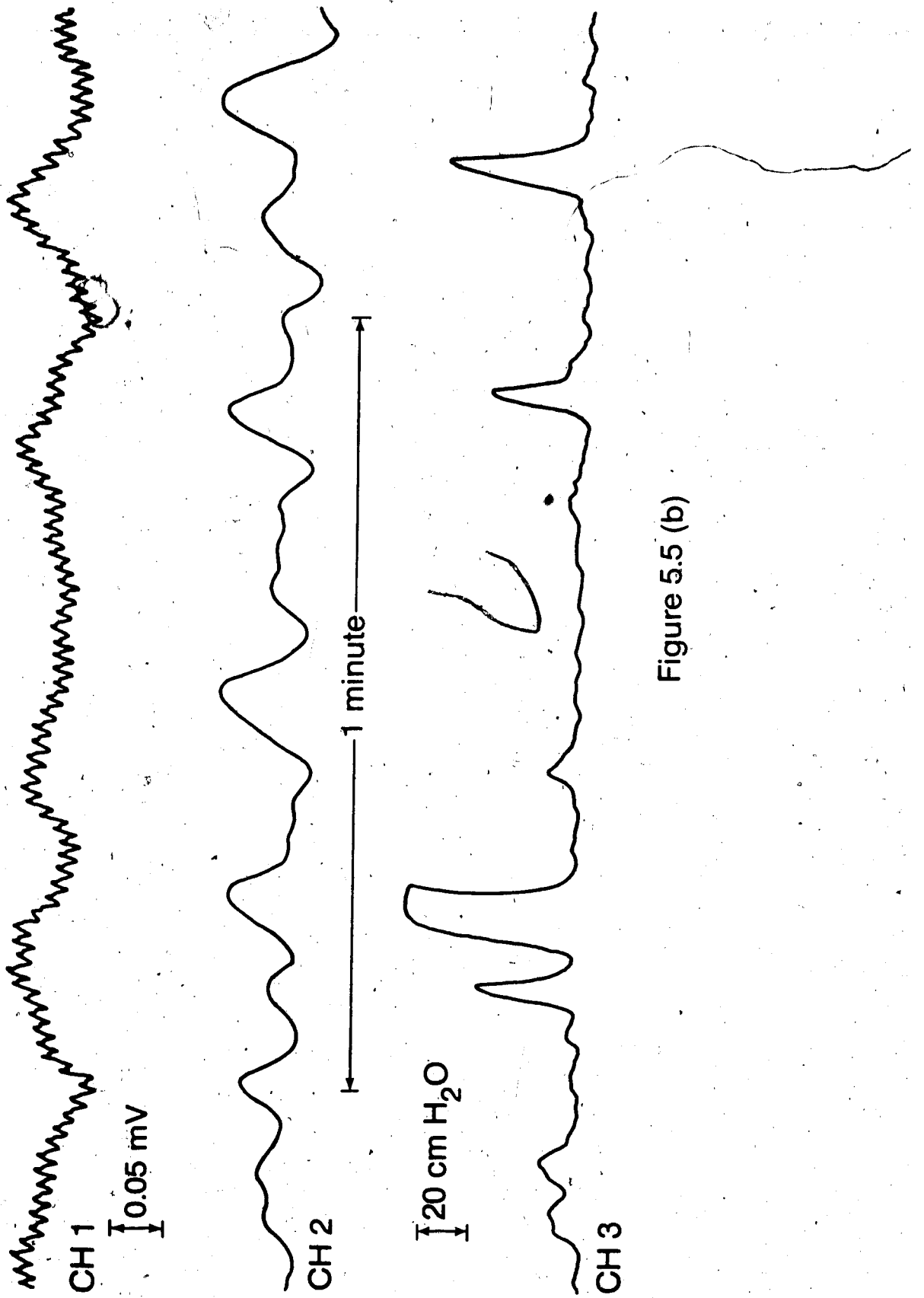


Figure 5.5 (b)

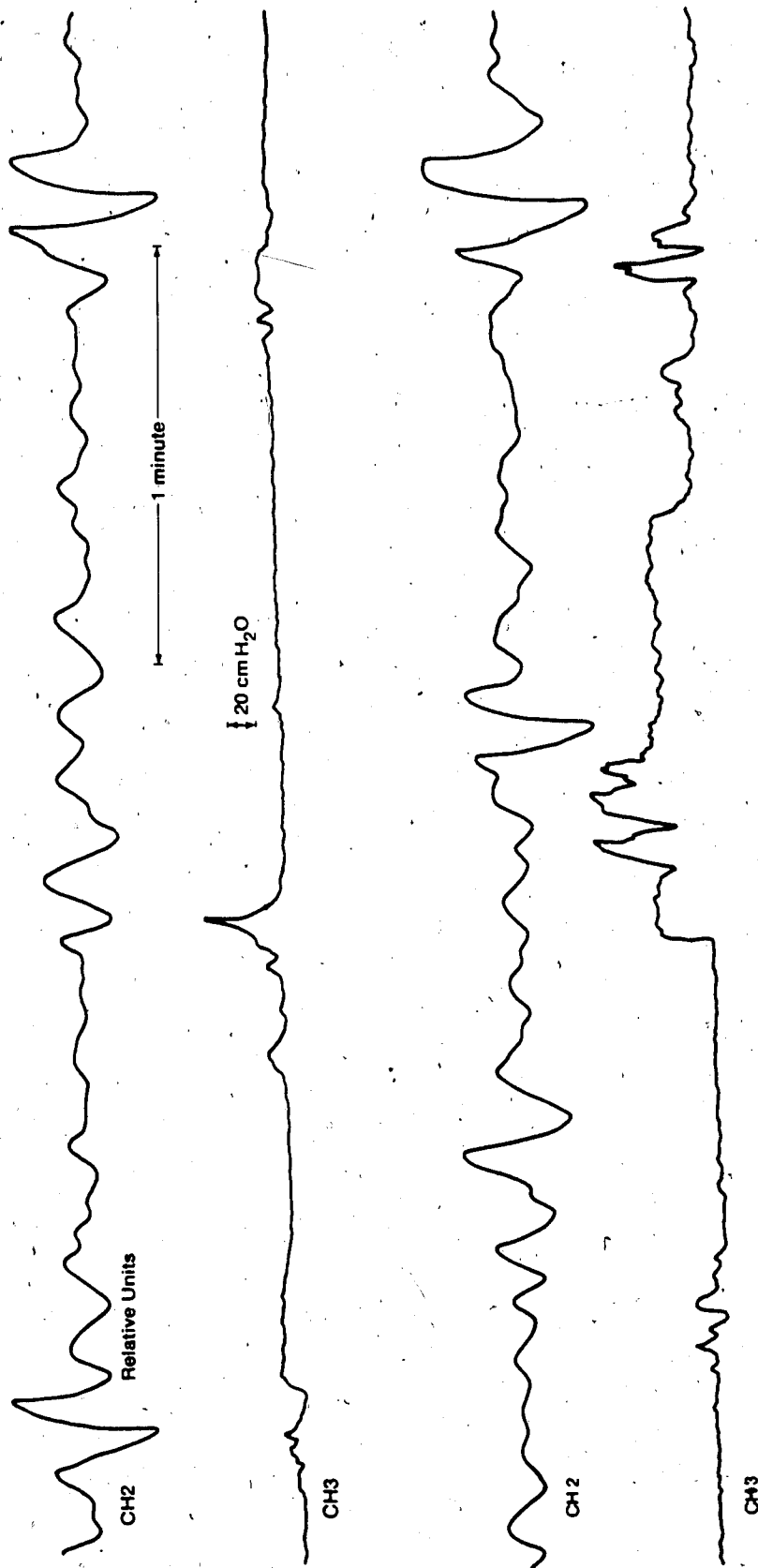


Figure 5.5c

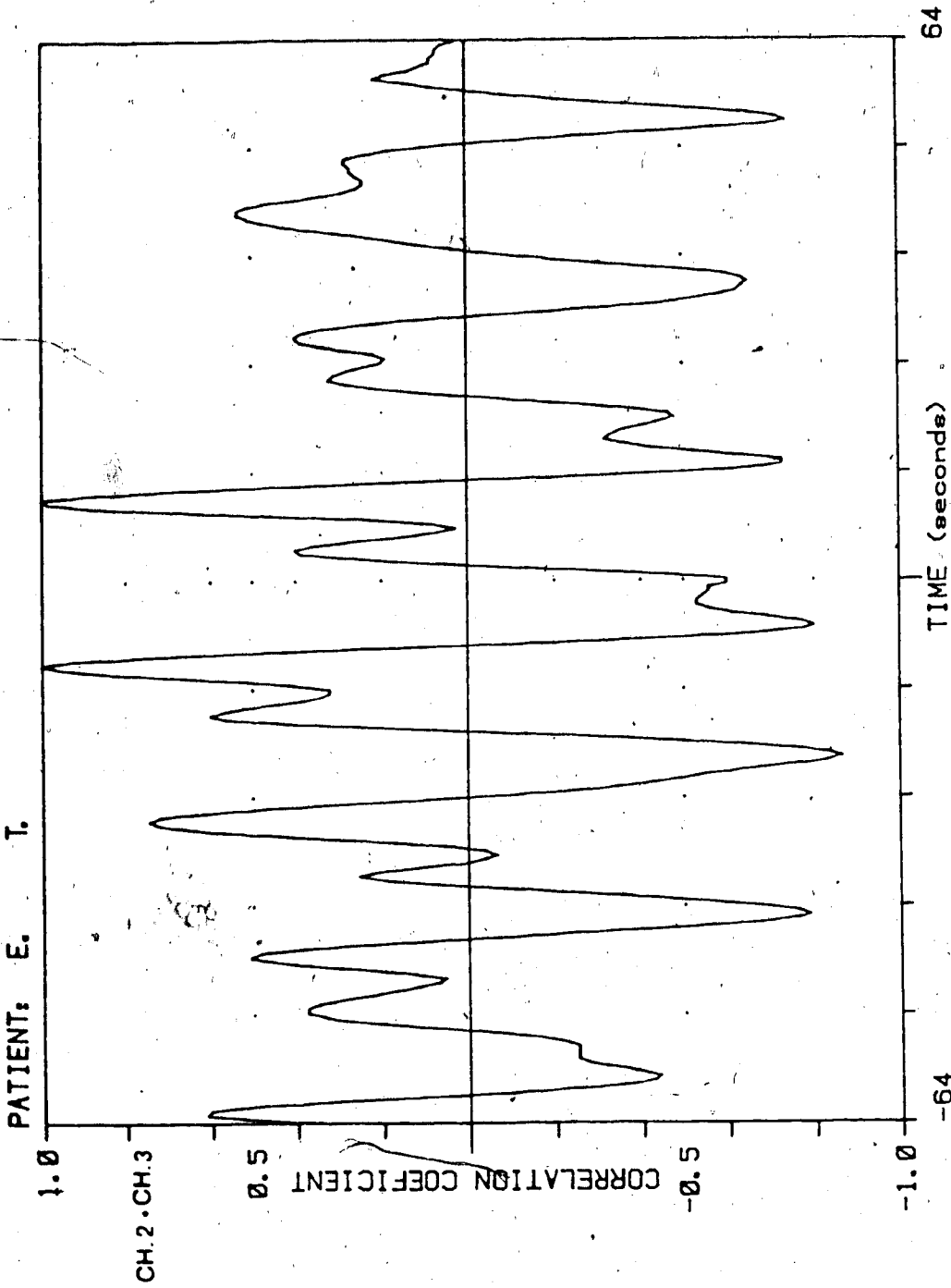


Figure 5.6
Correlation Plot

both the impedance channel and the intraluminal pressure channel simultaneously. This turns out to be 70% of the total duration for

TABLE 5.2
RESULTS OF TRANSCUTANEOUS IMPEDANCE AND INTRAGASTRIC
PRESSURE MEASUREMENTS

# ₀	#	T ₀	T _P	T _Z	T _{PZ}	P%	Z%
(Minutes)							
9	7	531	141.5	154.9	99.5	70.32	64.23

#₀ - Total number of participants.

- Number of successes

T₀ - Total recording duration in minutes

T_P - Duration with contractions indicated on the Intra-gastric Pressure channel (in minutes)

T_Z - Duration with contractions indicated on the impedance channel (in minutes)

T_{PZ} - Duration with contractions indicated simultaneously on both the intra-gastric pressure and impedance channels (in minutes)

$$P\% = \frac{T_{PZ}}{T_P} \cdot 100\%$$

$$Z\% = \frac{T_{PZ}}{T_Z} \cdot 100\%$$

which contractile activity is indicated on the pressure sensor. This

means that the extracorporeal impedance technique mirrors the intraluminal pressure 70% of the time in this study.

However, it is not uncommon to see signals of some sort on the impedance channel without the same showing up on the intraluminal pressure sensor. This may be due to a variety of reasons.

1. The amplitude of the signal may not be large enough to register as a detectable change in the intraluminal pressure.
2. The transference of antral contractions into a change in the intraluminal pressure sensed by the perfused catheter is only efficient when both the lower oesophageal and pyloric sphincters are closed. This condition is not always satisfied throughout the duration of an experiment. [18]
3. The contractile activity may occur at some distance from the opening in the perfused catheter and therefore not register on the sensor. The impedance channel on the other hand, sees a global picture of the area under the electrodes and therefore picks up the activity.
4. Since the impedance channel monitors the activity over a larger area than the catheter does, the catheter may be right in not picking up the signal if it arises from some other organ such as the large bowel.

It is not all that easy to sort out these confusing alternatives.

For one thing, the intraluminal pressure method is somewhat suspect even though it is presently the state of the art in the assessment of gastric motility. This means that the impedance method is compared to another method that is in itself prone to errors.

6. DISCUSSION

6.1 MODEL OF GASTRIC ELECTRICAL ACTIVITY

Figure 4.6a is a plot of the calculated potential at the skin for electrode positions $M_1(A, 160^\circ, .3)$ and $M_2(A, 60.0^\circ, .292)$, with M_2 designated as the neutral electrode. The difference in the slope of the rising and falling edges of both plots is perhaps the most important feature of this model as far as this study is concerned. It is important to note from the onset that the relative positions of the neutral and active electrodes are very important in the following results and conclusions.

The rising slope of the slow wave for an aborally propagating SD is steeper than the falling edge i.e. $\gamma > 1$. The opposite is the case for the retrograde SD source in the model, $\gamma < 1$. Figures 4.7a and b show experimental extracorporeal measurements of GEA that are similar in wave shape to those calculated in the model (figures 4.6a and b).

Hence, one may be able to tell the direction of propagation of antral electrical and consequently, contractile waves by inspection of the wave shape of EGGs. The proviso being that the electrode positions are very important. For one thing, if their positions relative to each other are switched, the results have to be interpreted backwards as discussed earlier. Perhaps more important than this is the fact that the SNR of the EGG depends a great deal on the electrode positions [43]. If the recorded signal is seriously corrupted by ECG, respiratory and other artifacts, interpretation of its wave shape may not yield information regarding the direction of propagation or worse still, be misleading. Such cases are covered further in section 6.3.

It is worth noting that values of $\frac{dV}{dt}|_1$, $\frac{dV}{dt}|_t$ and γ were obtained in this study without any particular attention being paid to

the contractile state of the stomach at the time of the experiment. Joseph H. Szurszewski reported that gastrin (G_{17}) and acetylcholine (ACh) increased the amplitude and duration of the plateau potential in his study [60]. One effect of this is a decrease in the duration from the plateau potential to the rest or base potential. This implies an increase in $\left. \frac{dV}{dt} \right|_t$ and consequently a decrease in γ .

Mirrizzi and Scafoglieri [43] reported that the optimal signal is obtained in human transcutaneous EGG with electrodes lined up above the antral axis. This is tested in the model by calculating the surface potential from an array of electrodes. The active electrodes are located at $M_1(A.155.0^\circ, z_j)$ and the neutral electrodes at $M_2(A.60.0^\circ, z_j)$, $j=1,2,\dots,25$ as shown in figure 6.1. In figure 6.2 the power in the calculated slow waves is plotted against the electrode position z . Figure 6.2 shows that the power in the slow wave reaches a maximum when the two electrodes are lined up above the L discrete oscillating regions representing the antrum.

6.2 COMPARISON OF EXTRACORPORAL AND TRANSMUCOSAL ELECTRO-GASTROGRAMS

Extracorporal EGG was recorded from 3 electrodes and a neutral spaced 3 cm apart and colinear above the antral axis as shown in figure 6.3. Intraluminal EGG's were also simultaneously recorded as discussed earlier. Figure 6.4 is typical of such records.

Table 6.1 shows values of θ' and θ_m where θ_m is θ averaged over 6 slow wave cycles centered around the 256 sample frame constituting the crosscorrelation in a particular record.

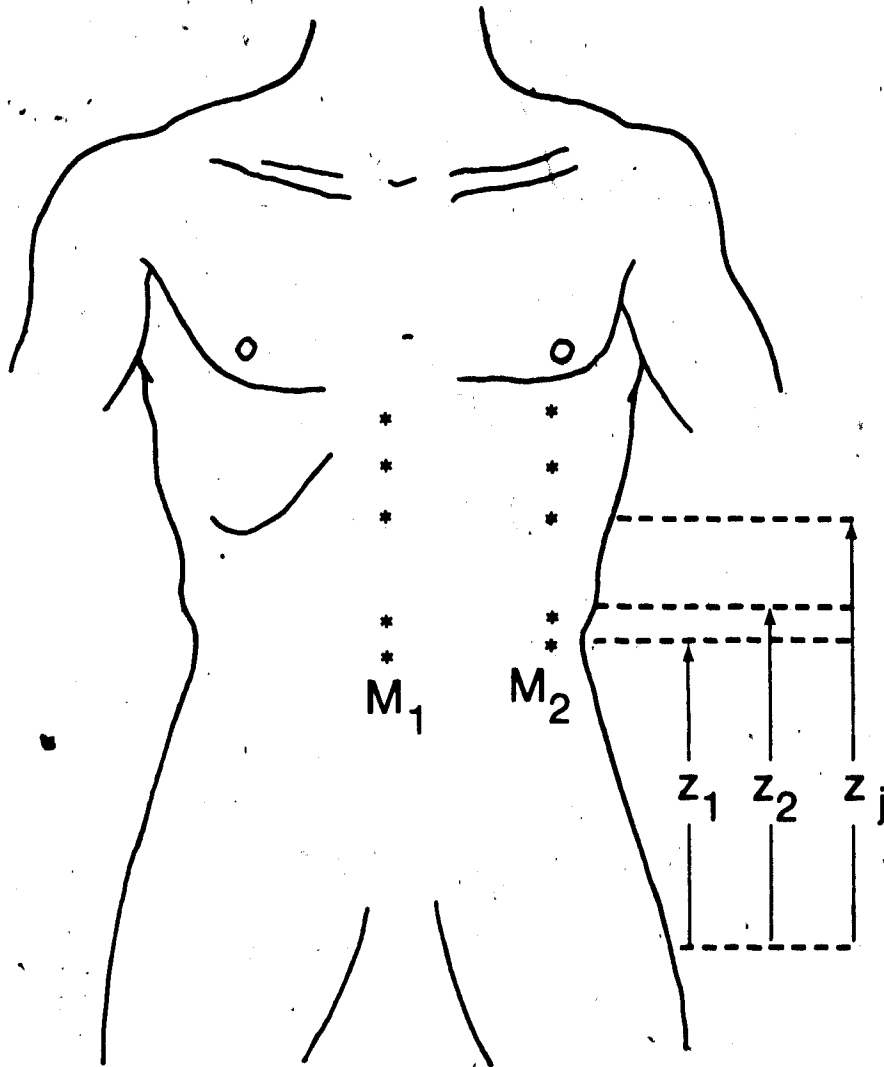


Figure 6.1

Electrode Positions for Array Calculation

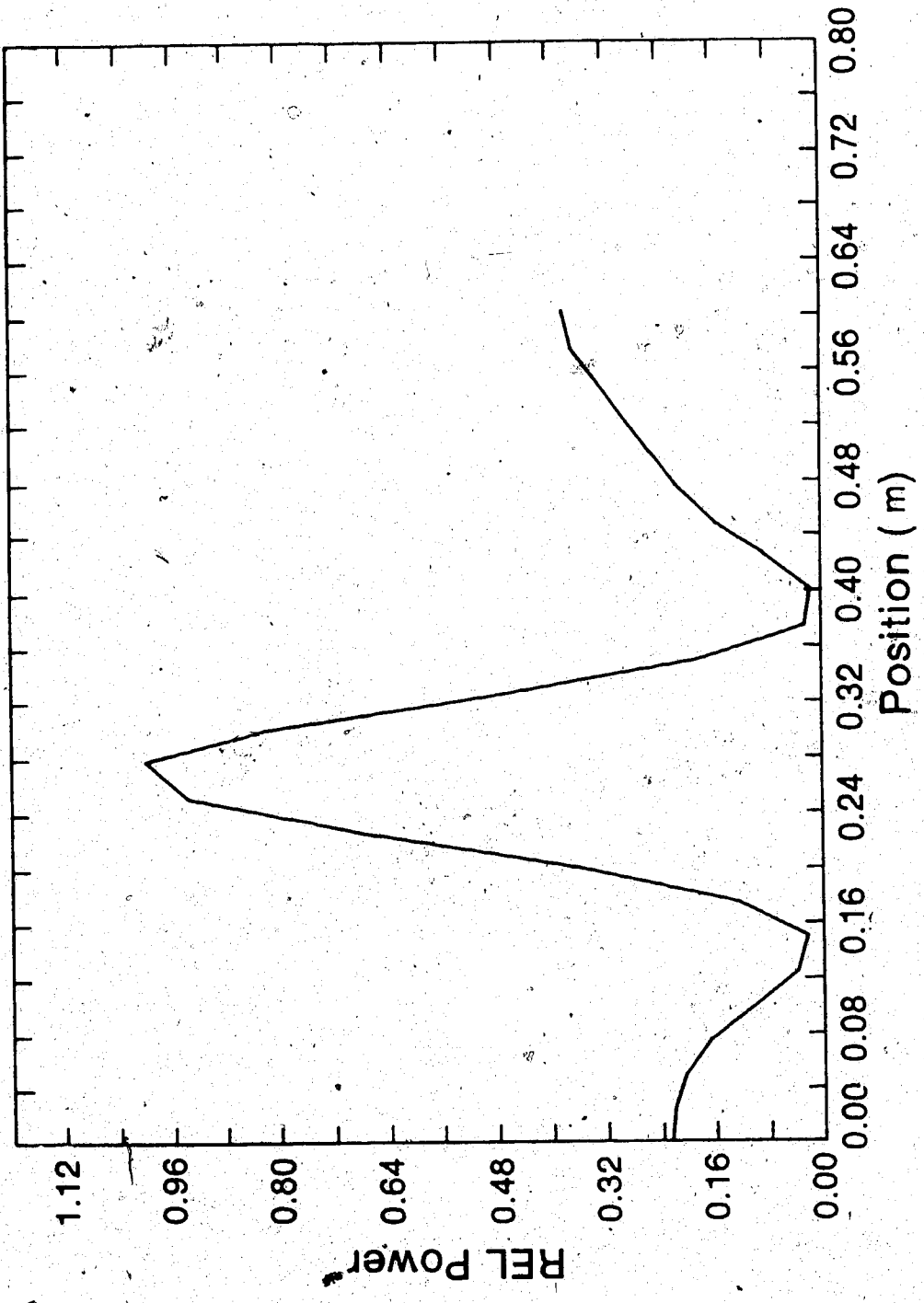


Figure 6.2
Power in Simulated GEA vs. Electrode Position

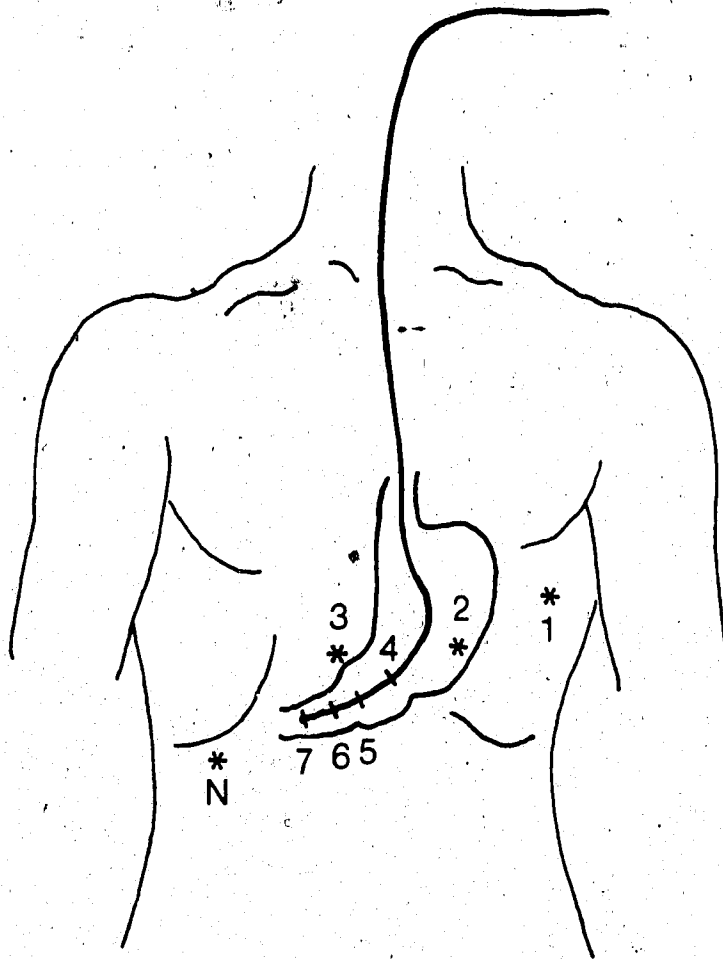


Figure 6.3
Electrode positions
1, 2, 3, & N on the skin
4, 5, 6 & 7 intraluminal

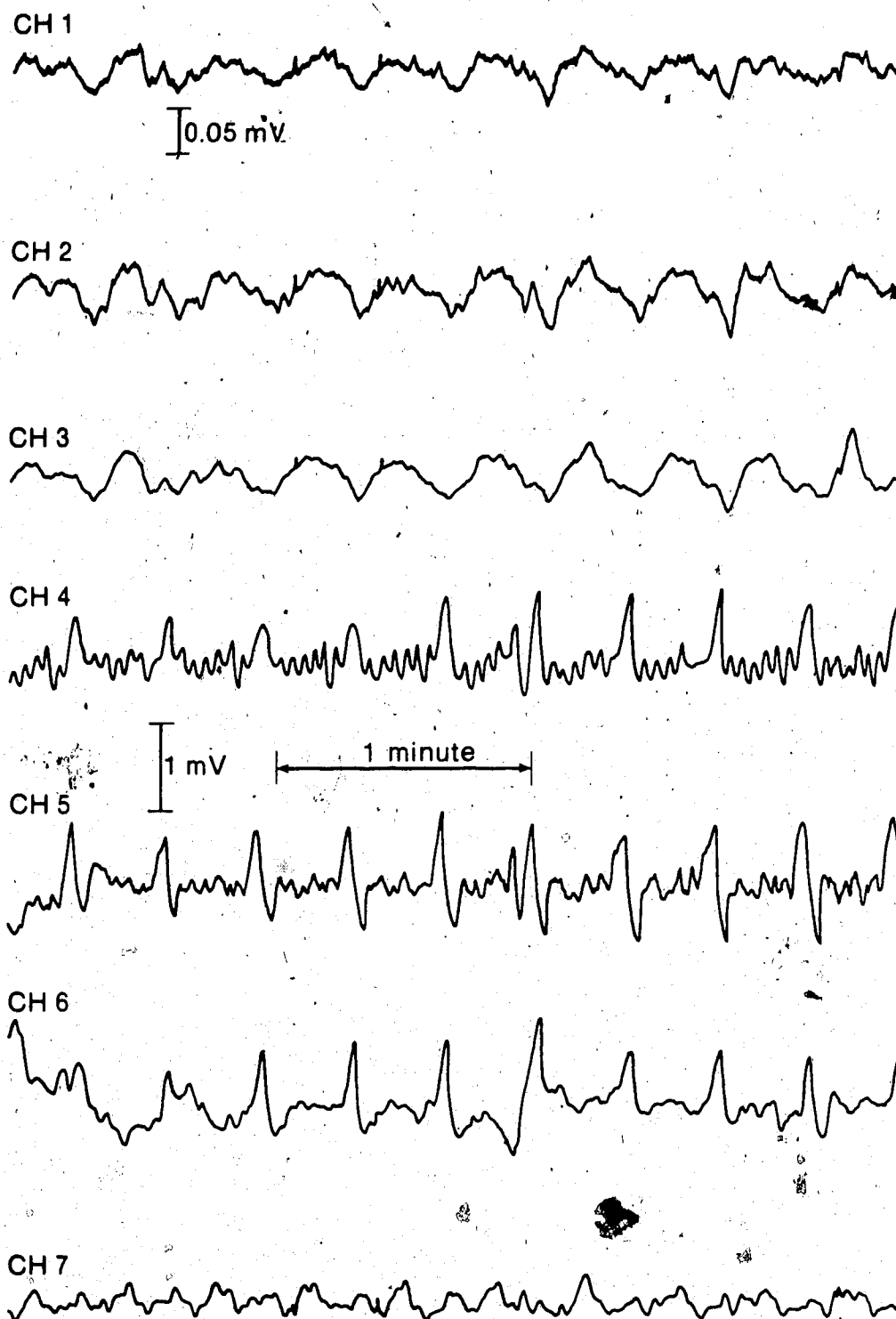


Figure 6.4

Record of Simultaneous Extracorporeal and Intraluminal EGGs

TABLE 6.1

PHASE SHIFT BETWEEN CHS. IN DEGREES					
	EXTERNAL (d=3 cm)			INTRALUMINAL (d=2 cm)	
	1 * 2	2 * 3	5 * 6	6 * 7	7 * 8
θ_m	6.0	-10.0	142.5	76.8	55.4
θ'	0	0	140	86.7	50

1.

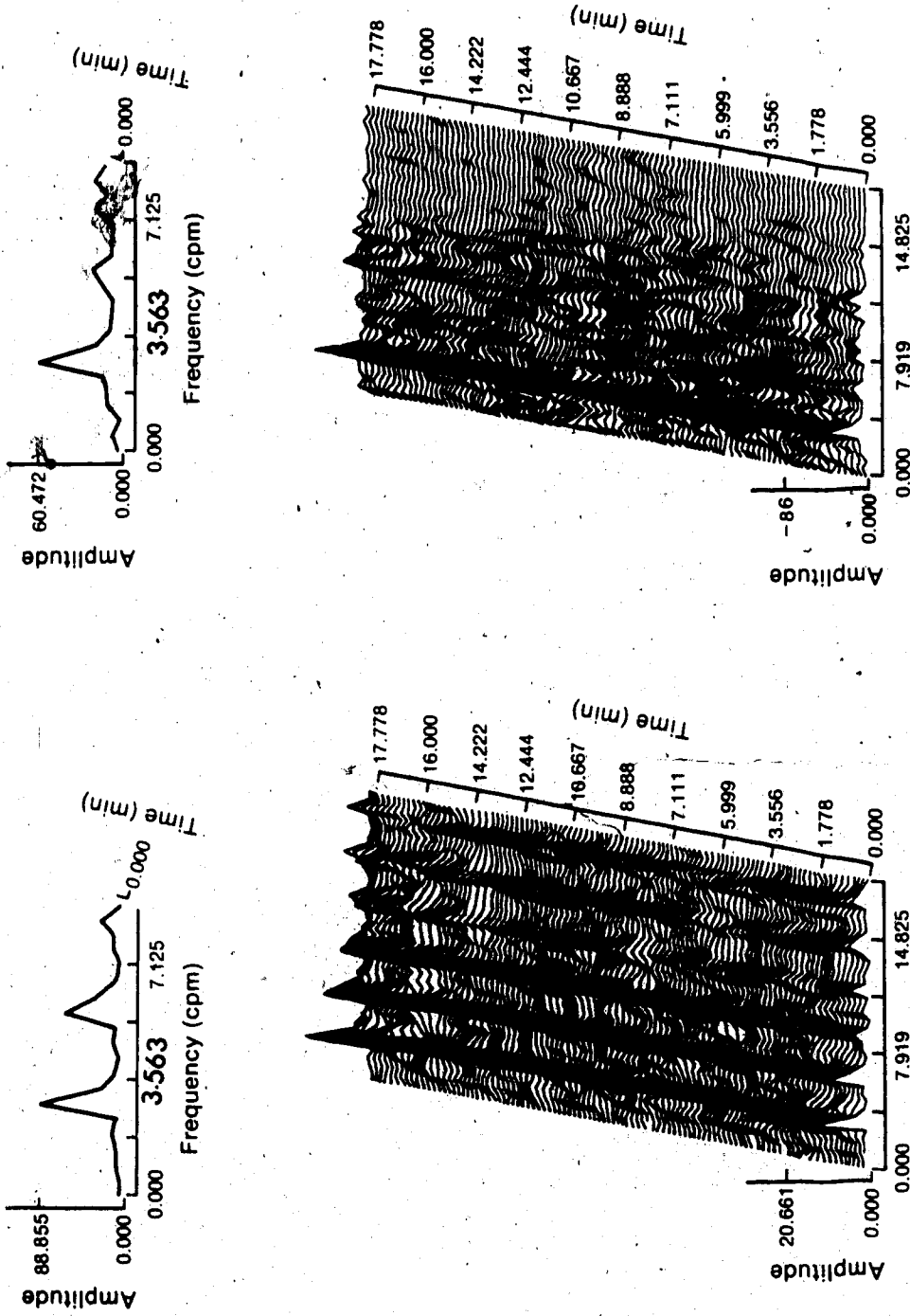
In all good records, both the extracorporeal and intraluminal EGGs occurred at the same frequency (mean 2.96 ± 0.22 cpm for the intraluminal records and 2.98 ± 0.3 cpm for the extracorporeal records). Figure 6.5a and b show power spectrum plots for the extracorporeal and the intraluminal records respectively. The dominant frequencies may be obtained from the 2-D plots while the 3-D plots show temporal variations (if any) in the dominant frequencies. The fact that they are of the same origin could be shown by crosscorrelation [10].

2.

The average amplitude of the intraluminal signal was 1.2 ± 0.4 mV while that of the extracorporeal signal was 0.07 ± 0.01 mV.

3.

No discernable coupling was noticeable in the extracorporeal EGGs whereas coupling, phase shift and direction of propagation information could be extracted from the intraluminal records both visually and by crosscorrelation. This is reflected in the average phase angles recorded.



a) Extracorporal EGG

b) Intraluminal EGG

Frequency (cpm)

Frequency (cpm)

4.

The average phase angle seen in normal subjects with the intraluminal method was $46.8^{\circ}/\text{cm} \pm 15.6$

6.3 EXPANSIONS

The last five chapters encompassed the scope of the present study. Possible improvements and/or expansions of some of the areas are examined in this section.

a)

In developing the mathematical model of the GEA, the primary aim was to extract information regarding the direction of propagation from the wave shape. Therefore, particular attention has not been paid to the absolute amplitude of the signals. By this, one infers that dc errors may exist in the amplitude of the calculated signal.

A more rigorous solution of the problem posed in section 4.1 can be attempted. However, such a solution cannot be expressed in closed form and will therefore have to be evaluated by numerical methods. The relative increase in the machine time required for the computation will be astronomical.

Finally, the "best fit" values of $\underline{P}(P_r, P_{\theta}, P_z)$ and z_0 depend a great deal on the SNR of the values y_j to which they are fitted (see section 4.1). Unfortunately, transcutaneous GEA cannot be measured as accurately as the ECG because of the corrupting ECG and respiration signals. Figure 6.6a and b show a typical trace of transcutaneous GEA and its FFT derived power spectrum respectively. Respiratory and ECG artifacts often corrupt these records as is quite evident from the records shown throughout this study. The ratio of the power in the 3.1

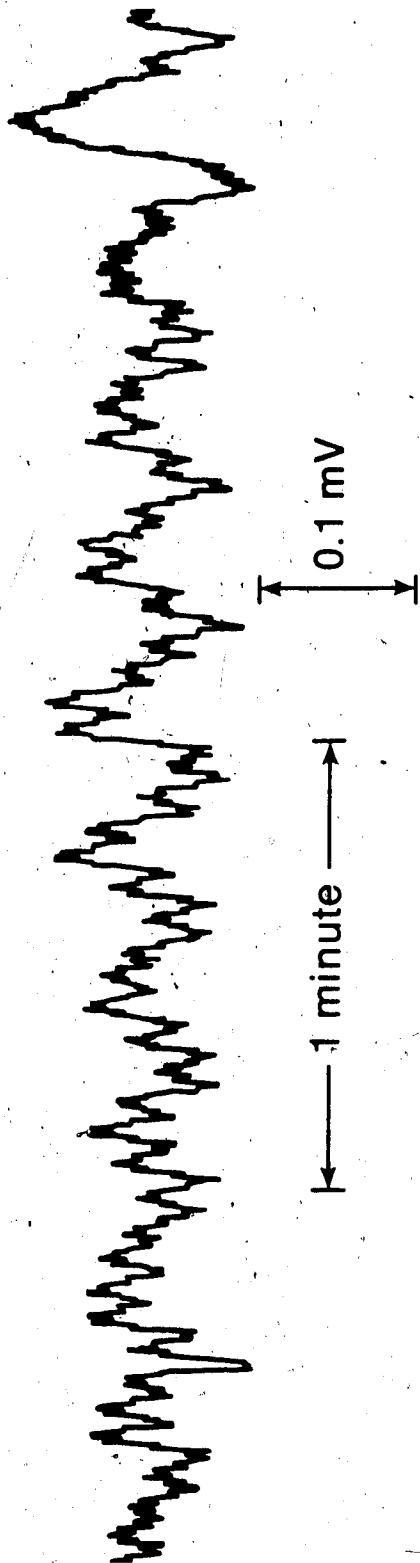


Figure 6. 6a.

Typical ECG Corrupted by ECG and Respiratory Artifacts

2.521 Patient: F.B.

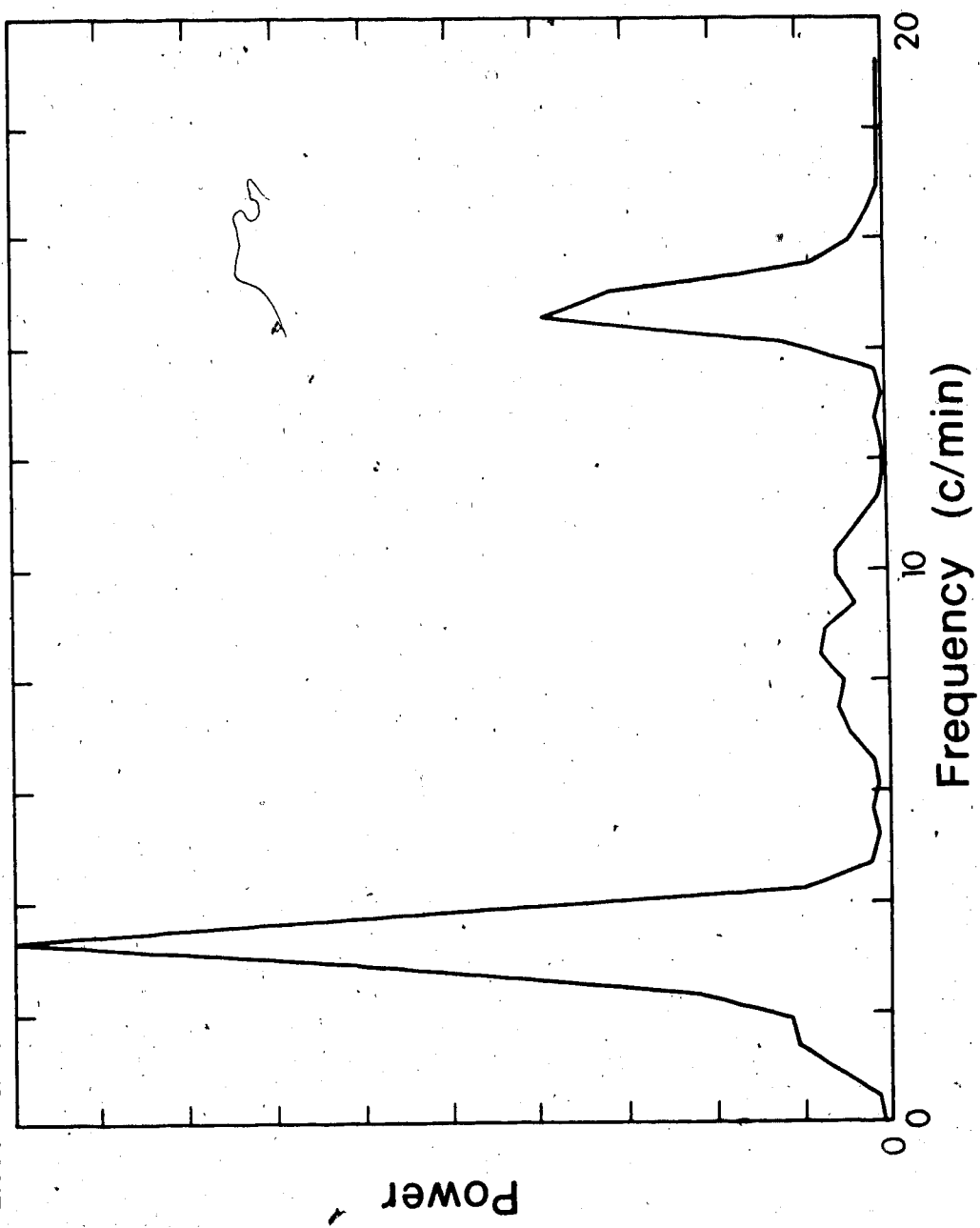


Figure 6.6 (b) Power Spectrum

cycles/minute signal (GEA) to that of the power in the respiratory component at 13.7 cpm is 1 to 0.42. This can play havoc with the convergence and/or accuracy of the finite difference Levenberg-Marquardt algorithm employed to determine the model parameters. A way round this noise problem might be to apply the difference algorithm to a filtered version of the measured signal. On the other hand, one might optimize the model parameters with the power in the fundamental and first few harmonics of the measured signal.

b)

In the determination of the direction of propagation from the slope of measured waveforms, it is essential that the signal possess a high SNR. Adaptive filtering of the recorded signal in the region of GEA may be considered. This has the advantage of

- 1) improving the SNR without a priori knowledge of the signal,
- 2) tracking the signal when the frequency drifts (which an ordinary band pass filter will not do unless its parameters are changed externally).

c)

It is conceivable that the direction and velocity of propagation of contraction waves may be extracted directly from measurements of extracorporeal electrical impedance. To do this, the impedance monitor needs to be equipped with more than one channel. That is, the impedance may be monitored at say three electrodes M_1 , M_2 and M_3 to constitute a 2 channel device with the same current electrodes I_1 and I_2 . The direction and velocity of propagation of contraction waves may then be determined in the same manner that the direction and velocity of propagation is determined in multi site EGG measurements.

6.4 CONCLUSIONS

In this section, a brief summary of what has been accomplished in this study is presented.

1. We have developed a hybrid electrode formed on a stainless steel base. In studies requiring the implantation of electrodes in animals and human beings, the overriding safety concerns often necessitate the use of the stronger metals (stainless steel and platinum) rather than the silver-silver chloride electrode with its lower electrode impedance and noise. The hybrid electrode developed in this study (section 2.2B) combines the mechanical strength of the stainless steel electrode with the good impedance and noise properties of the Ag-AgCl electrode. Such an electrode could be invaluable in long duration in vivo studies.

2. The intraluminal electrode assembly developed in this study and reported in chapter 3 has two main advantages over similar devices [1,10,26] reported to date.

a) Its unique design precludes possible separation of the mucosa from the muscle wall due to suction. This results in a good SNR.

b) It makes it possible to study myogenic potential at four evenly spaced sites simultaneously. Therefore, information regarding the direction of propagation of the myogenic potential, coupling between the four sites and the velocity of propagation may be extracted from measurements made with this probe.

3. The importance of gastric motor function in digestion and emptying has been elucidated at length. Studies of the motor activity are often made invasively as in the perfused catheter method of monitoring intragastric pressure. The few noninvasive techniques hitherto reported often involve complex instrumentation as in x-rays or ultrasound.

In this study, a new noninvasive technique is developed. The technique has the following advantages

- a) It is noninvasive
- b) It requires simultaneous measurement of EGG which in itself may aid in the diagnosis of certain gastric conditions
- c) The instrumentation involved is relatively simple
- d) The cost of constructing a unit of the design is only about \$270 and 35 technician man-hours

Such a system may find application in the study of gastric motility and in the clinical diagnosis of particular gastric motor dysfunctions.

REFERENCES

- 1] ABELL, T.L., MALAGELADA, J.: Glucagon evoked gastric dysrhythmias in humans shown by an improved electrogastrographic technique. *Gastroenterology* 88(6):1932-1940, 1985.
- 2] ALLISON, R.D.: Clinical applications of impedance plethysmography. *Clinical Med.*:33-41, Feb. 1967.
- 3] ALVAREZ, W.C.: The electrogastrogram and what it shows. *J.Am.Med. Assoc.* 78:1116-1119, 1922.
- 4] ARTHUR, R.M. and GESELOWITZ, D.B.: Effect of inhomogeneities on the apparent location and magnitude of a cardiac current dipole source. *IEEE Trans. BME-17*:141-146, 1970.
- 5] ARTHUR, R.M., GESELOWITZ, D.B, BRILLER, S.A., and FROST, R.F.: Quadrupole components of the human electrocardiogram. *Amer. Heart J.*, 83:663-667, 1972.
- 6] BANNISTER, C.H.: Analysis of electrical and pressure signals of human colon. An M.Sc. thesis. Univ. of Alberta, Edmonton. 1980.
- 7] BARNARD, A.C.L., DUCK, I.M., LYNN, M.S., and TIMLAKE, W.P.: The application of electromagnetic theory to electrocardiology. II. Numerical solutions of the integral equations. *Biophys. J.* 7:463-491, 1967.
- 8] BARR, R.C., SPACH, M.S. and HERMAN-GIDDENS, G.S.: Selection of the number and positions of measuring locations for electrocardiography. *IEEE Trans. BME*, BME-18:125-138, 1971.
- 9] BASS, P.: In vivo electrical activity of the small bowel. *Handbook of Physiology: Alimentary Canal Sect.* 6 Vol. 4. Edited by C.F. Code. pp. 2051-2074. 1968.

- 10] BELLANSENE, B.E., HAMILTON, J.W., WEBSTER, J.G., BASS, P. and REICHFELDER, M.: An Improved Method for Recording and Analyzing the Electrical Activity of the Human Stomach. IEEE Trans. Biomed. Eng., BME-32(11):911-915, 1985.
- 11] BORTOFF, A.: Configuration of intestinal slow waves obtained by monopolar recording techniques. Am. J. Physiol. 213(1):157-162. 1967.
- 12] BORTOFF, A.: Electrical transmission of slow waves from longitudinal to circular intestinal muscle. Am. J. Physiol., 209(6):1254-1260. 1965.
- 13] BORTOFF, A.: Slow potential variations of small intestine. Am. J. Physiol. 201:203. 1961.
- 14] CARSLAW, H. and JAEGAR, J.: Conduction of heat in solids. Oxford Press, 2nd edition. 1959.
- 15] CLARK, J. and PLONSEY, R.: A mathematical evaluation of the core conductor model. Biophysical Journal. 6:95. 1966.
- 16] CLARK, J.W. and PLONSEY, R.: A mathematical study of nerve fiber interaction. Biophysical Journal. 10:937. 1970.
- 17] CODE, C.F., SZURSZEWski, J.H., KELLY, K.A. and SMITH, I.B.: A concept of control of gastrointestinal motility. Handbook of Physiology: Alimentary Canal Sect. 6, Vol. 5. Edited by C.F. Code. pp. 2881-2896. 1968.
- 18] CHRISTENSEN, J. and WINGATE, D.L.: A guide to gastrointestinal motility. Wright. PSG. Chap. 4:101-127. 1983.
- 19] DANIEL, E.E. and CHAPMAN, K.M.: Electrical activity of the gastrointestinal tract as an indication of mechanical activity. Am. J. Dig. Dis. 85:54. 1963.

- 20] DURDLE, N.G.: Measurement and analysis of electrical slow wave activity of the colon. A Ph.D. Thesis. Univ. of Alberta. 1983.
- 21] DURDLE, N.G., KINGMA, Y.J., and BOWES, K.L.: Origin of slow waves in the canine colon. Motility of the Digestive Tract. Edited by Wienbeck. Raven Press. N.Y. 1982.
- 22] EL-SHARKAWY, T.Y., MORGAN, K.G., and SZURSZEWski, J.H.: Intracellular electrical activity of canine and human gastric smooth muscle. J. Physiol. London. 279:291-307. 1978.
- 23] EL-SHARKAWY, T.Y., BARDAKJIAN, MACDONALD, W.M. and DIAMANT, N.E.: Origins of the multiple patterns of electrical control activity in the colon. Motility of the Dig. Edited by M. Wienbeck. raven Press, N.Y. 1982.
- 24] ETTISCH, G.H. and PETERFI, T.: Zur Methodik der Elektrometric der Zelle. Arch. ges. Physiol. 208:348-355, 1925.
- 25] FAMILONI, B.O., KINGMA, Y.J., RATCHEV, I. and BOWES, K.L.: Noninvasive measurement of gastric electrical and mechanical activity. Proceedings of the 10th International Symposium on Gastrointestinal Motility. Rochester. Minnesota. Sept. 1985. Abst. Dig. Dis. and Sci., 30:8, 1985.
- 26] FIORAMONTI, J., BUENO, L. and FREXINOS, J.: Sonde endoluminale pour l'exploration electromyographique de la motricite colique chez l'homme. Gastroenterol. Cli. Biol. 4:546-550. 1980.
- 27] GEDDES, L.A.: Electrodes and the measurement of the bioelectric events. Wiley-interscience. 1972.
- 28] GESELOWITZ, D.B.: An application of electrocardiographic lead theory to impedance plethysmography. IEEE Trans. BME. 18:38-41, 1971.

- 29] GOUY, M.: Sur la Constitution de la charge électrique a la surface d'un électrolyte. J.Phys. (Paris) 9:457-468. 1910.
- 30] GRAHAM, M.: Guard ring use in physiological measurements. IEEE Trans. on Biomedical Engineering, July/Oct. 1964.
- 31] GRAY, MATHEWS and MACROBERTS: Bessel functions. MacMillan, 2nd Edition, 1922.
- 32] HAMILTON, J. W. BELLAHSENE, B.E., CANTER, D.S., BASS, P. and WEBSTER, J.G.: Improved method of recording the human gastrogram. Proceedings of the annual meeting of the American Gastroenterological Association and Digestive Week. Pg. A230. 1985.
- 33] HELMHOLTZ, H.: Studien Über elektrische Greneschichten. Ann.Phys.Chem., 7:337-382, 1879.
- 34] HEPNER, D.B., and PLONSEY, R.: Simulation of electrical interaction of cardiac cells. Biophysical Journal. 10:1057, 1970.
- 35] HERINGA, A., STEGEMAN, D.F., UIJEN, G.J. and DEWEERD, J.P.C.: Solution methods of electrical field problems in physiology. IEEE Trans. on BME, 29:34, Jan. 1982.
- 36] HILL, D.W., and DOLAN, A.M.: Intensive care instrumentation. Academic Press. 1982.
- 37] INOMATA, H. and KAO, C.Y.: Ionic currents in an intestinal smooth muscle. Physiology of Smooth Muscles. Edited by F. Bulbring and M.F. Shuba. Raven Press. N.Y. 1976.
- 38] KAVANAGH, R.N., DARCEY, T.M., LEHMANN, D. and FENDER, D.H.: Evaluation of methods for three dimensional localization of electrical sources in the human brain. IEEE Trans. Bio. Med.

- Eng., BME-12:421-429. 1978.
- 39] KINGMA, Y.J., DURDLE, N.G., LENHART, H., BOWES, K.L. and CHAMBERS, M.M. Improvements on Ag/AgCl pressure electrodes. Med. and Biol. Eng. and Comput. 21:351-357, 1983.
- 40] KINGMA, Y.J., DURDLE, N.G., BOWES, K.L., KOCYLOVSKI, M., and SZMIDT, J.: Size of oscillating regions in the canine colon. Gastrointestinal motility. Edited by J. Christensen. Raven Press. N.Y. 1980.
- 41] LEHR, J.: A vector derivation useful in impedance plethysmographic field calculations. IEEE Trans. BME-18:156-157. 1972.
- 42] McCLELLAND, G.R. and SUTTON, J.A.: Epigastric impedance: a non-invasive method for the assessment of gastric emptying and motility. Gut. 26:607-614, 1985.
- 43] MIRRIZI, N. and SCAFOGLIERI, U.: Optimal direction of the electrogastrographic signal in man. Med. and Biol. Eng. and Comput. 21:385, 1983.
- 44] MORRIS, I.R., HAMMOND, P.H., DARBY, C. and TAYLOR, I.: Relationship between motility and myoelectrical activity in the canine small and large intestine studied by a common electrode. Motility of the Dig. Tract. Edited by M. Wienback. Raven Press N.Y. 1982.
- 45] MORSE, P.M., FESHBACK, M.: Methods of theoretical physics. McGraw Hill, 1953.
- 46] NYBOER, J., BAGNO, S., BARNETT, A. and HALSEY, R.H.: Radiocardiograms: Electrical impedance changes of the heart in relation to electrocardiograms and heart sounds. J.Clin.Inves. 19:963, 1940.

- 47] OKADA, R.H.: Potentials produced by an eccentric dipole in a circular finite length conducting cylinder. IRE Trans. on Medical Electronics. ME-7:14. 1956
- 48] PLONSEY, R.: The bioelectric phenomena. McGraw Hill. 1969.
- 49] RAMIREZ, W.: The FFT Fundamentals and Concepts. Prentice-Hall Chap. 8:154-160. 1985.
- 50] RUSH, S., ABILDSKOV, J.A. and McFEE, R.: Resistivity of body tissues at low frequencies. Circ. Res. 12:40-50, 1963.
- 51] SAVARD, P., ROBERGE, F.A., PERR, J., and NADEAU, R.A.: Representation of cardiac electrical activity by a moving dipole for normal and ectopic beats in intact dog. Circ. Res. 46:415-425. 1980.
- 52] SHEARIN, N.L., BOWES, K.L. and KINGMA, Y.J.: In vitro electrical activity in canine colon. Gut. 20:780-786. 1978.
- 53] SIEGEL, G., ROEDEL, CH., NOITE, J., HOFER, HW., and BERTSCHE, O.: Ionic Compositions and ion exchange in vascular smooth muscle. Physiology of smooth muscle. Edited by E. Bulbring and M.F. Shuba. Raven Press. N.Y. 1976.
- 54] SNAPE, W.J., CARLSON, G.M., MATARAZZO, S.A. and COHEN, S.: Evidence that abnormal myoelectrical activity produces colonic motor dysfunction in the irritable bowel syndrome. Gastroenterol. 72(3):383. 1977.
- 55] SRAMEK, BO. B.: Electrical Bioimpedance. Medical Electronics. 95-105. April 1983.
- 56] STERN, O.: Zur theorie der elektrolytischen Doppelschicht. Z. Elektrochem. 30:508-516, 1924.

- 57] STODDARD, C.J., SMALLWOOD, R.H., and DUTHIE, H.L.: Electrical arrhythmias in the human stomach. *Gut*. 22:705-712. 1981.
- 58] STOUT, D.F. and KAUFMAN, M.: Handbook of operational amplifier design. McGraw Hill. 1976.
- 59] SWANSON, D.K. and WEBSTER, J.G.: Simple design for an impedance plethysmography. *Med. & Biol. Eng. and Comput.* 20:461-465. 1982.
- 60] SZURSZEWski, J.H.: Electrical basis for gastrointestinal motility. *Physiology of the gastrointestinal tract*, edited by Johnson, L.R., Raven Press N.Y. Vol. 2:1435-1466, 1981.
- 61] THANSANDOTE, A., STUCHLY, S.S., SMITH, A.M. and WIGHT, J.S.: Monitoring variations of biological impedances at microwave frequencies. *IEEE Trans. on Bio. Med. Eng.* BME 30(9):561-565. 1983.
- 62] SIN, B., USTACH, T.J. and SCHUSTER, M.M.: Electrical and mechanical activity of human and dog colon in vitro. *Hopkins Med. J.* 34:201-209. April 1974.
- 63] WARBURG, E.: Uber das verhalten sogenannter unpolarisierbarer elektroden gegen wechselstrom. *Ann.Phys.Chem.*, 67:493-499, 1899.
- 64] WATSON, G.N.: Theory of bessel functions. Camb. Univ. Press. 2nd edition. 1980.
- 65] WEISS, J.S.: A data acquisition and transmission system. An M.Sc. Thesis. Univ. of Alberta. 1982.
- 66] WOODBURY, J.W. and CRILL, W.E.: The potential between two abutting cells. *Biophysical Journal*. 10:1076. 1970.
- 67] WOODBURY, L.A., WOODBURY, J.W. and HECHT, H.: Membrane resting and action potentials of single cardiac muscle fibers. *Circulation*. 1:264-266. 1950.

- 68] YOU, C.H., LEE, K.Y., CHEY, W.Y. and MENGUR, R.:
Electrogastrographic study of patients with unexplained nausea,
bloating and vomiting. *Gastroenterol.* 79:311-314. 1980.
- 69] YOU, C.H. and CHEY, W.Y.: Study of electromechanical activity of
the stomach in humans and in dogs with particular attention to
tachygastria. *Gastroenterol.* 86:1460-1468. 1980.

APPENDIX A

SETTING UP THE IMPEDANCE MONITOR

Power Supply:

Start with the charger.

Step 1

Disconnect the terminals from the batteries. replace each battery with a 1Kohm, 1 Watt resistor. This represents the approximate internal resistance that the gel cells present to the charger. Insert the mains cable into the socket provided at the back of the instrument. Turn the power switch (S1 in figure 4.9) to the CHARGE position. The charge LED should light up. Check to see that the secondary voltage at the transformer is 16V AC. put a voltmeter across the 1K load and adjust pot R88 till the voltage reads 13.2V or whatever the charging voltage for the battery installed is. Turn the power switch off.

Step 2

Now disconnect the 1K load and reconnect the batteries, inserting an ammeter in the circuit to monitor the charging current. Turn the power switch back to the CHARGE position. The Gel cell employed in this instrument is a 12V, 2.6AH Elpower^R battery. Its 20 hour discharge rate is 130 mA. When the battery is flat (6 to 10V), the initial charging current should be about 3 to 4 times the 20H discharge rate. Therefore the ammeter should register between 340 mA and 512 mA. If the current is much higher than this, either reduce the charging voltage following the procedure in step 1 or increase the regulating resistance R85 in figure 4.16.

Charging should take about 12 to 18 hours. When the battery is fully charged, the charging current (termed float current) should be

about 10 percent of the 20H discharge rate; that is about 13 mA. This concludes the test on the charger. Turn the power switch off and disconnect all the meters used in the test.

Step 3

Turn the power switch to the ON position: the ON LED should light up. Check to see that the regulated supplies read -9V and +9V DC respectively. If not, adjust the regulating pots R64 and R66. Put a scope on each supply and verify that the AC ripple is lesser than 5%. Otherwise check the filtering tantalum capacitors C27 to C30 on the regulators shown in the power supply circuit.

Step 4

Oscillator and Current Source:

Connect a 100 ohm resistor across the current source, i.e. at terminals I_1 and I_2 . Put a scope on the 100 ohm resistor and adjust pot R1 until the frequency of the signal is 100 KHz or whatever else the desired frequency is in the range 90 KHz to 110 KHz. Adjust pot R6 until the voltage indicated shows the current that is desired i.e.: 100 mV for 1mA rms 200 mV for 2 mA. Change the 100 ohm load to 200 and then 500. Verify that the current regulation obtained is 2% or better.

Step 5

Input Circuit:

Connect up the test circuit of figure A1. Check that the voltage at pin 12 of the instrumentation amplifier (A3) is about 3 to 4 times the voltage across the input resistor (this depends on the turns ratio of transformer T2) and that the signal does not saturate. Repeat this procedure for the op-amps A4 and A5. A4 should have a gain of 10 and A5's gain is variable by way of pot R18. Check that the signal at pin

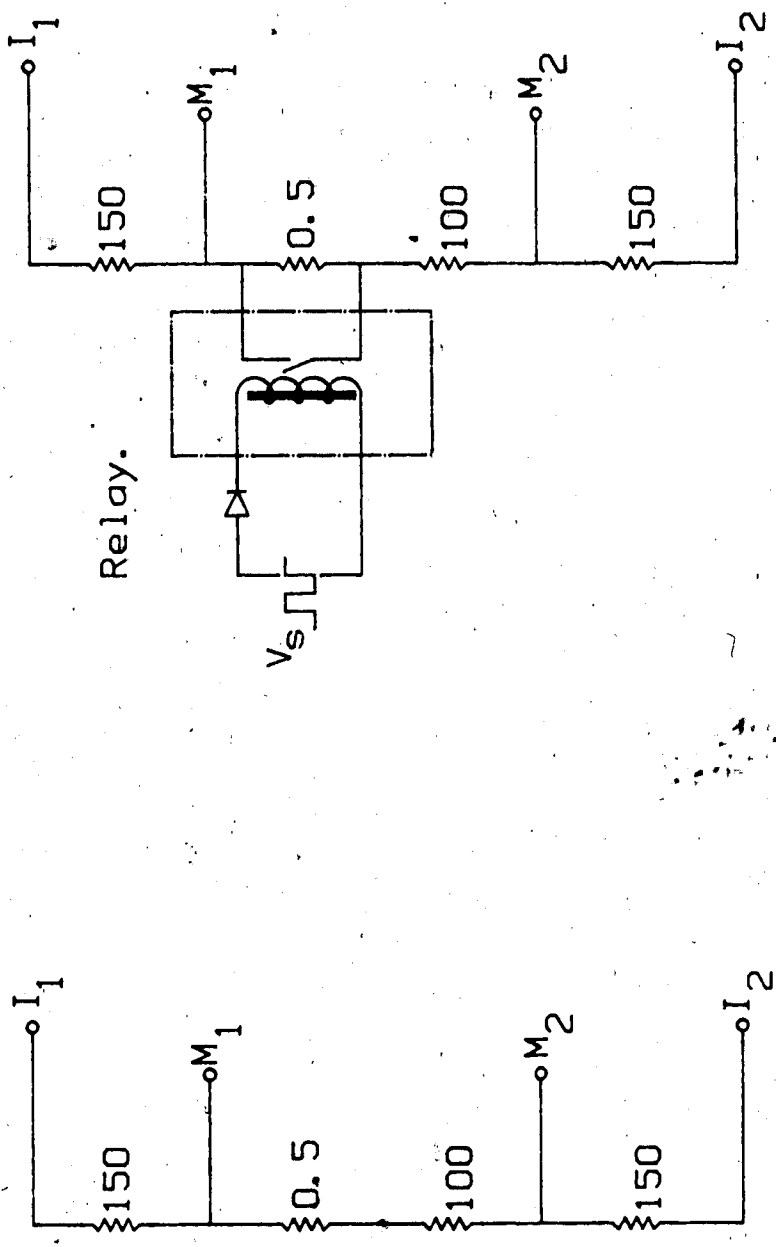


FIGURE A1
Test Circuit 1

FIGURE A2
Test Circuit 2

6 of A6 is not saturated.

Step 6

Now connect up the circuit of figure A2 where the driving signal V_g is a square wave of about 1 to 10 cpm. Make sure that its amplitude is large enough to drive the relay employed. The signal at M_1 and M_2 should now be an amplitude modulated signal at 0.5% modulation.

Now check the output signal $Z_0 + Z(t)$ at pin 6 of A7. It should be a DC level when the relay is not operated. It may be nulled to zero by adjusting pot R10 on the front panel. (If this is a first run, you might need to first null it to zero with the coarse adjust pot, R18 on the auxiliary detector.) The NULL LEDs on the front panel will indicate a balanced or near balanced condition by lighting up alternately at the slightest touch on the adjusting pot. Now switch on the modulating signal. The output should follow the relay with a time delay of a few seconds determined by the filters. The amplitude of the output should be at least 5 volts for a 0.5 ohm modulating resistor in figure A2. Of course this amplitude can be adjusted with switch S2 on the front panel.

This concludes the general testing routine that can also be used to trouble shoot the system.

Step 7

This is the last step required to set the system up for patient monitoring. Like the rest of the test routine, it only need be run if one adjusts any of the gain pots in the interior of the box. Otherwise, the operating point should be in the linear range for the demodulator.

Attach four ECG electrodes to the torso as described in the text for patient monitoring. Connect up the terminals I_1 , I_2 , M_1 and M_2 as

suggested. Adjust the gains and/or the current to the desired limits without saturation to the input amplifiers.

A.1 RESPONSE TIME OF THE IMPEDANCE MONITOR

In section 5.1, the mean delay introduced by the impedance monitor obtained by inspection of the experimental measurements is 10.55 ± 3.39 seconds. To determine the delay introduced into a test signal V_s , the test arrangement of figure A2 was employed. The signal V_s was monitored by a dc coupled Beckmann recorder between the diode and the relay. The test signal was set at a frequency of 4.3 cpm. At a time t_0 , the test signal was switched on to drive the relay. The output of the impedance monitor monitored by a second dc coupled channel on the Beckmann recorder remained zero until a time t_1 . This implies a delay of 2.8 seconds (see figure A3). The test signal was switched off at a time t_s . The time t_2 at which the impedance monitor responded to this control was determined by comparing the decaying waveform to that in the preceding cycles. The delay was determined to be 2.8 seconds.

We therefore conclude that the monitor introduced a delay of 2.8 seconds.

It is important to note that this figure may be off by several milliseconds. This is due to the fact that the relay modulating the input current probably did not switch at t_0 or t_s . The value of V_s at these instants may not be at the threshold at which the relay responds. This is because the input square wave has a finite rise time as indicated in figure A3.

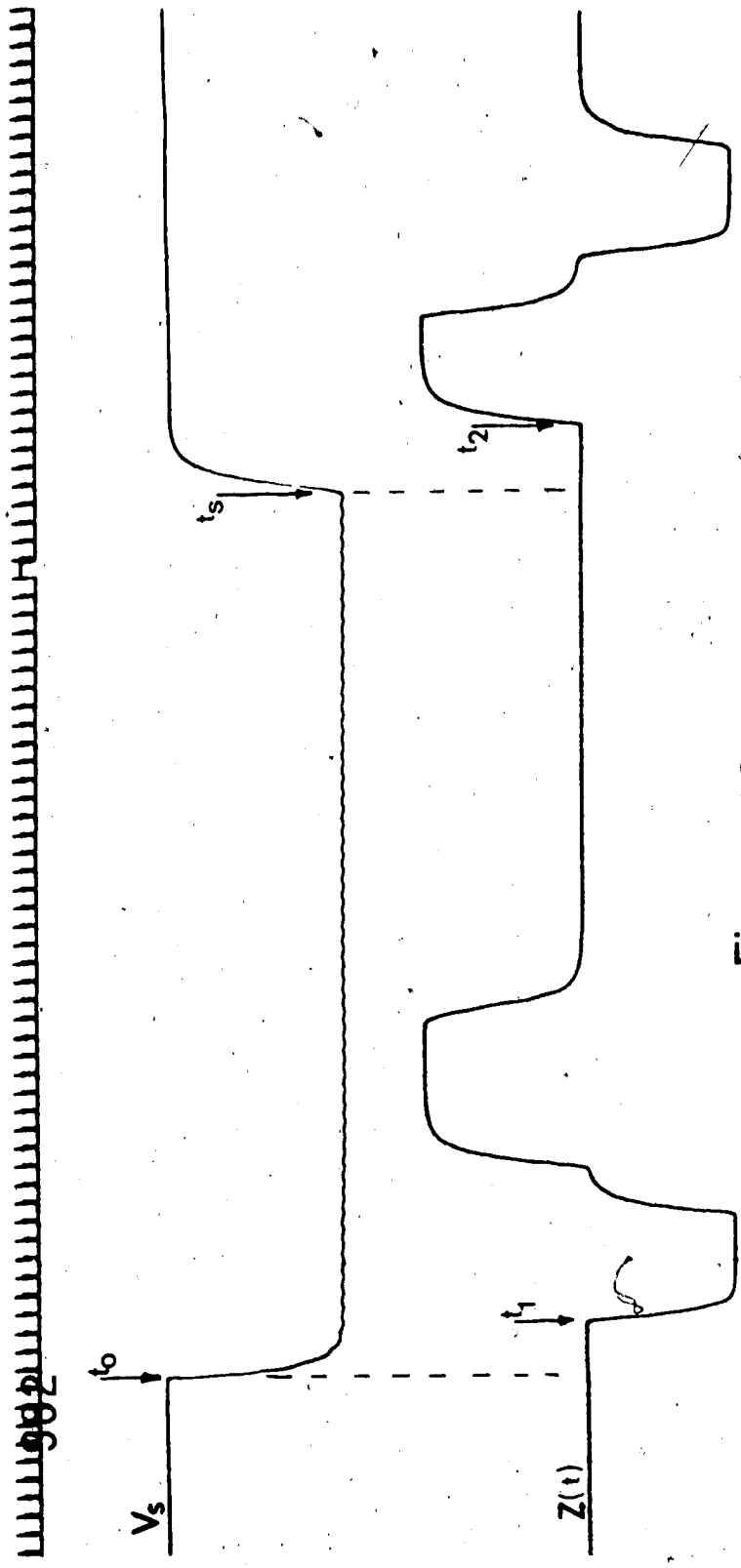


Figure A3

Test Signal and its Monitor-Delayed Output

A.2

PARTS LIST

OSCILLATOR AND CURRENT SOURCE

A1,A2	LF356
C1,C2	330 pF, 60V
C3,C4	0.1 μ F, 60V
D1,D2	1N914
Q1	2N4403
T1	101F

VOLTAGE SENSING AND DETECTION CIRCUIT

A3	AD521 JD
A4,.....,A6	LF351
A7,A9,A11	LF356
A8	LM311
A10	741
D3,D4	1N914
D5,D6	5.6V ZENER
D7,D8	LED
Q2	2N4401
Q3	2N5461
T2	LA2511, MULLARD

OUTPUT AND AUTO RESET CIRCUIT

A12 to A15	LF351
A18 to A20	741

REGULATORS AND CHARGERS

A21	LM317T
A22	LM337T
A23,A24,A25	741
Batteries	2 Elpower ^R 2.6AH, 12V Gell cell
D13,D21,D27	LED
D14,D22 to D25	1N4005
D15,D16	9V ZENER
D17,D18,D26	2*5V,5.6V ZENER
D19,D20	7V ZENER

APPENDIX B

CONSTRUCTION OF THE INTRALUMINAL ELECTRODE

Materials Required:

Gastric tube (Levine type #900-51)

Polyethylene tubing: $\phi = 3\text{mm}$

Heat shrinkable tubing: $\phi = 2\text{mm}$

Silver wire: $\phi = 1\text{mm}$

Tetrahydrofuran

4 strands 32 gauge stranded pick-up cable

Super glue

The mucosal electrode described in section 3.1 is made out of a Levine type stomach tube #900-51 manufactured by Cutter (Canada) Ltd.

This tube has 4 oval holes cut into its distal end from the factory. The holes are 2 cm apart on alternating sides of the tube. Widen the two holes on each side of the tube and cut two more to obtain the holes (A) and (B). Do not throw away pieces cut from the tubing. Soak them in tetrahydrofuran in a little bottle. The rubber solution so obtained will be used to seal holes in the finished product.

Cut out rubber membranes (M) (slightly larger than the holes (A)) on which the electrodes should be mounted with cement. Make 4 Ag/AgCl electrodes of the type described by Kingma et. al. [35] by replacing the capillary tubing in their description with heat shrinkable tubing. Dimension the electrodes to be flush with the surface of the tube at openings (B). Cement the electrode-membrane assembly on to the holes (A).

Using the dissolved rubber, seal off the end of the tube completely. Upon application of a light vacuum (25 cm H₂O), the

membranes (M) deformed inwards causing the electrodes to be pushed outwards. In this way good contact with the mucosa pressed against the smooth muscle tissue could be made.